

11-23-03
2
2006



This is to certify that the
dissertation entitled

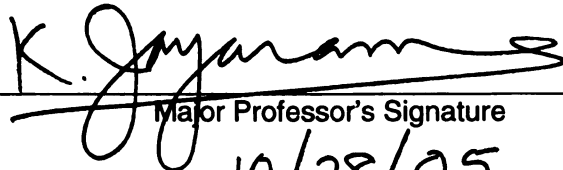
EFFECTS OF COUPLING AGENTS ON DISPERSION AND
STRUCTURE IN POLYPROPYLENE / CLAY
NANOCOMPOSITES

presented by

Sharad Kumar

has been accepted towards fulfillment
of the requirements for the

Ph.D. degree in Chemical Engineering and
Materials Science



Major Professor's Signature

10/28/05

Date

PLACE IN RETURN BOX to remove this checkout from your record.
TO AVOID FINES return on or before date due.
MAY BE RECALLED with earlier due date if requested.

DATE DUE	DATE DUE	DATE DUE
JAN 27 2008		
08 2 07		

**EFFECTS OF COUPLING AGENTS ON DISPERSION AND STRUCTURE IN
POLYPROPYLENE / CLAY NANOCOMPOSITES**

By

Sharad Kumar

A DISSERTATION

**Submitted to
Michigan State University
in partial fulfillment of the requirements
for the degree of**

DOCTOR OF PHILOSOPHY

Department of Chemical Engineering and Materials Science

2005

ABSTRACT

EFFECTS OF COUPLING AGENTS ON DISPERSION AND STRUCTURE IN POLYPROPYLENE / CLAY NANOCOMPOSITES

By

Sharad Kumar

This work focuses on improving the interactions of layered silicates with bulk polypropylene to optimize the nanolayer exfoliation. Silane coupling agents were selected based on their affinity with the bulk polypropylene: this was obtained by solubility parameter calculations. Maleated polypropylenes with different extents of bound maleic anhydride were also evaluated for their effectiveness in nanolayer exfoliation.

To study the interactions with silane coupling agents, the clay pretreated with a C18-surfactant was treated additionally with phenyl-trimethoxy silane. 5 wt% of this clay was melt blended with 10 wt% maleated polypropylene PP-g-MA and with 85 wt% of two different polypropylene grades having widely different molecular weights. The resulting nanocomposites were analyzed for microstructure and mechanical performance using X-ray diffraction (XRD), transmission electron microscopy (TEM), melt rheology and tensile modulus measurements. Nanocomposites with the most exfoliated structure were obtained when the chosen silane was located at the edges of the organoclay. This was confirmed with higher (almost twice) relative viscosity of the composites with silane modification at the organoclay edges as compared to composites with organoclay. The analysis of several TEM images also supports the rheology data. The improvements in

tensile modulus were greatest for the composites with this clay, indicative of improved coupling. The effects of shear and extensional flows on nanolayer morphology were investigated by extrusion through uniform bore and converging dies. Nanolayer restacking was observed; the levels for which were reduced for the nanocomposites reinforced with edge silated clay particularly at higher residence times in shear flows, as quantified by image analysis of the nanocomposite extrudates. Our results also show that compatibilizers having greater amounts of covalently bound maleic anhydride yield the most exfoliated structure.

ACKNOWLEDGMENTS

I would like to sincerely thank my advisor Dr K. Jayaraman for his help through the different stages of the Ph.D. work. He was always available to answer my queries and helped me understand the fundamental concepts behind the research work. His mentoring has given me the ability to handle challenging assignments with ease. I would also like to thank my committee members Dr Baker, Dr Lee and Dr Ofoli for serving on my committee and providing valuable guidance.

I would also take this opportunity to thank my parents, my sister Deepshikha and her family and Pooja for the immense love and support they have extended to me always. Without their support, this task would not have been possible. Their faith in me provided the required courage to cope with the stresses involved during the difficult stages of the research work and I am highly thankful to them.

I would also like to express my gratitude to my fellow colleagues, who provided me with the technical skills during the early stages of my research work. I would especially like to thank Giri, Darrell and Bhaskar, who helped me a lot in shaping my experiments.

Finally yet significantly, I would also like to thank my friends Hemant, Madhu, Anish, Srivatsan, Krishnan, Shireesh, Patil, Tanmay and John. It was an enjoyable and rewarding experience, which I had during my five years at Michigan State in your company. Thanks are also due to my other friends: Kartik, Nehru and Ritesh. You all have provided me with your support, whenever I was in need and I thank you.

TABLE OF CONTENTS

LIST OF TABLES	vii
LIST OF FIGURES	viii
CHAPTER 1	
INTRODUCTION	
1.1 BACKGROUND.....	1
1.2 RESEARCH OBJECTIVES.....	13
CHAPTER 2	
POLYPROPYLENE NANOCOMPOSITE PREPARATION AND CHARACTERIZATION	
2.1 NANOCOMPOSITE PREPARATION.....	15
2.2 SILANE TREATMENT FOR CLAYS.....	18
2.3 X-RAY DIFFRACTION.....	18
2.4 TRANSMISSION ELECTRON MICROSCOPY.....	20
2.5 RHEOLOGY.....	21
2.5.1 <i>Oscillatory Shear Measurements</i>	21
2.5.2 <i>Creep Compliance Measurements</i>	24
2.6 NANOLAYER MORPHOLOGICAL CHANGES IN EXTRUSION.....	25
2.7 MECHANICAL PERFORMANCE.....	27
CHAPTER 3	
THE USE OF SILANE COUPLING IN MELT MIXED POLYPROPYLENE CLAY NANOCOMPOSITES	
3.1 INTRODUCTION.....	31
3.1.1 <i>Objective</i>	31
3.1.2 <i>Background</i>	33
3.2 EXPERIMENTAL DETAILS.....	36
3.2.1 <i>Materials</i>	36
3.2.2 <i>Procedures</i>	37
3.2.2.1 <i>SILATION</i>	37
3.2.2.2 <i>MELT PROCESSING</i>	38
3.2.2.3 <i>EXTRUSION</i>	39
3.2.3 <i>Structural Characterization</i>	40
3.2.4 <i>Rheological and Mechanical Characterizations</i>	41
3.3 RESULTS AND DISCUSSION.....	41
3.3.1 <i>Silation and Clay Structure</i>	41
3.3.2 <i>Morphology of Nanocomposites</i>	42
3.3.2.1 <i>COMPRESSION MOLDED SPECIMENS</i>	42
3.3.2.2 <i>EXTRUDED SPECIMENS</i>	44

3.3.3	<i>Oscillatory Shear Rheology</i>	47
3.3.4	<i>Mechanical Performance</i>	49
3.4	CONCLUSIONS.....	50

CHAPTER 4

CHARACTERIZATION OF COMPATIBILIZER EFFECTIVENESS ON RHEOLOGY AND STRUCTURE

4.1	INTRODUCTION.....	69
4.1.1	<i>Objective</i>	69
4.1.2	<i>Background</i>	70
4.2	EXPERIMENTAL.....	73
4.2.1	<i>Materials</i>	73
4.2.2	<i>Melt Mixing</i>	74
4.2.3	<i>Structural Characterization</i>	74
4.2.4	<i>Rheological Characterization</i>	75
4.3	RESULTS AND DISCUSSION.....	76
4.4	CONCLUSION.....	82

CHAPTER 5

CONCLUSIONS AND RECOMMENDATIONS

5.1	CONCLUSIONS.....	101
5.2	RECOMMENDATIONS.....	104

BIBLIOGRAPHY	108
---------------------------	-----

LIST OF TABLES

Table 3.1:	Composition of various composite samples by weight %.....	52
Table 3.2:	Uniform bore and profile dies used for extrusion studies.....	53
Table 3.3:	Distribution of particle structures for composites before and after extrusion through uniform bore die (Die-1) at different rates from TEM Image analysis.....	54
Table 4.1:	Molecular Information on Compatibilizers.....	84
Table 4.2:	Composite identification and compatibilizer grade in each composite.....	85
Table 4.3:	Nature and concentration of maleic anhydride in maleated polypropylenes obtained by titration and average length of clay platelet.....	86

LIST OF FIGURES

Figure 2.1.	Representative DSC scans for melting transitions for polypropylene and corresponding silicate free melts: (—) Homopolymer PP, (—) Silicate free melt.....	29
Figure 2.2.	Capillary Rheometer setup for Extrusion Studies with Die Profiles.....	30
Figure 3.1.	Coupling between the matrix and the nanolayer faces is achieved with PP-g-MA chains and coupling between the nanolayer edges and the matrix can be achieved with selected silanes.....	55
Figure 3.2.	XRD patterns of organoclays with different silane treatment showing no change in d-spacing with phenyl trimethoxysilane (SiPh) but a noticeable increase in d-spacing with a different silane used in I.31PS. The organoclay I.30P was heated for 12 hours at 100°C to match the drying step in silation.....	56
Figure 3.3.	FTIR Spectra of I.30P and I.30PSiPh.....	57
Figure 3.4.	XRD patterns for polypropylene/clay nanocomposites with 5 wt% of different clays and 10 wt% of the same PP-g-MA (AC 950)	58
Figure 3.5.	Transmission electron micrographs of the composites (a) PP1-I.30P, (b) PP1-I.30PSiPh, (c) PP2-I.30P, (d) PP2-I.30PSiPh (The scale bar in each picture is 200 nm)	59
Figure 3.6.	Different particle structures identified in transmission electron micrographs.....	60
Figure 3.7.	Length distributions of "single particles" in nanocomposites (—) PP1-I.30P, (—) PP1-I.30PSiPh, (....) PP2-I.30P, (— • —) PP2-I.30PSiPh.....	61
Figure 3.8.	Transmission Electron Micrographs for the composite extrudates through Die-1 (a) PP2-I.30P-195 sec ⁻¹ , (b) PP2-I.30PSiPh-195 sec ⁻¹ , (c) PP2-I.30P-3650 sec ⁻¹ , (d) PP2-I.30PSiPh-3650 sec ⁻¹ . The scale bar in each picture is 500 nm.....	62

Figure 3.9.	Transmission Electron Micrographs for the composite extrudates through Die-2 (a) PP2-I.30P-1 sec ⁻¹ , (b) PP2-I.30PSiPh-1 sec ⁻¹ . The scale bar in each picture is 500 nm.....	63
Figure 3.10.	Dynamic viscosity curves for three composites and the corresponding silicate free melt of PP6323 and PP-g-MA: (Δ) PP1-I.30P, (○) PP1-I.30PSiPh, (■) PP1 and PP-g-MA.....	64
Figure 3.11.	Dynamic viscosity curves for two composites and the corresponding silicate free melt of PP6523 and PP-g-MA at 180°C: (▽) PP2-I.30P, (□) PP2-I.30PSiPh, (◆) PP2 and PP-g-MA.....	65
Figure 3.12.	Storage Modulus (G') curves versus frequency (ω) for the composites with different clays at 180°C: (Δ) PP1-I.30P, (○) PP1-I.30PSiPh.....	66
Figure 3.13.	δ versus Complex Shear Modulus (G*) for the composites with different clays at 180°C: (Δ) PP1-I.30P, (○) PP1-I.30PSiPh.....	67
Figure 3.14.	Tensile Moduli of PP6323 based nanocomposites with 5 wt% of different clays and 10 wt% of the same PP-g-MA (AC 950)	68
Figure 4.1:	XRD patterns for polypropylene/clay nanocomposites: Curve A: I.30P organoclay, curve B: NC11, curve C: NC12, curve D: NC13, curve E: NC14. All composites have a fix loading of 85wt% PP6323, 10 wt% PP-g-MA and 5wt% I.30P Clay. The composite NC11 is based on PP-g-MA1 (Acid Number =7), the composite NC12 is based on PP-g-MA2 (Acid Number=10), the composite NC13 is based on PP-g-MA3 (Acid Number=9) and the composite NC14 is based on PP-g-MA4 (Acid Number =23)	87
Figure 4.2:	Transmission Electron Micrograph for the composite NC12. The composite NC12 consists of 85wt% PP6323, 10wt% PP-g-MA2 (Acid Number =10) and 5wt% I.30P clay. The scale bar in the picture is 200 nm.....	88
Figure 4.3:	Transmission Electron Micrograph for the composite NC13. The composite NC13 consists of 85wt% PP6323, 10wt% PP-g-MA3 (Acid Number =9) and 5wt% I.30P clay. The scale bar in the picture is 200 nm.....	89

Figure 4.4:	Transmission Electron Micrograph for the composite NC14. The composite NC14 consists of 85wt% PP6323, 10wt% PP-g-MA4 (Acid Number =23) and 5wt% I.30P clay The scale bar in the picture is 200 nm.....	90
Figure 4.5:	Length distributions of single particles for composites: (– –) NC12, (....) NC13 and (—) NC14. All composites have a fix loading of 85wt% PP6323, 10 wt% PP-g-MA and 5wt% I.30P Clay. The composite NC12 is based on PP-g-MA2 (Acid Number=10), the composite NC13 is based on PP-g-MA3 (Acid Number=9) and the composite NC14 is based on PP-g-MA4 (Acid Number =23)	91
Figure 4.6:	Dynamic viscosity curves for composite NC11 (∇) and the silicate free melt of PP6323 and PP-g-MA1 (▼) at 180°C. The composite NC11 consists of 85wt% PP6323, 10wt% PP-g-MA1 (Acid Number =7) and 5wt% I.30P clay.....	92
Figure 4.7:	Dynamic viscosity curves for composite NC12 (Δ) and the silicate free melt of PP6323 and PP-g-MA2 (▲) at 180°C. The composite NC12 consists of 85wt% PP6323, 10wt% PP-g-MA2 (Acid Number =10) and 5wt% I.30P clay.....	93
Figure 4.8:	Dynamic viscosity curves for composite NC13 (□) and the silicate free melt of PP6323 and PP-g-MA3 (■) at 180°C. The composite NC13 consists of 85wt% PP6323, 10wt% PP-g-MA3 (Acid Number =9) and 5wt% I.30P clay.....	94
Figure 4.9:	Dynamic viscosity curves for composite NC14 (○) and the silicate free melt of PP6323 and PP-g-MA4 (●) at 180°C. The composite NC14 consists of 85wt% PP6323, 10wt% PP-g-MA4 (Acid Number =23) and 5wt% I.30P clay.....	95
Figure 4.10:	Relative viscosity curves obtained for the composites with different compatibilizers at 180°C: (∇) NC11, (Δ) NC12, (□) NC13, (○) NC14. All composites have a fix loading of 85wt% PP6323, 10 wt% PP-g-MA and 5wt% I.30P Clay. The composite NC11 is based on PP-g-MA1 (Acid Number =7), the composite NC12 is based on PP-g-MA2 (Acid Number=10), the composite NC13 is based on PP-g-MA3 (Acid Number=9) and the composite NC14 is based on PP-g-MA4	

(Acid Number =23) 96

Figure 4.11: Storage Modulus (G') curves versus frequency (ω) for the composites with different compatibilizers at 180°C: (∇) NC11, (Δ) NC12, (\square) NC13, (\circ) NC14. All composites have a fix loading of 85wt% PP6323, 10 wt% PP-g-MA and 5wt% I.30P Clay. The composite NC11 is based on PP-g-MA1 (Acid Number =7), the composite NC12 is based on PP-g-MA2 (Acid Number=10), the composite NC13 is based on PP-g-MA3 (Acid Number=9) and the composite NC14 is based on PP-g-MA4 (Acid Number =23) 97

Figure 4.12: Phase Angle (δ) versus Complex Shear Modulus (G^*) for the composites with different compatibilizers at 180°C: (∇) NC11, (Δ) NC12, (\square) NC13, (\circ) NC14. All composites have a fix loading of 85wt% PP6323, 10 wt% PP-g-MA and 5wt% I.30P Clay. The composite NC11 is based on PP-g-MA1 (Acid Number =7), the composite NC12 is based on PP-g-MA2 (Acid Number=10), the composite NC13 is based on PP-g-MA3 (Acid Number=9) and the composite NC14 is based on PP-g-MA4 (Acid Number =23) 98

Figure 4.13: Phase Angle (δ) versus Complex Shear Modulus (G^*) for the silicate free composite matrices at 180°C: (\blacktriangledown) NC11, (\blacktriangle) NC12, (\blacksquare) NC13, (\bullet) NC14. All composites have a fix loading of 85wt% PP6323, 10 wt% PP-g-MA and 5wt% I.30P Clay. The composite NC11 is based on PP-g-MA1 (Acid Number =7), the composite NC12 is based on PP-g-MA2 (Acid Number=10), the composite NC13 is based on PP-g-MA3 (Acid Number=9) and the composite NC14 is based on PP-g-MA4 (Acid Number =23) 99

Figure 4.14: Creep Compliance $J(t)$ as a function of time at a stress of 10 Pa at 180°C: (∇) NC11, (Δ) NC12, (\square) NC13, (\circ) NC14 All composites have a fix loading of 85wt% PP6323, 10 wt% PP-g-MA and 5wt% I.30P Clay. The composite NC11 is based on PP-g-MA1 (Acid Number =7), the composite NC12 is based on PP-g-MA2 (Acid Number=10), the composite NC13 is based on PP-g-MA3 (Acid Number=9) and the composite NC14 is based on PP-g-MA4 (Acid Number =23)..... 100

Figure 5.1: Proposed mechanism for the enhancement in the stability of nanolayers by careful control of the interactions between the different system components. This is achieved by favorable interactions of the phenyl end-capped silane with the bulk polypropylene and also increased hydrogen bonding interactions between the PP-g-MA and the hydroxyl groups.

107

INTRODUCTION

CHAPTER-1

1.1 BACKGROUND

Polymer-layered silicate nanocomposites have been a focus of great interest over the last decade after the pioneering work done by researchers at Toyota for nylon-6 based materials[1-5]. The high aspect ratio of delaminated or exfoliated platelets has the potential for producing striking improvements in a variety of polymer properties with the incorporation of small amounts of nanoclays[6-14]. These nanoclays have aspect ratios of the order of 200 and provide considerable enhancement in stiffness at a much lower loading as compared to conventional fillers (mica and talc), which need to be used at a rather high loading of 20 to 40 wt% in order to provide similar improvements in mechanical performance. The final part weight with nano-clays also has a lower density as compared to traditional talc filled composites owing to low filler loadings. Another main advantage of nano-clays is that they are impervious to gases and when they are well dispersed and oriented, can yield greatly improved barrier properties[15] as well as flame retardancy [16-20] in the composite. The earliest success in nanocomposite production was restricted to polar polymers, i.e. nylon and epoxy[21]. Limited success has been achieved with the most common commodity polymer polypropylene, which is non-polar in nature. Polypropylene (PP) is used in a wide range of products ranging from automotive bumpers to packaging applications such as pouches for meals-ready-to-eat (MRE's) and other food containers and therefore the prospects of improved nano-clay

dispersion in PP in order to perk up the properties needs careful and detailed investigations.

The silicate clay widely used for reinforcing polymers is Montmorillonite (MMT). The silicate clays exist naturally in a tactoid structure comprised of several tens of stacked layers (nanolayers) with a typical lateral dimension of 100-200 nm, a layer thickness of 1 nm, and an interlayer spacing of about 1 nm and have surface areas of greater than 700 m²/g [22, 23]. Each nanolayer is comprised of an aluminum-oxygen-hydroxyl octahedral sheet sandwiched between two silicon-oxygen tetrahedral sheets for the 2:1 smectite clays used for this work. The nanolayers can be separated by the introduction of water or other swelling agents into the Van-der-Waals gap between the clay layers. The gap contains exchangeable cations (usually sodium) to compensate the unbalanced charge in the interior of the clay layers due to isomorphous substitutions. This exchange capacity of the clays (cation exchange capacity) is an important variable, which dictates the effectiveness of the clay to be used as reinforcements for different polymer matrices [24]. Another important property of these clays is that they have hydroxyl groups at the slightly positive edges of the platelets (as opposed to fibrous clays like sepiolite).

The clay nano-layers need to be separated and dispersed in the polymer matrix; the procedure termed as clay exfoliation or clay delamination. In some cases, the polymer chains swell (intercalate) the clay galleries, but don't lead to complete separation of the layers. The resulting composite contains ordered clay tactoids with increased layer spacing and are termed as intercalated composites. Exfoliated clay composites yield

enhanced mechanical and barrier performance as compared to intercalated composites and therefore constitutes the desired structure.

The clay in its pristine form is hydrophilic and so has to be modified before it can be used as reinforcement for different polymer systems. For a nanocomposite formation, the polymer chain has to first penetrate between the clay galleries and then by employing certain processing strategies, the clay layers are separated far apart resulting in exfoliation of the nanolayers. Due to the 1 nm spacing between the closely packed sheets, there is a large entropic barrier, which the polymer has to overcome in penetrating this gap and hence, becoming intermixed with the clay. In order to enhance the interaction between the mineral and the organic polymer, the hydrophilic face of the clay platelets is modified by pre-intercalating long chain alkyl ammonium ions as surfactants. The onium ion is tethered to the surface of the clay and the hydrocarbon tails swell the clay and improve its dispersibility in organic materials. Theoretical studies by Vaia and coworkers[25, 26] and by Balazs and coworkers[27-42] suggest that the hydrocarbon tail makes interactions between the gallery faces and the polymer more enthalpically favorable and thereby compensates for the entropic reduction owing to polymer chain confinement in the clay galleries. Here the length of the surfactant chain is an important variable that influences the level of exfoliation. Reichert and coworkers[43] investigated the effectiveness of the chain length by exchanging synthetic sodium fluoromica with various protonated alkyl amines such as butyl (C4), hexyl (C6), octyl (C8), dodecyl (C12), hexadecyl (C16), and octadecyl (C18) amine. They concluded that the degree of dispersion went up with the alkyl chain length up to C18. Manias et al.[18] have reported that clay treated with a surfactant having two C18 tails mixes readily with a variety of

functionalized polypropylenes. Ton-that et al.[44] have compared the performance of polypropylene nanocomposites prepared with 2 wt % of two different surfactant treated clays - Cloisite 30B with one tallow tail and Cloisite 15A with two hydrogenated tallow tails (tallow composition is typically ~65% C18; ~30% C16; ~5% C14). They found that the nanocomposite with Cloisite 15A had a noticeably higher tensile modulus and tensile strength. Recent studies done by Hotta and Paul[45] indicate that the surfactant treatment with two alkyl tails yields better exfoliation in a polyethylene system as compared to a surfactant with just one long alkyl tail. The results from these studies with polyolefins are opposite to the results obtained for a Nylon-6 clay nanocomposite, where a surfactant treatment with 1 tallow tail was found to yield better dispersion levels as compared to a treatment with 2 tallow tails[46]. Surfactant with one tallow tail allowed efficient contact with the clay faces and the polyamide chains, while maintaining enough platelet spacing. The surfactant treatment with 2 tallow tails although instrumental in providing enough platelet spacing, weakened the platelet and polyamide chain interactions and led to poor clay delamination in the final composite. Manias et al.[18] have also indicated that the polymer-clay interactions should be more favorable than the surfactant-clay interactions in order to get improved dispersion levels.

Thermal characteristics of the organoclay play an important role in the final microstructure of the composite, since the melt intercalation is carried out usually at higher temperature. The loss of the interlayer surfactant present in the clay galleries during high temperature has been studied by Lee et al.[47] for two different surfactant treated clays- Cloisite 30B with one tallow tail and Cloisite 20A with two hydrogenated tallow tails and found that the amount of surfactant degradation was greater for Cloisite

30B and subsequently the reduction in the basal spacing was greater for the Cloisite 30B. The final dispersion levels of this clay were also found to be lower as compared to the Cloisite 20A for similar loadings in the final polypropylene nanocomposite. A recent numerical simulation study[48] on thermodynamic miscibility of a nanocomposite system also suggests that the surfactant loss can lead to the presence of a bare clay surface, which is highly detrimental for the exfoliation process.

In-situ polymerization techniques were initially used to fabricate clay/polymer hybrids. In the first step, the monomer was intercalated in the clay galleries followed by the polymerization in the second step, which led to an expansion of the clay galleries and resulted in an exfoliated morphology. The first polymer clay composite was synthesized in Nylon-6 using a similar monomer intercalation method by the Toyota group. The organophilic montmorillonite was ion exchanged with aminododecanoic acid, which was also the catalyst for the ring opening polymerization of the monomer ϵ -caprolactam. The polymerization of Nylon-6 occurs in the presence of MMT after ϵ -caprolactam is intercalated into the galleries. The resulting material provided significant improvements in mechanical, thermal and gas barrier properties at loadings of only 2-5wt% MMT. The in-situ polymerization technique for fabricating exfoliated nanocomposites was extended to epoxy systems as well. Pinnavaia et al.[49, 50] accomplished this by controlling the catalyst concentration in the galleries to obtain higher polymerization rates in the clay galleries. Recently an in-situ polymerization technique has also been reported[51] for making high performance polyolefin nanocomposites.

Melt intercalation in mixing instruments like twin-screw extruder still remains the convenient and the commercial inexpensive way for nanocomposite production. The

technique involves intercalating the polymer directly in the clay interlayer galleries directly through heating the mixture and then applying shear to separate the clay platelets. This method can be applied to a range of commodity polymers from essentially non-polar polypropylene to weakly polar polyethylene terephthalate, to strongly polar nylon. The melt mixing requires effective stress transmission between the matrix and the layered silicates particularly while the layers are still stacked to facilitate layer sliding and thereby have high exfoliation levels. Fornes et al.[52] studied melt processed nylon/montmorillonite nanocomposites and showed that if the molecular weight is lower than a critical value, the nanocomposite had a significant fraction of intercalated structures. This is because, only with a polymer of molecular weight higher than the critical molecular weight for entanglement can a sufficient level of shear stresses be transmitted from the matrix to a stack of nanolayers for sliding them apart.

In case of non-polar polypropylene, the dispersion of polar silicates is facilitated by the addition of functionalized polyolefin oligomers (compatibilizers), where the polar functionality (usually maleic anhydride) wets the clay surface and the oligomers are soluble in the bulk matrix. Using this approach, Okada and co-workers[53] synthesized the first PP-clay hybrids using maleic anhydride functionalized PP oligomers. The procedure involved the dissolution of functionalized polyolefin oligomer in toluene followed by intercalation of this mix in the clay galleries. The toluene was then evaporated and this mixture of functionalized polyolefin and clay was then melt blended with bulk PP to prepare the polymer clay hybrid. A solvent free procedure was also demonstrated to work for preparing PP-clay intercalation compounds using two different functionalized PP oligomers: maleic anhydride (MA) functionalized and a polypropylene

oligomer with telechelic OH groups (PP-OH)[9, 10, 54]. The need to have a significant level of polar functionality to interact with the nanolayer faces has since been established by Hasegawa et al.[54-57], Gopakumar et al.[58] for polyethylene and by Ishida et al.[59] for a wide range of polymers. Theoretical studies done by Balazs et al.[38, 40] have also established that adding functionalized polymers improves the clay exfoliation levels. Strong interactions between the maleic anhydride moieties and the organoclay results in an increase in system enthalpy, which compensates for the reduction in entropy due to the polymer chain intercalating in the 1 nm gap between the clay platelets and leads to greater separation of the clay nanolayers. A recent molecular dynamics study by Minisini and Tsobnang[60] calculates the interaction energy between functionalized polypropylenes and the organoclay surface. The interaction energy was highly favorable with the presence of maleic anhydride moieties and therefore should lead to improved organoclay dispersion.

The loading of the maleic anhydride functionalized polyolefins (PP-g-MA), the molecular weight of the PP-g-MA and the molar ratio of the maleic anhydride functionality[61] dictate the choice of compatibilizer for polyolefin nanocomposites. It is well established that functionalization with maleic anhydride leads to chain scission of the polypropylene[62]. Therefore large amounts of low or modest molecular weight PP-g-MA will lead to unacceptable mechanical properties. Wang et al[63, 64] have earlier investigated the effects of different molecular weight compatibilizers, maleic anhydride contents and the compatibilizer loadings on the clay exfoliation in polypropylene nanocomposites. Their results showed that the compatibilizer with lower molecular weight and higher MA content could lead to good clay dispersion in PP/clay composites,

yet there was some deterioration in both mechanical and thermal properties. A high maleic anhydride content in the maleated polypropylene while favorable for improved interactions with the clay surface results in a lower molecular weight wax, which will not entangle adequately with the bulk polypropylene during compounding[61]. Okada and coworkers[9, 10] used a 3:1 ratio and found that with the higher MA content, this ratio led to phase separation of the polar and non-polar polypropylenes.

The nature of the maleic anhydride functionality itself influences the exfoliation levels of the nanoclay. The maleic anhydride moieties in these materials may exist in three distinct forms. First as an un-reacted small molecule, second as a maleic anhydride oligomer and third as maleic anhydride bound to a polymer chain [65, 66]. The stronger bond between the clay and the compatibilizer will allow more effective stress transfer from the polymer to the clay in shear and ease the separation of the clay nanolayers. Hence a greater fraction of bound maleic anhydride should yield a greater degree of exfoliation. In one part of this study, four nanocomposite formulations with a 10 wt% loading of compatibilizers and 5 wt% organoclay were investigated for rheological and mechanical improvements, wherein the chosen compatibilizers had different bound maleic anhydride contents from 0.37-2.6 wt%. The detailed rheological analysis and detailed image analysis of the transmission electron micrographs revealed that the distribution of maleic anhydride in maleated polypropylene plays an important role in the process of clay delamination and the clay exfoliation levels were higher for compatibilizers with more bound maleic anhydride.

A few research groups have also focused on alternate methods to exfoliate the clay in PP. Intercalation of olefinic monomers followed by in-situ polymerization[67] and

in-situ melt phase ultrasonication[68] have been used to delaminate the clay in polypropylene. Manias and coworkers[18, 69] have used functionalized polypropylenes to improve the polymer/clay interactions; they also investigated a semi-fluorinated surfactant having a poor affinity for the clay surface in order to decrease the surfactant/clay interactions. In both cases, they obtained a mix of intercalated/exfoliated structures with improved mechanical and flame retardant properties. Liu and Wu[70] used a co-intercalation clay modification, which involved treating the clays with alkyl-ammonium surfactants followed by treatment with epoxy-propyl methacrylate, the latter to tether to the polypropylene. They obtained an intercalated morphology and improved mechanical properties with increased silicate loading. In a recent work, Kato and coworkers[71] use a water based slurry treatment of the clay, which doesn't involve alkyl ammonium surfactant treatment; this clay was compounded with PP and PP-g-MA in a twin-screw extruder. They obtained nanocomposites with high levels of clay exfoliation, which had comparable properties to a conventionally prepared nanocomposite.

Another way to increase the interactions between polymer and the filler is to have favorable interactions of the bulk polymer with the hydroxylated edges of the silicate layer[72]. The OH groups on the clay edges can be modified with appropriate silane coupling agents, which should provide the necessary interfacial coupling during the process of melt compounding and facilitate the nano-layer sliding, when the layers are still stacked. Previous studies[73] have used silane-modified clays, which have resulted in nanocomposites with improved mechanical properties. However with the layered morphology of clays, some silanes can actually move into the interlayer galleries. Fluoro-alkyl silanes were used by Manias and coworkers, which led to silane intercalation in the

clay galleries and increased the basal spacing from 1.98 to 2.4 nm. Other silanes have been shown to react with the edges mainly [74-77], which is evident by similar interlayer spacing before and after silane treatment. One of the objectives of this work was to investigate the effectiveness of the latter class of silanes in enhancing exfoliation levels of clay in polypropylene nanocomposites.

The silanes used in this study were selected based on thermodynamic compatibility between the filler and the polymer matrix. In previous studies, the filler-matrix compatibility and its resulting effects on interfacial adhesion have been investigated. Miller and coworkers [78-80] have worked with different organo-functional silanes and indicate that there is an enhanced interfacial strength in systems with more favorable thermodynamic mixing. Their study includes both crystalline and amorphous polymer composites and suggests that thermodynamic compatibility as quantified by the free energy of mixing ($-\Delta G_{\text{mix}}$) provides a convenient means for predicting the interfacial strength between silane treated surfaces and polymers. A solubility parameter match between the polymer and the silane organo-functional group has been suggested as a criterion for compatibility.

Investigating the nanolayer morphological stability to further melt processing was the other objective of this work. Once the nanoclay is exfoliated in the polymer matrix, it is used for applications ranging from automotive [81, 82] to food packaging to flame retardant materials [16-20, 83]. This production step is accomplished by additional melt processing steps like injection molding and extrusion: both involving different extents of straight and converging-diverging flows. Additional melt blending can affect the nanolayer morphology as illustrated by the work of Reichert et al. [84] and Manias et

al.[18]. Shear induced flocculation of nanolayers has also been observed by Okamoto et al.[85]. Reichert et al.[84] conducted annealing studies of injection molded polypropylene nanocomposites and observed a coarsening of the nanolayers after annealing. The ability of the nanocomposites to withstand additional processing effects indicates improved coupling between the clay and the bulk polymer. Similar studies were conducted by Manias et al.[18] for two polypropylene nanocomposite systems with the same organoclay for each case but with two different matrices: neat PP alone for one case and PP-g-MA alone for the second. The structure before and after annealing was studied by X-ray diffraction and it was observed that the composite with the neat PP matrix turned from an exfoliated structure to strongly intercalated after annealing cycle of 15 min. The other structure with PP-g-MA as matrix was stable over a period of 30 min indicating better coupling for this case.

The clay platelets being anisotropic orient differently based on the type of flow, and therefore processing induced orientation assumes a lot of significance[86]. Recent studies indicate that along with exfoliation, the orientation of the nanolayers is also an important variable, which dictates the levels of improvements in material properties of the polymer[87]. This study assumes vital importance when these materials have to be fabricated for use as barrier materials or for flammability reductions[16, 83], where greater alignments of silicate nanolayers yield better properties. Qian et al. did permeability measurement on cast films as well as blown films of a 7-wt% clay reinforced polypropylene nanocomposite[15]. The reduction in permeability for the blown film was about 60% for the blown film and 30% for the cast film as compared to the silicate free polypropylene film. These nanocomposites had a large fraction of

intercalated structures. Greater orientation of the nanolayers in the plane of the film was obtained in the film blowing process, which led to lower relative permeability. The degree of crystallinity in the matrix polymer also goes up in the presence of the nanolayers particularly as they are oriented. Increased crystallinity leads to further reduction in permeability to gases[88]. Greater reductions in permeability can be obtained with full exfoliation of the nanolayers in polypropylene, followed by even greater orientation of the high aspect ratio particles. Different studies have been conducted previously to investigate the nanolayer orientation in both shear flows[3, 89-92] as well as elongational flows[93]. Kojima et al.[3, 90] in their work with nylon-clay nanocomposite films observed that the clay platelets align parallel to the surface of the film and along the flow axis. Bafna et al.[89] observed a similar kind of behavior with PP-clay nanocomposite films. Varlot et al.[92] have observed that the clay platelets are aligned with normals both parallel and perpendicular to the thickness direction of the sample for injection molded nylon-clay nanocomposites. Schmidt et al.[91] have investigated the influence of shear on viscoelastic polymer-clay solutions by means of small-angle neutron scattering (SANS) and found that at higher shear rates, the scattering anisotropy increased due to the enhanced orientation of the clay platelets in the shear field. Okamoto et al.[93] conducted uniaxial elongational tests on their elongational flow opto-rheometer (similar to Meissner's elongational rheometer) in the melt state at constant Hencky strain rate on samples of PP-clay nanocomposites and observed a perpendicular alignment of the clay platelets to the stretch direction.

1.2 RESEARCH OBJECTIVES

The goal here is to develop a novel and more controllable approach to prepare polypropylene nanocomposites with mostly exfoliated clay structures and investigate the resulting nanocomposite for rheological and mechanical improvements. This approach is motivated by the need for better coupling between the matrix and the nanolayers. The task of coupling the matrix and the clay can be accomplished by providing improved interactions at the clay faces and at the hydroxylated clay edges. The incorporation of maleated polypropylenes serves to provide favorable interactions at the clay faces. The edge sites can also be functionalized with carefully chosen silane coupling agents in order to enhance the bulk polypropylene/clay interactions. The morphological stability of the anisotropic silicate layers to various flows was also investigated. The information hence obtained will allow us to design materials with high levels of clay exfoliation and also lead to evaluation of the nanolayer morphological stability during post processing compounding.

The various research tasks, which this work attempts to answer, are as follows:

- To investigate the effects of compatibilizers with varying maleic anhydride distribution on the rheological and mechanical performance of melt mixed polypropylene nanocomposites.
- Additional coupling provided on the hydroxylated clay edges with carefully chosen silane coupling agents in order to improve the interactions between the silicate layers and the bulk polypropylene. To investigate the nanolayer exfoliation levels and the concomitant improvements in flow and mechanical properties.

- To investigate the effects of extrusion through uniform bore and profile dies on the nanolayer morphology. The composites extruded for this study had fixed loadings of clay and compatibilizer and were verified to have a high degree of clay exfoliation initially by XRD, TEM and oscillatory shear rheology. The additional task was to investigate if the edge functionalization with silane coupling agents provides more stability to the silicate structure? A high morphological stability to additional melt processing will further provide evidence for improved interactions between the clay and the bulk polypropylene.

POLYPROPYLENE NANOCOMPOSITE PREPARATION AND CHARACTERIZATION

CHAPTER-2

2.1 NANOCOMPOSITE PREPARATION

All nanocomposites in this study were melt mixed using a batch mixing technique. The residence time in the mixing technique should be selected to provide enough shear while avoiding the degradation of surfactant; this can be manipulated by adjusting the throughput rate and the screw rpm[94]. For small batches, batch mixers like a DACA mixer[95], Gelimat[96] or a Banbury[61] can be used., where the shear rates in the batch mixers ranged from 50 to 200 s⁻¹ and the residence time was between 2 to 10 minutes.

The melt mixing technique for this research involved initial homogenization of the materials in the solid form by shaking them in a sample bag vigorously for 2 minutes. The homogenous powder-pellet blend is fed to a preheated mixer bowl in a batch size of 47 grams for 1 run. The bowl containing 2 Banbury impellers has a volume of 75 cm³ and was manufactured by CW Brabender Instruments Inc. A nitrogen purge port was also incorporated along with the mixing bowl to ensure minimum polymer degradation. Solomon et al.[97] and Lee et al.[47] have previously used similar mixing instrument for preparation of polypropylene nanocomposites.

The homogenous powder melt was melt blended in the pre-heated bowl at a temperature of 180°C at 150 rpm for 10 minutes. The rationale behind choosing the

mixing protocol was to maximize shearing time, minimize polymer degradation and limited availability of materials. The chosen temperature of 180°C was above the melting temperature of the polypropylene as well as the corresponding nanocomposites. The melting temperature of the polypropylene chosen for this study was greater than 160°C and had a specific gravity between 0.88-0.92, as indicated by the company literature. Representative DSC scans on the polypropylene and PP-maleated PP blends shown in Figure 2.1 further confirm that the melting point range for all the materials is between 160°C and 170°C. The temperature of 180°C was chosen to maximize polymer melt viscosity, so that enough shear stresses are generated during the process of melt mixing. Fornes et al.[52] have worked with a range of nylon-6 molecular weights and have concluded that a higher melt viscosity is much effective for sliding the clay platelets apart and therefore maximize clay exfoliation.

The time period of mixing should be sufficient enough to completely melt and mix the polymer. Higher melt mixing times have been established to be better in promoting clay exfoliation[94], however excessive mixing time can lead to possible material degradation as well. The mixing time for the instrument has been optimized by a previous work in our lab, in which constant torque readout from the instrument was observed in a time span of 5 minutes thereby indicating the material has been melted and mixed uniformly. The mixing speed was determined by the maximum permissible speed on the instrument and thus to impart the maximum possible shear into the material using the instrument.

The “clump” of the materials after the mixing was scrapped from the mixer bowl using a brass scraper and the clump was fed to a mini granulator to make small pellets,

the melt was chopped in a mini-granulator. The resulting granules were then compression molded to make 50 mm disks for rheological analysis and XRD measurements.

The compression molding procedure involved a Wabash Compression Molder, which was preheated to 200°C. The temperature was chosen to ensure homogenous melting of the polymer. The samples are molded using 2 thick steel plates, a multi cavity mold and a polyimide release film. The choice of the release film was based on its inertness to the material and its high temperature stability.

For molding the specimens, the assembly was as follows. One sheet of the polyimide release film was placed on the top of one of the thick steel plates. This was followed by the multi cavity mold on the top of the release film. The 9 cavities were filled with the required amount of pellets, which were calculated based on the thickness of the mold (about 1 mm), the mold diameter (close to 50 mm) and the density of the material (value chosen was 1 gm/cm³). The samples were then covered with another release film followed by the second thick steel plate. The complete mold assembly was transferred to the preheated compression-molding machine. The platens of the machine were closed and the material was lightly compression molded for 5 minutes at a low pressure of 2 tons. This was followed by another cycle of compression at 10 tons for an additional 5 minutes at the same temperature. Following this, the cooling water was introduced into the platens and the set point temperature was also reduced to 30°C to quench the assembly as quickly as possible, while maintaining the pressure at 10 tons. The assembly was taken out at a temperature around 65°C and the samples were removed from the molds carefully. These disks were used for further rheological analysis as well as X-ray diffraction measurements.

2.2 SILANE TREATMENT FOR CLAYS

For doing the silane treatment on the organoclay I.30P, 20 grams of the organoclay was stirred in a 2wt% silane solution in methanol for 2 minutes. The solution was allowed to stand for 10 minutes and then decanted. The particles were kept under ambient conditions for 24 hrs to cure the silane layer. A series of three wash cycles with methanol were done to remove any un-reacted silane. The resulting clay cake was dried in vacuum for a period of twelve hours at 100°C. The dried clay clumps were lightly ground and the resulting clay (referred to as I.30PSiPh in the subsequent discussion) was used for melt blending with the polypropylene and the compatibilizer. All clays were characterized by XRD for basal spacing. A different commercially available siliated clay I.31PS was received from Nanocor and compared with the I.30P clay as well as with the I.30PSiPh.

2.3 X-RAY DIFFRACTION

One of the structural characterization techniques used for this study is X-ray diffraction. X-ray diffraction is based on the fact that ordered structures act as scattering sites for x-ray radiation. Also since the wavelength of the X-ray is of the same order as the inter-atomic distance in a crystal, the diffraction from these sites can be analyzed using a detector and can provide insight into the microstructure. The mathematical expression for this diffraction phenomenon was established by Bragg and is given by equation 2.1.

$$n\lambda = 2d \sin \theta \quad (2.1)$$

Here “n” stands for the order of diffraction, “d” is the spacing between atoms or planes, and “ θ ” is the angle of diffraction. For this study, the first order peak was considered for analysis[98].

The natural montmorillonite clay has a basal spacing of about 0.95 nm. After the clay modification with octadecyl ammonium surfactants, the basal spacing for the organoclay I.30P increases to 2.3 nm. For polypropylene, the X-ray peak is obtained at a 2θ value of about 14 degrees. The powder x-ray diffraction of the clays is carried out by initially compacting the clay in a brass fixture with a 1"-1" cavity. For all the nanocomposite specimens, the compression-molded disks were used. These were first pasted onto glass slides to provide enough rigidity to the samples, so as to get enough diffraction intensities with the X-ray beam. The X-ray diffractometer used for the study was a Rigaku Rotaflex Ru-200BH X-ray diffractometer, which is equipped with a Ni-filtered Cu K α radiation source and operated at 45 kV and 100 mA. The sample is scanned over a 2θ range of 0.5° to 15° at a rate of 0.5°/min and measurements are recorded at equal increments of 0.01°.

The chosen voltage and current were the recommended parameters for the instrument. The scan range was chosen to encompass the various diffraction peaks (clay, polypropylene) required for the research. The lower scan angle was chosen as 0.5° and the higher scan angle (15°) was chosen, since the polypropylene peak occurs around 14°. The scan speed was found to be optimum for the analysis, since a higher scan speed might not show the diffraction intensities accurately at low 2θ values. The sampling interval of 0.01° was chosen to provide efficient resolution in the quality of diffracted data over the entire investigated range. The other instrument setting was the choice of

diffraction slits. There are 4 slits overall, one between the x-ray source (diffraction slit) and the sample; two after the sample on the goniometer and the last slit is on the detector. The first two slits are of the same width by convention and $1/6^\circ$ slits were used for this work. The $1/6^\circ$ slits were the smallest available and were used to obtain diffraction intensities at low angles with accuracy. The other two slits were both 0.3° and were chosen based on the outcomes of a few trial runs.

2.4 TRANSMISSION ELECTRON MICROSCOPY

Transmission electron microscopy (TEM) is a valuable analytical tool, which is based on scattering of electrons. Since the electron wavelength is much smaller than light, the TEM resolution is far better than that from a light microscope. Therefore TEM micrographs can provide information about the finest details of internal structure. The microscope involves an electron beam (produced by an electron gun), which passes through a series of lenses (condenser lens, objective lens) and then through the sample. The sample image is passed through a set of intermediate and projector lenses, being enlarged all the way. Finally the image is formed on a phosphorescent screen, which is then digitized using a digital camera. The dark areas (clay in our work) represent those areas of the sample through which fewer electrons were transmitted, whereas the lighter areas correspond to the bulk polymer phase.

The technique however probes very small areas of the samples and is a big limitation. Also to get a uniform passage of electrons through the sample, it has to be thin (about 90 nm) and of uniform thickness, which is another big limitation of the technique. For polypropylene samples, which have glass transition temperatures below room

temperature, cryosectioning is required to ensure enough polymer rigidity. The sectioning was done using the following procedure. Initially a small trapezoid was carved on a small compression molded section of the specimen at room temperature using a razor blade. This was followed by placing the sample in a cryo-assembly maintained at -120°C using a liquid nitrogen reservoir. Sections of thickness close to 90 nm were chipped from the trapezoidal structure using a diamond knife and transferred to a copper grid of 300-mesh size. For some specimens, a copper grid of 450-mesh size was also used. The choice of the grid was governed by the fact, that they should provide enough rigidity to the thin sections and should not be damaged due to the electron beam. The cryomicrotomed sections for extruded strands were prepared carefully from the strand core to get a much more representative estimate of the composite morphology. The thin sections were then viewed under a microscope JEOL 100 CX equipped with a 120 KeV electron accelerator. The digital images obtained using a digital camera were analyzed using commercial image analysis software (Sigma Scan Pro 5.0, SPSS Inc) to calculate the percentage of single platelet structures, stacked structures as well as agglomerates in the sample. The procedure is laid out in detail in Chapters 3-4.

2.5 RHEOLOGY

2.5.1 Oscillatory Shear Measurements

The rheological properties of a polymer yield useful information about the material microstructure, which dictates its end product performance and processing ease. The viscoelastic (a combination of viscous and elastic) response of polymers as a

function of frequency (time) and temperature can be obtained by using rotational rheometers. The structure of a material can typically be accessed by its response to small strain amplitude oscillatory strains.

$$\gamma = \gamma_0 \sin \omega t \quad (2.2)$$

$$\tau = \tau_0 \sin(\omega t + \delta) \quad (2.3)$$

The stress can be decomposed into two components – an elastic component in phase with the strain and a viscous component 90° out of phase with strain. This yields two dynamic moduli — G' (in-phase elastic or storage modulus) and G'' (out-of-phase viscous or loss modulus). The phase tangent provides information regarding the melt elastic nature (equation 2.4)

$$\tan \delta = \frac{G''}{G'} \quad (2.4)$$

A complex viscosity may be defined, with its magnitude is given by,

$$\left| \eta^* \right| = (\eta'^2 + \eta''^2)^{1/2} = \left[\left(\frac{G''}{\omega} \right)^2 + \left(\frac{G'}{\omega} \right)^2 \right]^{1/2} = \frac{|G^*|}{\omega} \quad (2.5)$$

The rheometer used for this work was an RMS 800 instrument from Rheometrics Inc. The strain limit to be used for oscillatory testing has to be in the linear viscoelastic limit. This limit is obtained by running a strain sweep test. The strain sweep test involves varying the strains for the material at a fixed frequency and monitoring the viscoelastic properties (G' , η') as a function of strain. The strain at which the chosen viscoelastic property shows a decrease indicates the onset of non-linearity. The strains utilized in this research were confirmed to be in the linear viscoelastic regime. Typically a 2 % strain for the composites was in the linear viscoelastic regime and was used for the oscillatory shear measurements. The chosen strain percentage also resulted in torque values greater than 2 g-cm, which is the lowest limit for acceptable torque values for the instrument. The lower strain values also preclude any nano-layer alignment, which has been earlier observed to occur with large amplitude oscillatory strains[99-101]. The chosen frequency range was 0.01-100 rad/s for all the composite specimens, whereas a frequency range of 0.5-100 rad/s was used for the silicate free matrices. The lower frequencies were used for the composites to investigate any possible pseudo-yield behavior, typically observed with nanocomposites[97, 100, 102]. A lower frequency of 0.05 rad/s was sufficient for the silicate free matrices, since all the materials reached a steady plateau in the viscosity curve. All the data reported in this work were only considered if the corresponding torque values were above the acceptable lower torque-sensing limit of the instrument.

2.5.2 Creep Compliance Measurements

The creep compliance measurements are an efficient tool to monitor the low frequency micro-structural changes and yield phenomenon associated typically with filled materials[103]. Creep is a slow, progressive deformation of a material under constant stress. A creep test involves application of a constant shear stress and monitoring the resulting shear strain as a function of time. The creep compliance is the ratio of the time dependent strain to the constant stress. For a viscoelastic liquid, the creep compliance $J(t)$ can be defined by the equation 2.6.

$$J(t) = \frac{t}{\eta_0} + \sum_i J_i (1 - e^{-t/\lambda_i}) \quad (2.6)$$

A higher value for the creep compliance is typically a characteristic of a liquid like response and a lower creep compliance value is typically observed for materials having a solid like response. For sufficiently higher creep times, the zero shear viscosity can be obtained by making a plot of $t/J(t)$ versus time and reading the steady plateau value of the curve slope[104].

The creep compliance measurements for this research are obtained with an AR 2000 rheometer at 180°C from TA Instruments. 40mm steel plates were utilized for this research. The 50 mm compression molded disks were reduced in diameter to 40mm to be used in the instrument by cutting the disk carefully with a sharp razor blade. The samples were initially homogenized for 10 minutes before starting the run. The creep tests were performed at a stress of 10 Pa. Similar values of stress have been previously used by other researchers for creep compliance measurements[103, 104] with polypropylene and

polypropylene clay hybrids as well. The chosen stress value of 10 Pa was confirmed to be in the linear viscoelastic regime, since similar compliance values were obtained at a higher stress of 15 Pa. The tests were performed at a temperature of 180°C and the samples were melted for 10 minutes before starting the test. The gap spacing used for the runs ranged from 0.8 mm-0.9 mm. The spacing was chosen so as to get enough normal force and for making sure that both plates are in sufficient contact with the sample.

2.6 NANOLAYER MORPHOLOGICAL CHANGES IN EXTRUSION

To investigate the morphology of the silicate nanolayers in different flows, the granulated pellets were passed through a uniform bore die and a converging die providing logarithmic tensile (Hencky) strain of 5. The specifications of the two dies and the extrusion parameters have been shown in Figure 2.2.

The dies were mounted in a Dynisco LCR6000 Capillary rheometer (Figure 2.2) and extrusion was carried out at 200°C. The procedure for extruding with the straight and profile dies involves the following sequence of steps: (1) the capillary barrel of the rheometer was heated to the test temperature (200°C) and the die was attached to it; (2) a total of 6 g of nanocomposite pellets was loaded into the capillary barrel in 2+2+2 gms increments, after adding each 2 gm batch, the sample was allowed to melt for 2 minutes to ensure homogenous melting, (6) the test was programmed in and run from the instrument software window. Two different rates of extrusion were used with Die 1- 195 sec⁻¹ (piston rate of 16 mm/min) and 3650 sec⁻¹ (piston rate of 300 mm/min) in order to contrast the effects of low and high strain rates. These rates were obtained based on the following equations for straight shear flows.

$$\dot{\gamma} = \frac{4Q}{\pi R_e^3} \quad (2.7)$$

$\dot{\gamma}$ = Apparent Shear Rate, Q= Volumetric Flow Rate, R_e = Die Exit Radius

$$Q = \frac{V_p \pi R_b^2}{4} \quad (2.8)$$

R_b = Inlet Die Radius, V_p = Piston Speed

$$\bar{u} = \frac{Q}{\pi R_e^2} \quad (2.9)$$

\bar{u} = Average velocity

$$t = \frac{L}{u} \quad (2.10)$$

t = Residence Time, L= Die Length

The converging die used in this study has a semi-hyperboloidal profile, which provides a fixed extensional (Hencky) strain, ε_H on the melt.

$$\varepsilon_H = \ln\left(\frac{R_B^2}{R_E^2}\right) \quad (2.11)$$

In the above equation, R_B is the inlet radius of the semi-hyperboloidal die (same as barrel diameter) and R_E is the exit radius of the die. The capital letters “B” and “E” used as subscripts are used to distinguish the semi-hyperboloidal die (Die 2) with the straight die (Die 1) as used in this work. The semi-hyperboloidal die provides an extensional strain rate ($\dot{\epsilon}$), over its entire length (L) for a given piston velocity (V_P).

$$\dot{\epsilon} = \frac{V_P}{L} \exp(\epsilon_H) \quad (2.12)$$

Both the dies used in these studies have a length of 20 mm. In order to draw the distinctions between the morphology in straight and converging flows, a similar piston ram rate was used for the converging die (Die 2), after adjusting it for the difference in the exit diameters. The equivalent ram speed turns out to be about 9.2 mm/min, which translates to an extensional strain rate of 1 sec^{-1} .

2.7 MECHANICAL PERFORMANCE

Exfoliated clay platelets result in large improvements in the mechanical performance of a composite. The composites in this study were evaluated for improvements in tensile modulus. The specimens for this evaluation were prepared by using a mini DSM injection molder. The choice of the instrument is based on the small nanocomposite batch size. Typically 1 kg of material is required with a conventional injection molder. Such amount of material wasn't possible to obtain with the Banbury Mixer and therefore the mini-injection molder was used for this research. The procedure involves initially feeding 12 gms of pellets into a DSM 15 cm^3 Micro-Extruder. The

extruder was operated at a uniform temperature of 180°C for all the zones and a run cycle of 5 rpm for 2 minutes was used to homogenize and melt the specimens. The 5 rpm screw speed was chosen to impart minimum shear to the instrument, so that the microstructure of the composite remains more or less intact. XRD scans run on specimens before and after DSM micro-extruder compounding are almost similar, which corroborate the idea that the clay microstructure remains almost the same. The melt from the DSM after the two minutes cycle is taken out by opening a side gate and collected in a melt holder, which is maintained at 180°C. The melt holder is loaded in the DSM Injection Molding machine and injection molded at 100 psi to make tensile coupons. The coupons obtained were devoid of any scratches and were mostly smooth.

The 1% tangent tensile moduli were obtained at a testing speed of 0.7 in/min using a United Universal Testing Machine. The tensile testing was carried out following the procedure ASTM D3039 with a 20 K load cell. The tensile specimens prepared by the DSM compounding didn't comply with ASTM standards, but were useful to provide a relative estimate of the improvements in tensile modulus as compared to the base polypropylene. At least 3 samples were tested for each measurement, and approximately 5% error was associated with the obtained values.

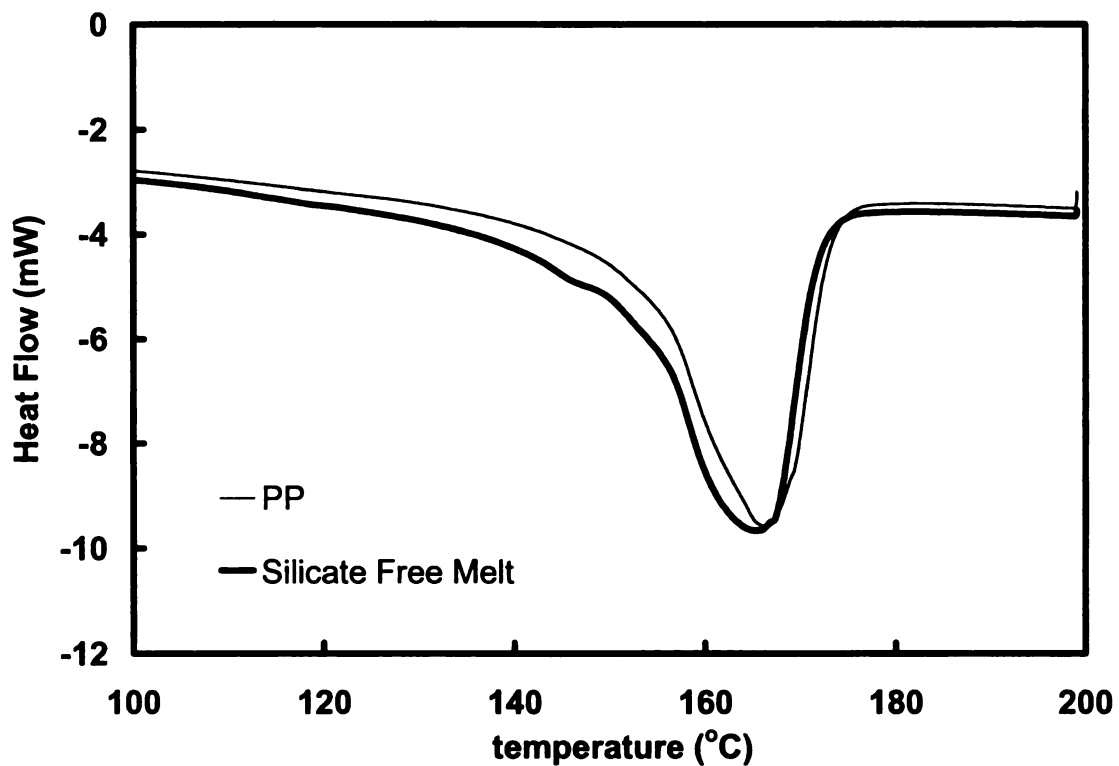


Figure 2.1. Representative DSC scans for melting transitions for polypropylene and corresponding silicate free melts: (—) Homopolymer PP, (—) Silicate free melt

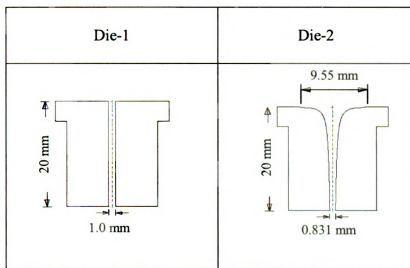
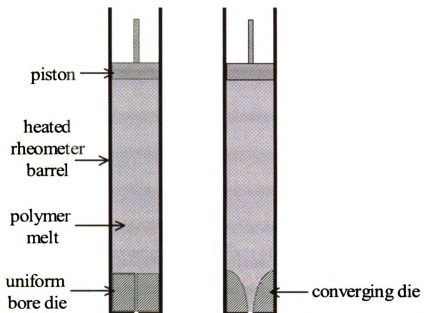


Figure 2.2. Capillary Rheometer Setup for Extrusion Studies with Die Profiles

THE USE OF SILANE COUPLING IN MELT MIXED POLYPROPYLENE CLAY NANOCOMPOSITES

CHAPTER 3

3.1 INTRODUCTION

3.1.1 *Objective*

In this chapter, we have investigated the effects of additional coupling at the clay edges on the clay exfoliation levels for melt mixed polypropylene nanocomposites and the associated improvements in flow and mechanical properties. Melt processing of nanocomposites requires effective stress transmission between the matrix and the layered silicates particularly while the layers are still stacked to facilitate layer sliding and result in high exfoliation levels. Montmorillonite pretreated with a C18-surfactant was treated additionally with a carefully chosen silane coupling agent and X-ray diffraction was used to confirm if the silane was located predominantly at the clay edges. A different commercially available siliated clay I.31PS was also used for nanocomposite preparation. 5 wt% of each clay was compounded with 10 wt% maleated polypropylene PP-g-MA (acid number =23 and $M_w=22000$) and 85 wt% of 2 grades of polypropylene (MFR= 4 and 11). The resulting nanocomposites were analyzed with X-ray diffraction, transmission electron microscopy (TEM), and melt rheology. The nanolayer stability to additional processing was also studied by monitoring the morphology of nanocomposite extrudates through different flow geometries and at different strain rates. The questions addressed in the present work are as follows.

- Does the incorporation of carefully chosen silane coupling agent enhance the interactions between the bulk polypropylene and the clay and thereby improve the delamination of the clay?
- How are the rheological response and the mechanical performance of the polymer/clay hybrids affected by different silane treatments on the clay?
- After effective dispersion of clay has been obtained initially, what is the morphological change when using clays with and without silane treatment on extrusion through straight and converging dies?

3.1.2 Background

The potential for significant improvements in mechanical[7, 12, 53, 73, 105-107], flame retardancy[16, 17, 83] and gas barrier properties[15] with small loadings (as low as 3 wt%) of layered silicates in various polymer matrices has stimulated the growth of polymer nanocomposites[6, 13, 81, 82] and has attracted both industrial and academic interest. However attempts to exfoliate the clay in non-polar systems like polypropylene have met with limited success. Absence of enough interfacial contacts between the nanoclay and non-polar polymers like polypropylene impairs the efficiency of stress transfer from the continuous polymer matrix and results in incomplete clay exfoliation. This efficiency is critical for the exfoliation process, since the clay platelets separate only when the attractive Van-der-Waals force between them is exceeded by the transmitted stress during melt blending[108]. More favorable interactions of the polymer/clay as compared to the surfactant/clay result in a favorable enthalpy of mixing[25, 26], and leads to better clay exfoliation.

Frequently with polypropylene nanocomposites, functionalized polyolefin oligomers (compatibilizers) are used[9, 10, 54-57, 63, 64], where the polar functionality (usually maleic anhydride) wets the clay surface and the oligomers are soluble in the bulk matrix. A high level of grafting (more than 5 wt% MA), which although desirable for favorable interaction with the clay surface causes PP chain scission[62] and is a primary limitation of using maleated PP as a polymeric compatibilizer.

Another way to increase the interactions between polymer and the filler is to have favorable interactions of the bulk polymer with the hydroxylated edges of the silicate

layer[72] by using silane coupling agents. The efficiency of the multifunctional silane-coupling agents is based on their bridging ability: the hydrolyzable moiety of the silane reacts with the hydroxyls present on the clay edges and the organo-functional group of the silane interacts with the bulk polymer. The latter interaction can be in the form of covalent bonding or the formation of interpenetrating networks (IPN's)[109] for non-reactive systems like polypropylene. Figure 3.1 shows a schematic of the various interaction sites with clay nanolayers. The maleic anhydride moiety in the PP-g-MA has favorable interactions with the clay faces. Even though the edge area is much smaller as compared to the nanolayer face area for a single clay platelet, the un-separated clay stacks should provide enough functionalization sites, which can be coupled to the bulk polypropylene. As is shown in the present work, use of carefully chosen silane coupling agents to functionalize the hydroxylated clay edges improve its interactions with the bulk polypropylene, and translates into enhanced clay delamination and improved nanocomposite mechanical performance.

Previous studies[73] have used silane-modified clays, which have resulted in nanocomposites with improved mechanical properties. However with the layered morphology of clays, some silanes can actually move into the interlayer galleries. Fluoro-alkyl silanes were used by Manias and coworkers[18], which led to silane intercalation in the clay galleries and increased the basal spacing from 1.98 to 2.4 nm. Other silanes have been shown to react with the edges mainly[74-77], which is evident by similar interlayer spacing before and after silane treatment. Song and Sandi[74] have investigated the surface properties of smectite clays modified with two different long chain organo-silanes and found a reduction in the surface area for the modified clays owing to the formation of

a hydrophobic coating as a result of the condensation reaction between the silane and the hydroxylated clay edges. Morris and coworkers[110] indicate that for layered clays, interlayer hydroxyls are normally inaccessible to silane coupling agents and found reactions between the clay edge hydroxyls and trimethylsilyl chloride for their system using Al-NMR. One of the objectives of this work was to investigate the effectiveness of silanes, which functionalize the clay edge hydroxyls in enhancing exfoliation levels of clay in polypropylene nanocomposites.

The study of nanolayer morphological changes to additional melt processing was the other objective of this research. Additional melt processing steps affect the nanolayer morphology as illustrated by the work of Reichert et al.[84] and Manias et al.[18]. Reichert et al.[84] conducted annealing studies of injection molded polypropylene nanocomposites and observed a coarsening of the nanolayers after annealing. The capacity of the nanocomposites to withstand additional processing effects is a measure of the improved coupling between the clay and the bulk polymer. Similar studies were conducted by Manias et al.[18] for two polypropylene nanocomposite systems with the same organoclay for each case but with two different matrices: neat PP alone for one case and PP-g-MA alone for the second. The structure before and after annealing was studied by X-ray diffraction and it was observed that the composite with the neat PP matrix turned from an exfoliated structure to strongly intercalated after annealing cycle of 15 min. The other structure with PP-g-MA as matrix was stable over a period of 30 min indicating better coupling for this case. Wang and co-workers[111] investigated the role of shear stress on dispersion of PP/clay nanocomposites by using dynamic packing

injection molding (DPIM) and concluded that the clay assumes an intercalated and oriented morphology in the skin region, whereas it is largely exfoliated in the core region.

In this work, we have investigated the effects of additional coupling using silane coupling agents on clay exfoliation levels for melt mixed polypropylene nanocomposites and the associated improvements in flow and mechanical properties. The nanolayer stability to additional processing was also studied by monitoring the morphology of nanocomposite extrudates through different flow geometries and at different strain rates.

3.2. EXPERIMENTAL DETAILS

3.2.1 *Materials*

The polypropylenes utilized in this research were Basell Profax 6323 with a molecular weight (M_w) of 248,000 and melt flow index (MFI) of 12g/10min and Profax 6523 with a molecular weight (M_w) of 390,000 and MFI of 4g/10min (molecular weight information provided by Basell). The maleated polypropylene AC950 (acid number =23 and M_w =22000) from Honeywell was used as a compatibilizer. The chosen compatibilizer with a total maleic anhydride content of 4wt% has 2.6 wt% bound maleic anhydride and has been established as an effective candidate for exfoliation of clay in polypropylene[112].

The basic organoclay used here was Nanocor I.30P, modified by the exchange of 95-98% of the sodium cations in the clay gallery with octadecyl-ammonium ions. The specific gravity of the clay was 1.9 and a gallery spacing of 2.3 nm. The silane employed for modifying I.30P was phenyltrimethoxy silane (trade name Z-6124) from Dow

Corning. The choice of the silane-coupling agent was based on a solubility parameter match between the polymer and the organo-functional silane group (typical silane structure is $(RO)_n\text{-Si-Y}$, where RO is a hydrolyzable group, such as methoxy or ethoxy and Y is an organo-functional group, such as amino, phenyl or isobutyl). This should result in the lowest system free energy, which directly correlates with the experimentally observed interfacial adhesion as observed by Miller and coworkers[78-80]. The solubility parameter (δ) was calculated using equation (3.1) by using the group molar attraction constants (G) for each group as discussed by Sperling[113].

$$\delta = \frac{\rho \sum G}{M} \quad (3.1)$$

Here “ ρ ” is the density and “M” is the molecular weight (for the polymer, M is the monomer molecular weight). The δ values calculated for the polypropylene was 8.0 $(\text{cal}/\text{cm}^3)^{1/2}$ and 8.3 $(\text{cal}/\text{cm}^3)^{1/2}$ for the phenyl group in the chosen silane for this work, which indicates that clay functionalized with the phenyltrimethoxy silane should have favorable interactions with the bulk polypropylene. A different commercially available silated clay I.31PS was received from Nanocor and compared with the I.30P clay as well as with the I.30P silated in this work.

3.2.2 Procedures

3.2.2.1 SILATION

For doing the silane treatment on the organoclay I.30P, 20 grams of the organoclay was stirred in a 2wt% silane solution in methanol for 2 minutes. The solution was allowed to stand for 10 minutes and then decanted. The particles were kept under

ambient conditions for 24 hrs to cure the silane layer. A series of three wash cycles with methanol were done to remove any un-reacted silane. The resulting clay cake was dried in vacuum for a period of twelve hours at 100°C. The dried clay clumps were lightly ground and the resulting clay (referred to as I.30PSiPh in the subsequent discussion) was used for melt blending with the polypropylene and the compatibilizer.

3.2.2.2 *MELT PROCESSING*

The bulk PP, PP-g-MA and clays were initially bag mixed for two minutes to insure a homogeneous mixture and the mix was then fed to a lab scale Banbury Mixer, where it was compounded at 180°C at 150 rpm for 10 min. The melt mixing was carried out under a nitrogen blanket to ensure minimum polymer degradation. The “clump” of material was removed from the mixer and pelletized in a mini-granulator. The composite formulations are laid out in Table 3.1. A fixed loading of 5wt% clay and 10wt% compatibilizer was used for this study. The pellets from the granulator were melted in a DSM 15 cm³ Micro-Extruder at 5 rpm with a minimum input of additional shear and then injection molded at 100 psi in a DSM Injection Molding Machine to make tensile coupons for mechanical testing.

The pellets were compression-molded at 200°C in a Wabash Compression molder. The materials were loaded on the hot plates and kept at 5 minutes for homogenous melting. This was followed by a 2 tons pressure cycle for 5 minutes and an additional 10 tons cycle for 5 min. Circular disks of 50 mm diameter and 1.0-1.2 mm in thickness were made and were used for X-ray diffraction, transmission electron microscopy and rheological characterization.

3.2.2.3 EXTRUSION

The stability of the nanocomposite morphology to further melt processing was determined by extruding the granulated pellets at two different strain rates through a uniform bore die and then through a converging die which provided a logarithmic tensile strain or Hencky strain of 4.9 at the center line. The specifications of the two dies and the extrusion parameters have been shown in Table 3.2. The converging die offers a fixed Hencky strain (ϵ_h) of 4.9 and the die profile is designed to provide a uniform extensional strain rate ($\dot{\epsilon}$) for a given piston velocity (V_p).

$$\dot{\epsilon} = \frac{V_p}{L} \exp \epsilon_h \quad (3.2)$$

Here L is the die length. The two composites PP2-I.30P and PP2-I.30PSiPh are used for the extrusion studies to contrast the effects of silane functionalization of the clay on the morphological stability.

The dies were mounted in a Dynisco LCR6000 Capillary rheometer and extrusion was carried out at 200°C. The extrusion procedure involves the following sequence of steps: (1) the capillary barrel of the rheometer was heated to the test temperature (200°C) and then the die was attached to it; (2) 6 g of nanocomposite pellets were loaded into the capillary barrel in 2+2+2 gm increments, after adding each 2 gm batch, the sample was allowed to melt for 2 minutes to ensure homogenous melting, (6) the test is programmed in and run from the instrument software window. Two different rates of extrusion were used with Die 1- 195 sec⁻¹ (piston rate of 16 mm/min) and 3650 sec⁻¹ (piston rate of 300 mm/min) in order to contrast the effects of low and high strain rates. In order to draw the

distinctions between the morphology in straight and converging flows, a similar piston ram rate was used for the converging die (Die 2), after adjusting it for the difference in the exit diameters of the two dies. The equivalent ram speed turns out to be about 9.2 mm/min, which translates to an extensional rate of 1 sec^{-1} . The detailed experimental setup and the extrusion layout for the various experiments have been discussed in Chapter 2 (section 2.5).

3.2.3 *Structural Characterization*

All nanocomposites were analyzed for morphology using TEM and XRD. The characterization of the structure by XRD is performed on the compression-molded disks with a Rigaku Rotaflex Ru-200BH X-ray diffractometer, which is equipped with a Ni-filtered Cu K α radiation source and operated at 45 kV and 100 mA. The sample is scanned over a 2θ range of 0.5° to 10° at a rate of $0.5^\circ/\text{min}$ and measurements are recorded at equal increments of 0.01° .

The TEM used in this study is a JEOL 100 CX with a 120 KeV electron accelerator. Ninety nanometer thin sections are prepared from the compression molded disk. The sections are cryomicrotomed at a temperature of -125°C in order to create the required rigidity to produce the uniform thin sections required to obtain clear reproducible images. Several of these micrographs were analyzed using image analysis software (Sigma Scan Pro 5.0, SPSS Inc.) to get a length distribution for the clay platelets. Particles were catalogued in several images for each composite so that a total of close to 100 single particles were analyzed for each composite. For imaging the nanocomposite extrudates, thin sections were prepared carefully from the core of the

extruded strand in order to get a better idea of a representative nanolayer microstructure. The FTIR spectra for the clay samples were obtained using compressed KBr pellets.

3.2.4 *Rheological and Mechanical Characterizations*

The oscillatory shear measurements were performed in a parallel plate fixture (50mm diameter plates) with a Rheometrics RMS 800 at 180°C and subjected to oscillatory shear over a frequency range of 0.05-100 rad/s and a strain amplitude of 2%, which was confirmed to be within the linear viscoelastic regime by performing a strain sweep. The data are recorded only when the torque amplitude is above the recommended threshold of 2 g-cm.

The tensile modulus was obtained at testing speeds of 0.7 in/min using a United Universal Testing Machine. At least 3 samples were tested for each measurement, and a 5% error was associated with the obtained values. For improvements in mechanical performance, the composites PP1-I.30P, PP1-I.30PSiPh and PP1-I.31PS were used, whereas the composites PP2-I.30P and PP2-I.30PSiPh were used for the extrusion study.

3.3. RESULTS AND DISCUSSION

3.3.1 *Silation and Clay structure*

Figure 3.2 shows the XRD patterns for the organoclay I.30P, I.31PS and the I.30PSiPh. The I.30PSiPh clay treated with the phenyl trimethoxy silane has similar basal spacing of 2.2 nm as compared to the unsilated organoclay (I.30P), indicating that the silane has functionalized the edge hydroxyls and doesn't intercalate the clay galleries. Song and Sandi[74] also obtained unchanged basal spacing after the treatment of the clay

with a different long alkyl trimethoxy silane. Additionally, they used the Near Edge X-Ray Absorption Fine Structure Spectroscopy to confirm that the silane has reacted with the clay edge hydroxyls.

For comparing the two clays in this study for basal spacing, the organoclay I.30P was heated under vacuum for 12 hrs at 100°C. The basal spacing was found to reduce from 2.3 nm to 2.2 nm for the I.30P after the heating cycle for 12 hours. The loss of interlayer water could have resulted in this decrease in basal spacing. A similar loss of 0.1 nm in the basal spacing was observed, when the I.30P was dried for 12 hrs under vacuum at 130°C. The other clay used in this work: I.31PS clay has a basal spacing of 2.7nm, thereby indicating that the silane treatment for this clay intercalates the clay galleries owing to an increase in the spacing. A comparison of the IR spectra shown in Figure 3.3 between the I.30P and I.30PSiPh shows the characteristic phenyl ring deformation modes in the range 560-420 cm^{-1} for the I.30PSiPh, indicating that the phenyl grafting has been successfully performed on the hydroxylated edges of the organoclay I.30P.

3.3.2 *Morphology of Nanocomposites*

3.3.2.1 *COMPRESSION MOLDED SPECIMENS*

Figure 3.4 shows the XRD patterns for the five composites. Lack of distinct features in the XRD curve implies the existence of random-well dispersed clay platelets. The presence of distinct peaks indicates the presence of ordered clay stacks and the corresponding 2θ values allows us to calculate the spacing of the stacked platelets. The X-ray diffraction pattern for the composite PP1-I.31PS shows an intercalation peak at

$2\theta=2.3^\circ$, which translates to an intercalated composite with 3.8 nm as the basal spacing, an increase of 1.1 nm over the base clay I.31PS (XRD spacing calculated from Figure 3.2) used for this composite. An intercalated morphology with the I.31PS have been also observed by Ellis and D'Angelo[105], who melt blended the polypropylene nanocomposites with the help of a masterbatch concentrate termed C.31PS that contained 50-60 wt% of the I.31PS along with the polymer and compatibilizer. The XRD pattern for the composite PP1-I.30P lacks distinct intercalation peaks and displays a “shoulder”, whose length indicates the population of intercalated as opposed to exfoliated species. The composites PP1-I.30PSiPh, PP2-I.30P and PP2-I.30PSiPh are the most featureless curves implying that the nanolayers have undergone the largest extent of separation in these composites.

Careful distinctions in morphology of the polypropylene clay hybrids can be made by analysis of the transmission electron micrographs (TEM's). The micrographs were obtained for the composites, which appear from the XRD results to be significantly exfoliated: PP1-I.30P, PP1-I.30PSiPh, PP2-I.30P and PP2-I.30PSiPh (Figure 3.5). The micrograph for the composite PP1-I.30PSiPh in Figure 3.5(B) has the most distinct and random particle structures as compared to all the other composites. A good amount of single platelet structures can be clearly seen in all the micrographs, implying a high level of clay exfoliation. Clay platelets sliding out of a stack when subjected to shear are seen in all micrographs analogous to the formation termed “skewed stack” by Fornes et al.[52] in their work with nylon-6-layered silicate nanocomposites.

Three different types of particle structures on several such images of these four composites were identified and are shown in Figure 3.6. A structure where no gaps can

be detected and that is at least half a particle length away from neighboring particles is termed a single particle. A stack refers to a structure containing particles arranged with significant face-to-face overlap and several discernible gaps ranging from 3 to 20 nm. The remaining structures can be categorized as agglomerates. A quantitative comparison of the degree of exfoliation in these composites can be obtained from an analysis of the length distribution of such particles. The results of this analysis are shown in Figure 3.7. The composite PP1-I.30P has a bi-modal distribution of single clay platelets with almost equal contributions from two most probable lengths of 125 nm and 210 nm. Although the composite PP1-I.30PSiPh has a most probable length around 180 nm, it also has a significant proportion of clay platelets with lengths >200 nm. Similar results were obtained for the composites PP2-I.30P and PP2-I.30PSiPh, with the latter having slightly greater platelet lengths. This clearly identifies that the composites prepared with the phenyltrimethoxy silane treated clay had improved levels of exfoliation as compared to the composites with the organoclay. Also the exfoliation levels of the clay with the lower molecular weight polypropylene PP6323 are slightly better than the composites with the higher molecular weight PP6523 as the matrix.

3.3.2.2 *EXTRUDED SPECIMENS*

Shear Flow

Representative micrographs for the nanocomposite extrudates through shear flow in a uniform bore die (Die 1) are shown in Figure 3.8 (A, B, C, D). The micrographs 3.8(A) and 3.8(C) correspond to the composite PP2-I.30P extruded at rates of 195 sec^{-1}

and 3650 sec^{-1} respectively, whereas 3.8(B) and 3.8(D) correspond to the composite PP2-I.30PSiPh extrudates at analogous rates.

A comparison of the as-mixed organoclay composite PP2-I.30P (earlier shown in Figure 3.5(C)) with 3.8(A,C) indicates that the additional extrusion step results in occurrence of stacking at both extrusion rates. The lower extrusion rate of 195 sec^{-1} leads to a large concentration of clay stacks [Figure 3.8(A)] as compared to the higher extrusion rate of 3650 sec^{-1} (Figure 3.8(C)). This could be attributed to the greater residence time ($\sim 0.82 \text{ sec}$) for the lower extrusion rate as compared to 0.04 sec for the higher rate. The extrudates for the composite PP2-I.30PSiPh with the edge siliated clay also indicate restacking after extrusion, especially at the lower extrusion rate of 195 sec^{-1} , as compared to the as-mixed composite (Figure 3.5(D)). Visual inspection of the micrographs indicate lower restacking at similar extrusion rates for the composite PP2-I.30PSiPh as compared to the extrudates corresponding to the composite PP2-I.30P. The composite extrudate for PP2-I.30PSiPh at 3650 sec^{-1} (Figure 3.8(D)) also indicates a large number of single platelet structures. Wang and co-workers[111] have indicated the positive influence of shear on the levels of clay exfoliation in the core region of injection molded nanocomposite specimens.

An analysis of the area fractions for the three structures: single platelets, stacks and aggregates shows that the aggregate structures present in the as-mixed composites from the Banbury mixer are broken into ordered stacks and single platelets after extrusion (Table 3.3). This is indicated by a decrease in the area fraction for the aggregate structures for both composites after extrusion. The tendency to re-stack upon extrusion is observed for both composites at both rates as evident by an increase in the area fraction,

however the area fractions of the stacks are much higher for the composite PP2-I.30P as compared to PP2-I.30PSiPh for both extrusion rates. This could be attributed to better interfacial coupling for the latter case with the edge silated clay, which results in additional stability to the clay morphology and limits the restacking levels.

Extensional Flow

In addition to flow through straight channels, extensional flows are also encountered in various processing techniques like injection molding and blown film extrusion. To examine the effects of extensional flows on clay nano-structure, the composites PP2-I.30P and PP2-I.30PSiPh were extruded through a semi-hyperboloidal profile die: Die 2 (specifications laid down in Table 3.2). The representative micrographs from the core region are shown in Figures 3.9(A) and 3.9(B). Figure 3.9(A) for the composite PP2-I.30P shows a high percentage of clay stacks in addition to the single platelets; on the contrary the morphology is largely preserved for the extrudate PP2-I.30PSiPh, which shows a high concentration of mostly single clay platelets in figure 3.9(B).

3.3.3 Oscillatory Shear Rheology

The dynamic viscosities for the composites based on the PP6323 as well as the corresponding polypropylene-compatibilizer matrix are shown in Figure 3.10. The composite PP1-I.30PSiPh has higher dynamic viscosity over the entire G^* range, with all the composites showing an abrupt increase in viscosity with decreasing stresses, thereby indicating the presence of a yield stress for these systems. Xu and coworkers[114] have analyzed the melt state viscoelastic properties of an exfoliated in-situ polymerized and

intercalated solution blended PS/organoclay composite. For intercalated composites, they obtained a limiting value for the complex viscosity up to 3wt% clay loading; a divergence in the complex viscosity was observed for higher loadings of 6.7 and 9wt%, consistent with the presence of a yield stress. For exfoliated composites, the yield stress was observed for loadings of 3.5 wt% and 3.9 wt%.

The dynamic viscosity curves are more conveniently related to the mean aspect ratio and therefore to the degree of exfoliation[61] because the intrinsic viscosity increases with the average aspect ratio of the particles as has been established for dilute suspensions[115] as well as for filled polymer melts[116]. The dynamic viscosity curves for the composites PP2-I.30P, PP2-I.30PSiPh and the corresponding silicate free melt are shown in Figure 3.11. The viscosity values are slightly higher for the composite PP2-I.30PSiPh as compared to the composite PP2-I.30P over the entire G^* range, indicative of better exfoliation.

The dynamic storage modulus (G') plotted in Figure 3.12 shows a plateau at low frequencies, which is consistent with the presence of a yield stress. Matsumoto and coworkers[117] observed a second plateau at low frequencies for high loadings of 10-30 wt% of spherical particles (styrene-divinylbenzene copolymers in polystyrene) in diethylphthalate (DEP), which indicated a yield stress. Aubry and coworkers[102] have worked with 0.5-10 wt% organoclay loadings with polyamide-12 as the bulk matrix. A second plateau was observed at lower frequencies for clay volume fractions higher than 1.5%. A percolated network structure for the anisotropic clay platelets at low frequencies results in this solid like behavior at larger time scales. A modified Carreau-Yasuda model has been fitted to the complex viscosity curves of PP nanocomposites in a recent study by

Lertwilmolnun and Vergnes[118] and it was found that the estimated yield stress value was around 800 Pa for a nanocomposite system prepared with 5-wt % of organoclay and a PP-g-MA containing 1 wt % maleic anhydride.

The plots of phase angle (δ) versus complex modulus (G^*) are shown in Figure 3.13 for the nanocomposite formulations, which indicate that the lowest phase angle is obtained for the composite PP1-I.30PSiPh. This plot was first used by Van Gorp and Palmén[119] to provide additional verification of the time temperature superposition. Trinkle and coworkers[120] have used it to elucidate the effects of molecular weight and polydispersity for polystyrene, poly (methylmethacrylate) and metallocene polyolefins and indicate that the minima in the plot can be used to identify the rubbery plateau modulus. The same authors[121] also extended the plot utility to study the viscoelastic response of long chain branched polymers.

A secondary minima was also observed at lower values of G^* for some of the nanocomposite specimens. From the secondary minima in the van-Gorp-Palmén (vGP) plots, we can calculate the yield stress values for the nanocomposite formulations. This allows reliable estimation of the yield stress than is possible by reading the plateau value of the storage modulus curve in the low frequency regime. The composite PP1-I.30PSiPh is around 2500 Pa, which is more than double as compared to the composites PP1-I.30P (~950 Pa). This may be attributed to better coupling between the phenyltrimethoxy silane modified clay and the polymer matrix as well as to a high concentration of single platelets in the composite PP1-I.30PSiPh.

3.3.4 Mechanical Performance

The mechanical performance for the three composites has been discussed in Figure 3.14. The more exfoliated composite PP1-I.30PSiPh shows the maximum increase in tensile modulus (~ 37%), whereas the nanocomposite PP1-I.31PS with I.31PS having significant intercalated structures shows the least improvement in tensile modulus (~18%). Typically composites with largely exfoliated clay platelets have an improved mechanical performance as compared to an intercalated composite. Ton-that et al.[44] worked with a fixed loading (2 wt%) of two different clays: Cloisite 15A and Cloisite 30B and found a better mechanical performance for the predominantly exfoliated nanocomposites obtained with the Cloisite 15A. For composites with largely exfoliated clay platelets, the increases in tensile modulus of up to 40 % have been obtained with clay loadings of 5wt%[43, 73], whereas about 25% increase in tensile modulus has been observed for similar clay loadings with intercalated composites[105, 107]. Ellis and D'Angelo obtained intercalated structures with I.31 PS, an organoclay with additional silane treatment. They also prepared composites with the help of a masterbatch concentrate termed C.31 PS that contained 50 to 60wt % of the I.31 PS with the other two components. By both compounding methods, a 5wt% intercalated nanocomposite exhibited a 25% improvement in tensile modulus.

Enhanced mechanical performance further illustrates the effect of increased coupling obtained at the clay edges with the phenyltrimethoxy silane treatment. Although di-alkoxy and tri-alkoxy silanes have been established to be superior to mono-alkoxy silanes[122] in terms of adhesion improvements owing to extensive interphases, care should be taken that the chosen silane for clay modification shouldn't participate in any

reactions with the maleic anhydride moieties of the PP-g-MA, since this will rule out favorable interactions between PP-g-MA/clay as compared to the surfactant/clay: essential for clay exfoliation. In previous studies[73], the silane coupling agent amino-propyl-trimethoxy silane has been used for clay treatment. The amine group can chemically bond with the PP-g-MA as shown by Nygard et al.[123] and Bikiaris et al.[124]. The silane treatment with the phenyltrimethoxy silane in our case serves two important functions. It is mostly located at the clay edges and provides additional coupling between the clay and the bulk polypropylene during melt blending, which facilitates nanolayer sliding and results in high exfoliation levels. Additional proof of improved coupling is obtained with an improved mechanical and rheological performance for the composites reinforced with this clay, with the yield stress values almost double as compared to the organoclay composites. Secondly it also leads to morphological stabilization to additional processing and limits the clay re-stacking. This provides further evidence of better interfacial contacts between the clay and PP and can serve as a useful tool to render morphological stability to the clay nanolayers in additional melt processing steps.

3.4. CONCLUSIONS

This study reveals that carefully chosen silane-coupling agents can improve the interfacial interactions between the edges of the nanolayer stack and the bulk polymer. This facilitates sliding of individual nanolayers from the clay stack during melt blending. The organoclay with additional edge functionalization using phenyltrimethoxy silane was exfoliated to a greater extent than the base organoclay in a melt processed polypropylene nanocomposite system, as quantified by rheological findings and image analysis of

various transmission electron micrographs. The silane-coupling agent for this study was chosen based on a solubility parameter match between the bulk polymer and the non-hydrolyzable group of the silane. The edge siled clay led to better improvements in mechanical performance, which was attributed to better coupling between the silicate layers and the bulk PP. The van-Gurp-Palmen plots were used to identify the yield stress for the nanocomposites and the yield stress values were higher (almost double), when the edge siled clay was used for compounding. A high level of nanolayer re-stacking was observed in extrusion studies particularly at higher residence times in shear flows, and these levels were found to be less for the nanocomposites reinforced with the edge siled organoclay.

Table 3.1: Composition of various composite samples by weight %

Material Id	PP6323	PP6523	PP-g-MA	I.30P	I.30P-SiPh	I.31PS
PP1-I.30P	85	—	10	5	—	—
PP1-I.30PSiPh	85	—	10	—	5	—
PP1-I.31PS	85	—	10	—	—	5
PP2-I.30P	—	85	10	5	—	—
PP2-I.30PSiPh	—	85	10	—	5	—

Table 3.2: Uniform bore dies and profile dies used in extrusion studies

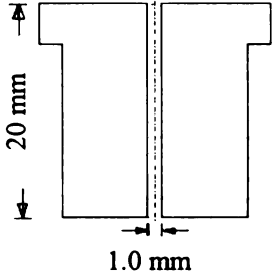
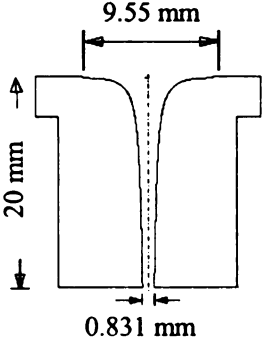
	Die-1	Die-2
	 <p>20 mm 1.0 mm</p>	 <p>9.55 mm 20 mm 0.831 mm</p>
Inlet radius (mm)	0.5	4.775
Outlet radius (mm)	0.5	0.4155
Length (mm)	20	20
Extrusion Temperature (°C)	200	200

Table 3.3: Distribution of particle structures for composites before and after extrusion through uniform bore die (Die-1) at different rates from TEM image analysis

Sample	Area Fraction		
	Single	Stacks	Aggregates
PP2-I.30P before extrusion	0.30	0.19	0.51
PP2-I.30P-195 sec ⁻¹	0.20	0.62	0.18
PP2-I.30P-3650 sec ⁻¹	0.45	0.47	0.08
PP2-I.30PSiPh before extrusion	0.37	0.20	0.43
PP2-I.30PSiPh-195 sec ⁻¹	0.44	0.49	0.07
PP2-I.30PSiPh-3650 sec ⁻¹	0.77	0.23	0.00

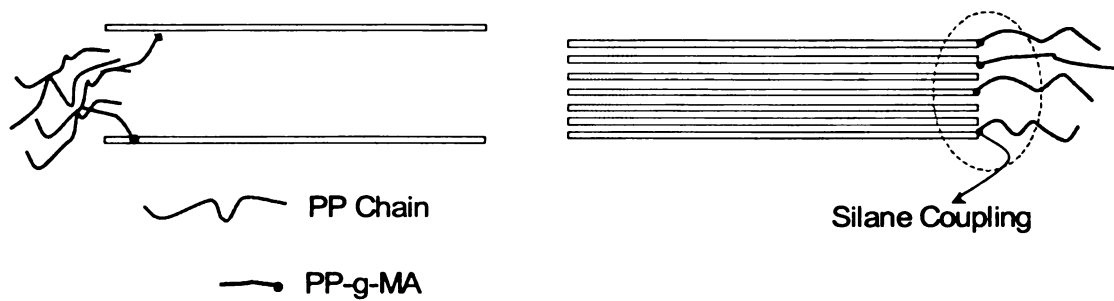


Figure 3.1. Coupling between the matrix and the nanolayer faces is achieved with PP-g-MA chains and coupling between the nanolayer edges and the matrix can be achieved with selected silanes

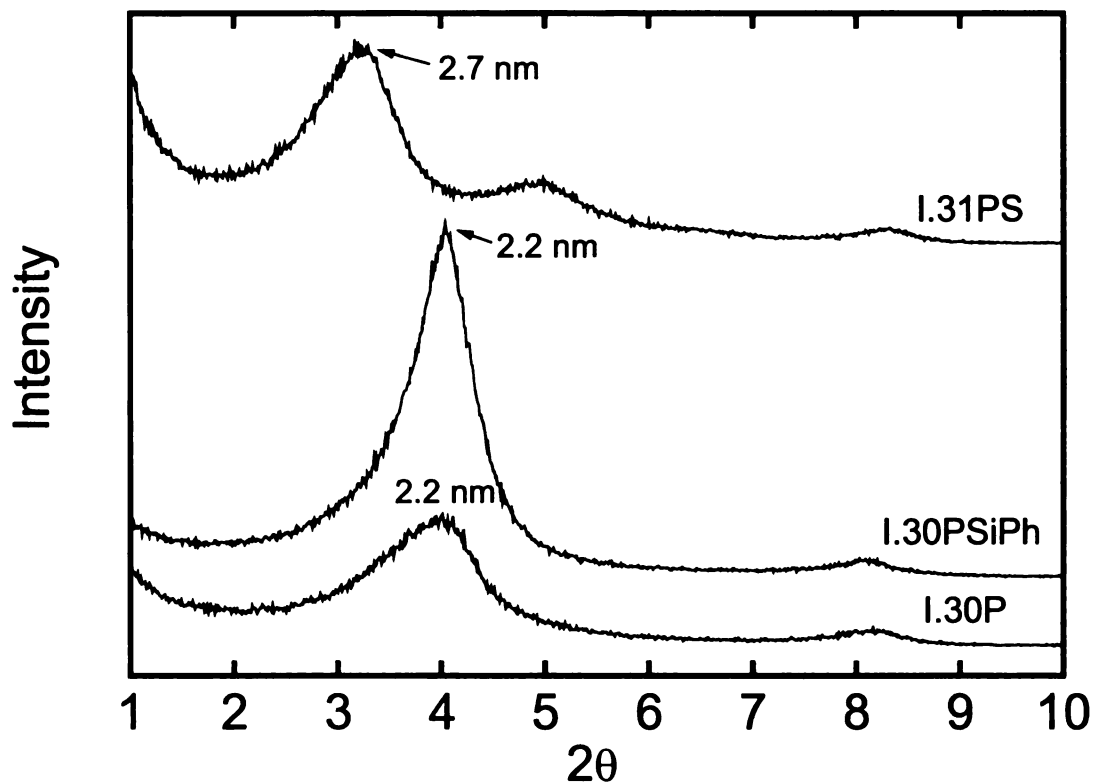


Figure 3.2. XRD patterns of organoclays with different silane treatment showing no change in d-spacing with phenyl trimethoxysilane (SiPh) but a noticeable increase in d-spacing with a different silane used in I.31PS. The organoclay I.30P was heated for 12 hours at 100°C to match the drying step in silation

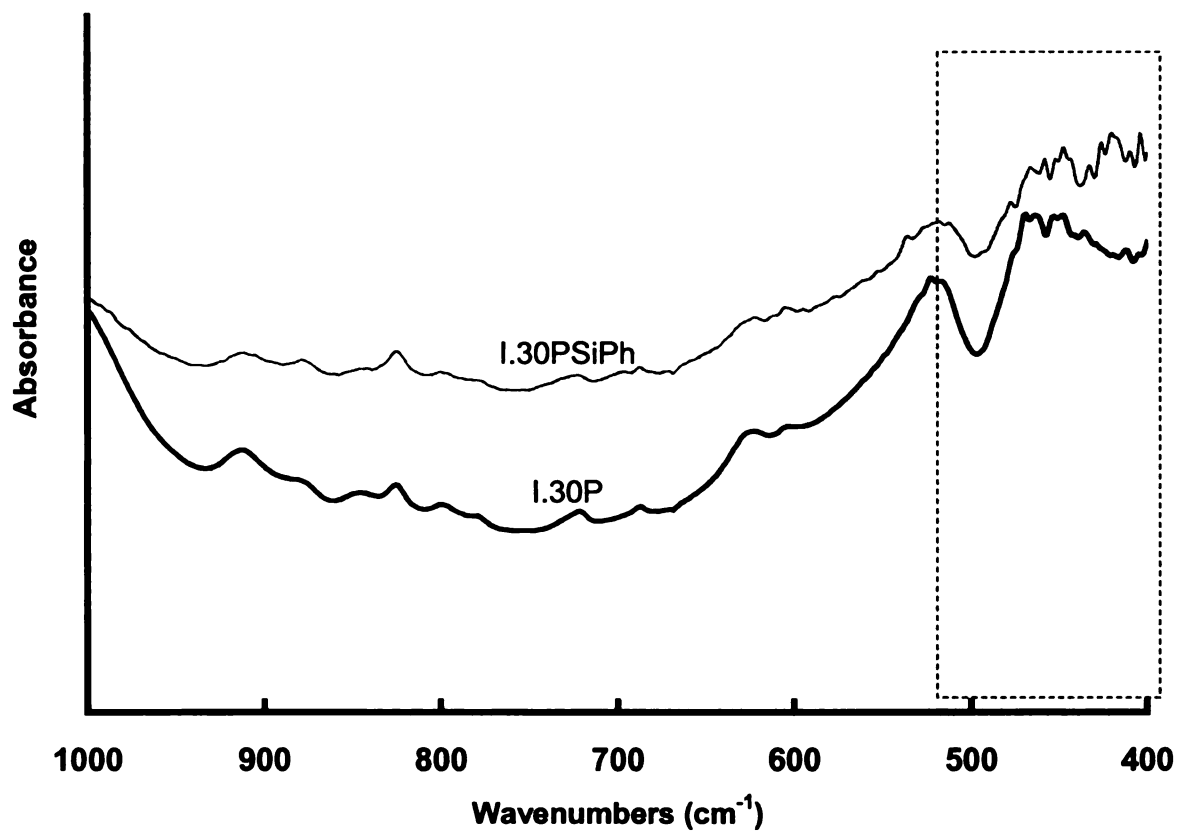


Figure 3.3. FTIR Spectra of I.30P and I.30PSiPh

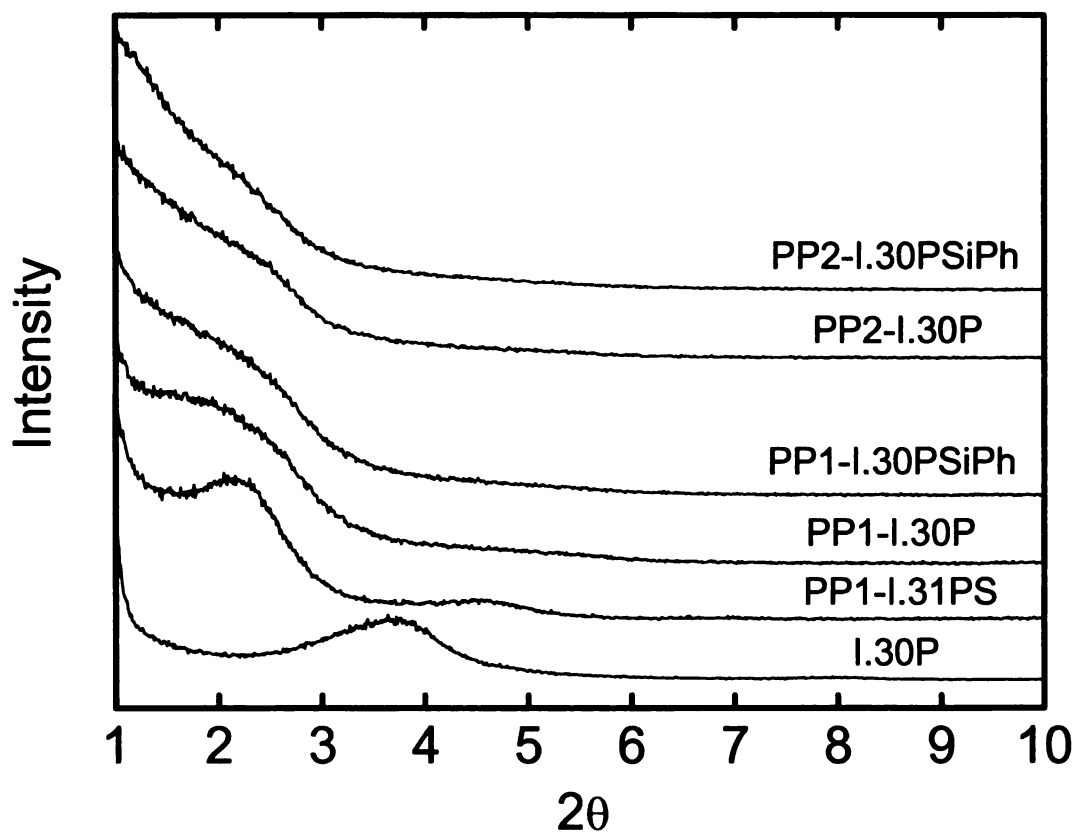


Figure 3.4. XRD patterns for polypropylene/clay nanocomposites with 5 wt% of different clays and 10 wt% of the same PP-g-MA (AC 950)

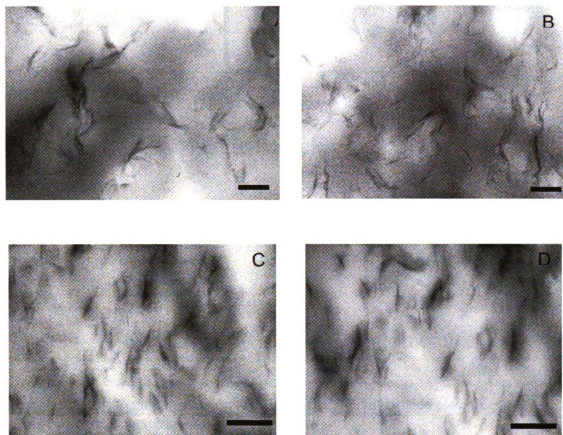
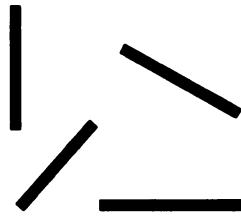


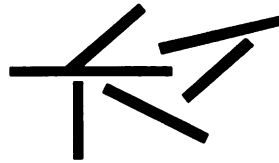
Figure 3.5. Transmission electron micrographs of the composites (a) PP1-I.30P, (b) PP1-I.30PSiPh, (c) PP2-I.30P, (d) PP2-I.30PSiPh (The scale bar in each picture is 200 nm)



Single Particles



Stacks



Agglomerates

Figure 3.6. Different particle structures identified in transmission electron micrographs

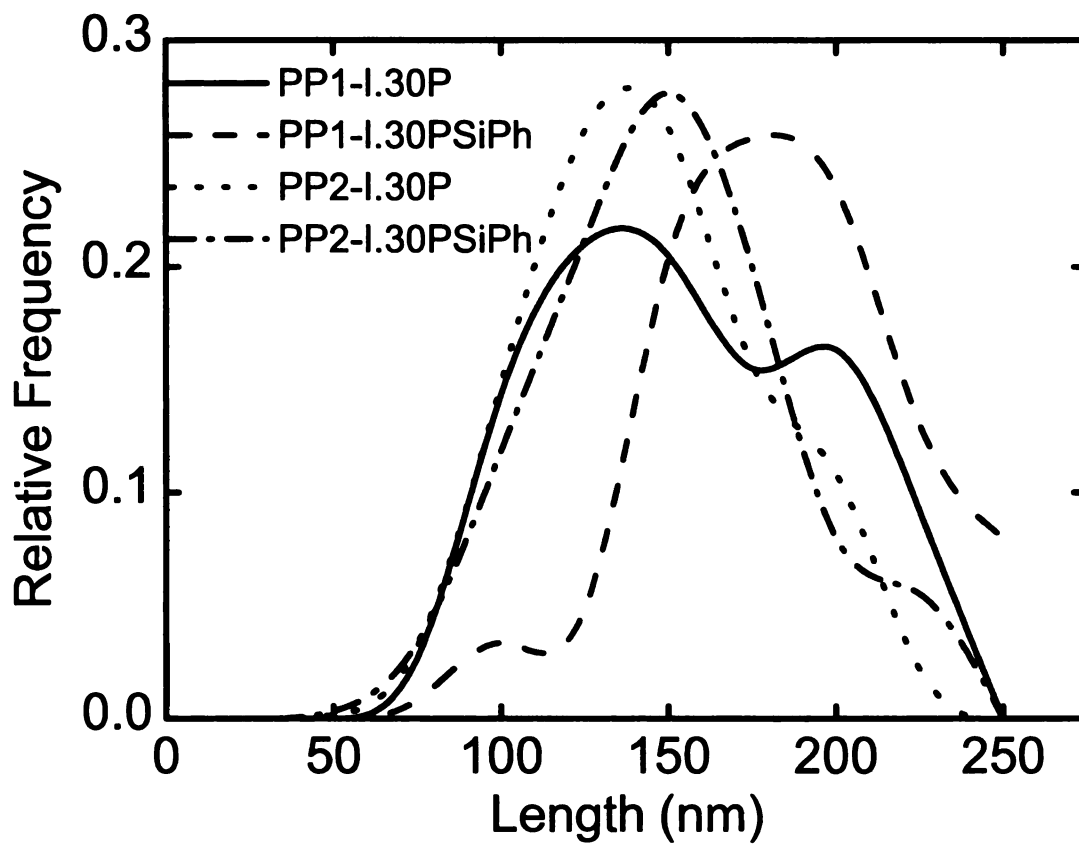


Figure 3.7. Length distributions of "single particles" in nanocomposites (—) PP1-I.30P, (---) PP1-I.30PSiPh, (.....) PP2-I.30P, (- · -) PP2-I.30PSiPh

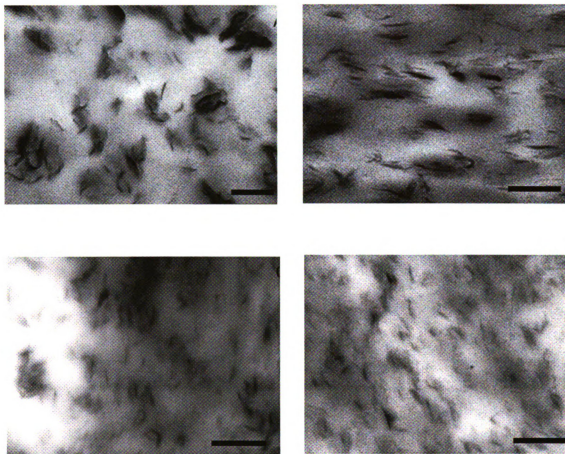


Figure 3.8. Transmission Electron Micrographs for the composite extrudates through Die-1 (a) PP2-I.30P-195 sec^{-1} , (b) PP2-I.30PSiPh-195 sec^{-1} , (c) PP2-I.30P-3650 sec^{-1} , (d) PP2-I.30PSiPh-3650 sec^{-1} . The scale bar in each picture is 500 nm

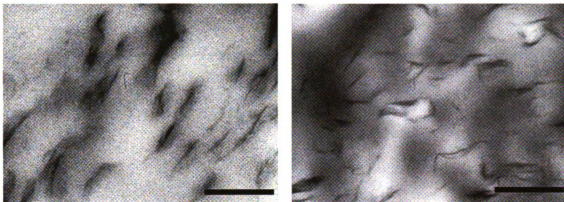


Figure 3.9. Transmission Electron Micrographs for the composite extrudates through Die-2 (a) PP2-I.30P-1 sec^{-1} , (b) PP2-I.30PSiPh-1 sec^{-1} . The scale bar in each picture is 500 nm

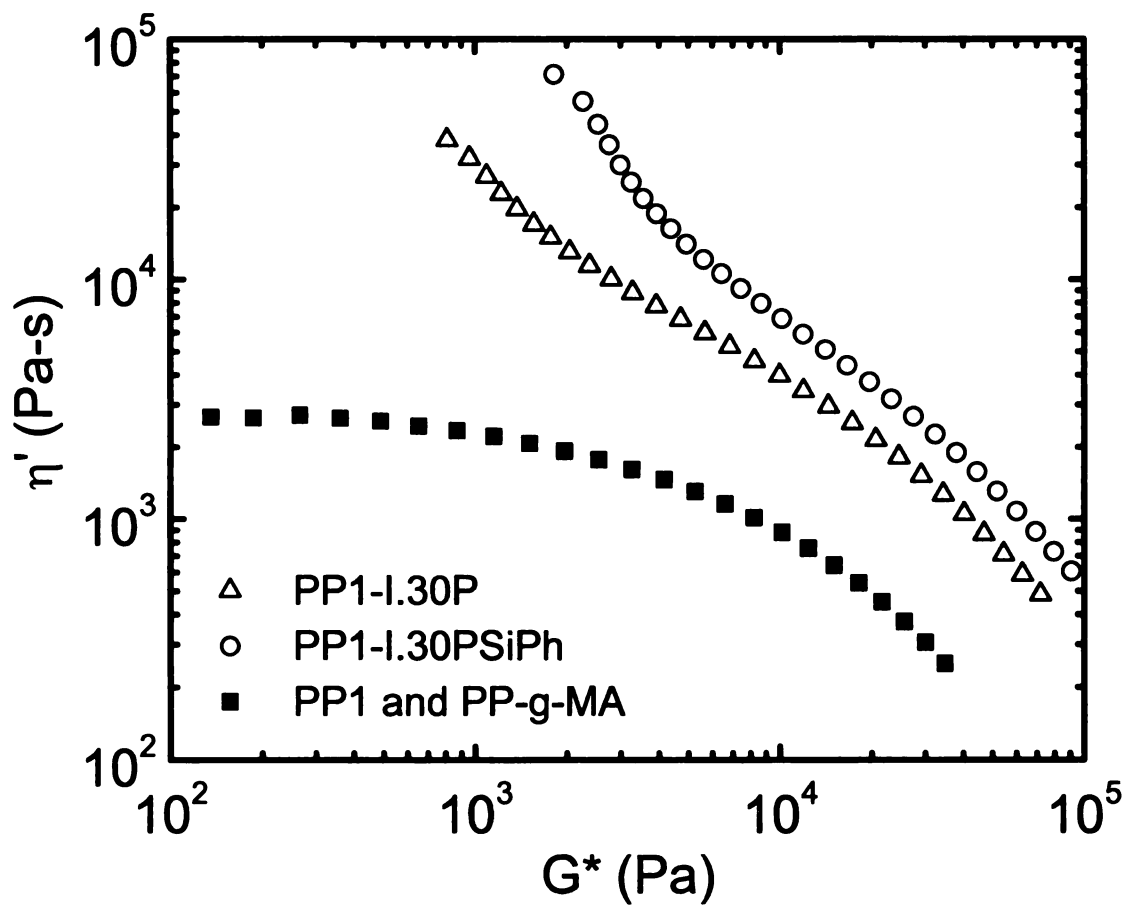


Figure 3.10. Dynamic viscosity curves for three composites and the corresponding silicate free melt of PP6323 and PP-g-MA: (Δ) PP1-I.30P, (\circ) PP1-I.30PSiPh, (\blacksquare) PP1 and PP-g-MA

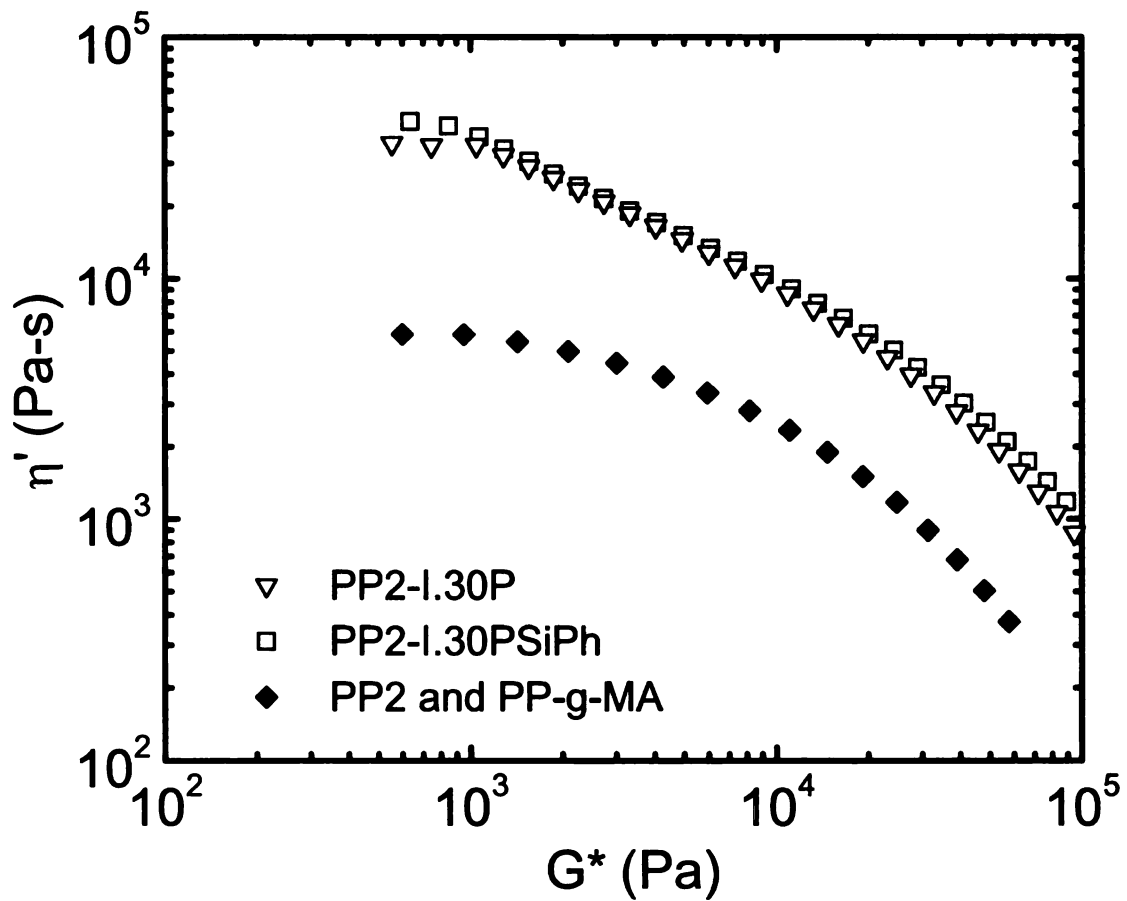


Figure 3.11. Dynamic viscosity curves for two composites and the corresponding silicate free melt of PP6523 and PP-g-MA at 180°C: (∇) PP2-I.30P, (\square) PP2-I.30PSiPh, (\blacklozenge) PP2 and PP-g-MA

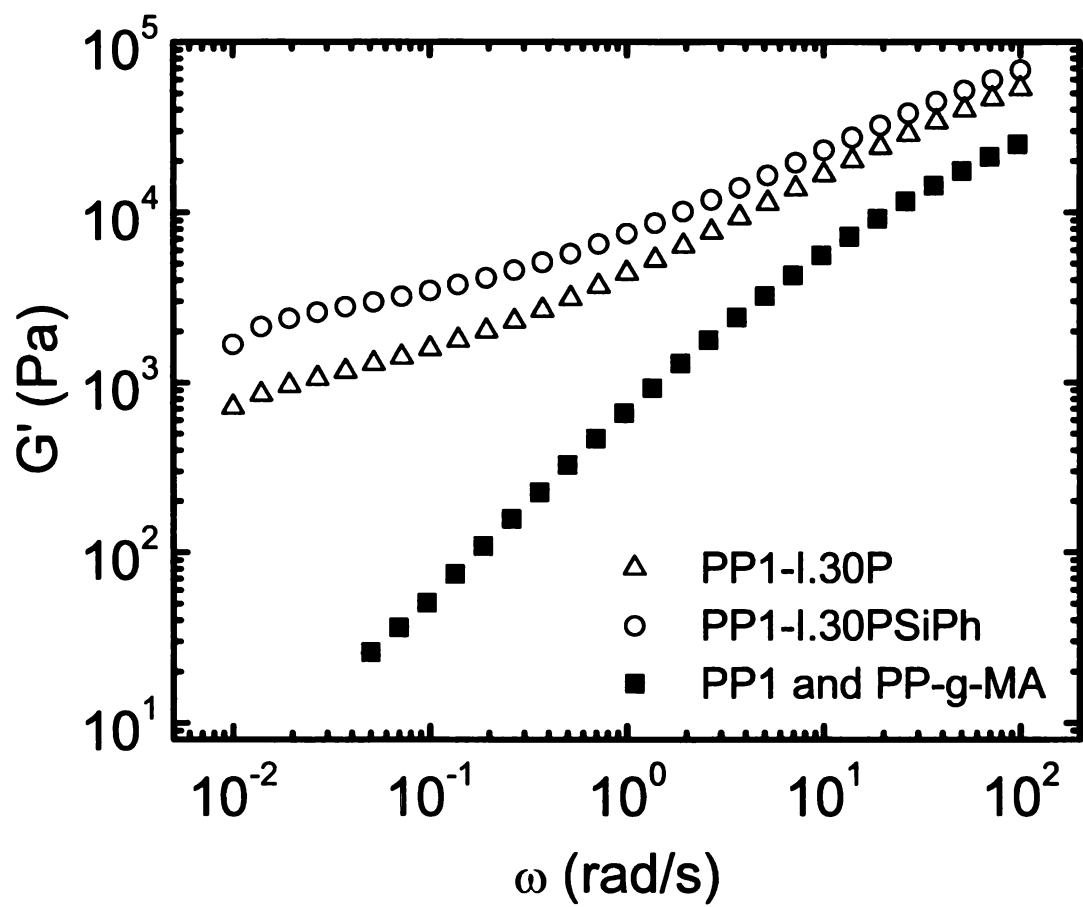


Figure 3.12. Storage Modulus (G') curves versus frequency (ω) for the composites with different clays at 180°C: (Δ) PP1-I.30P, (\circ) PP1-I.30PSiPh

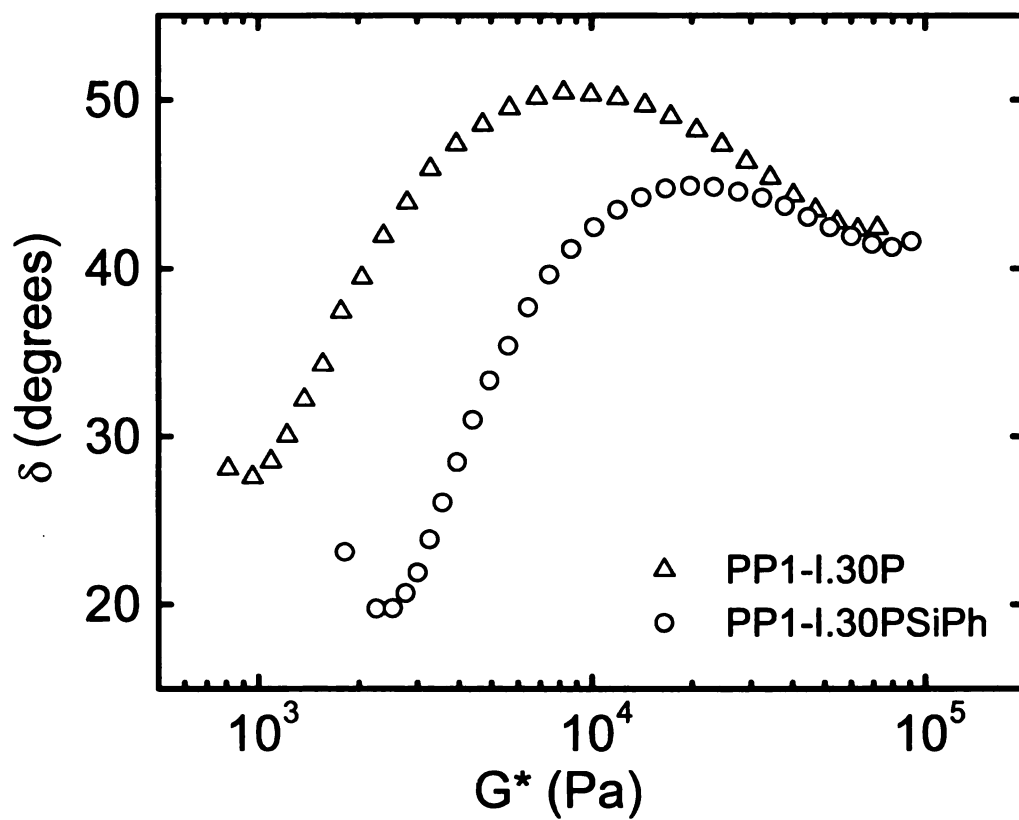


Figure 3.13. δ versus Complex Shear Modulus (G^*) for the composites with different clays at 180°C: (Δ) PP1-I.30P, (\circ) PP1-I.30PSiPh

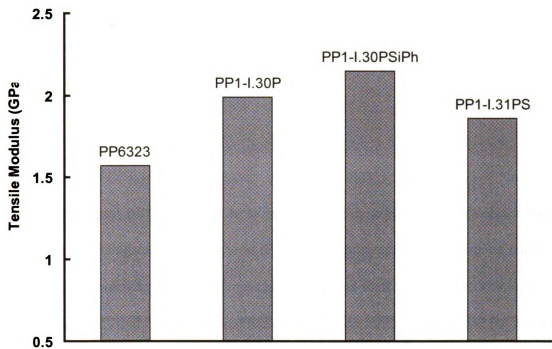


Figure 3.14. Tensile Moduli of PP6323 based nanocomposites with 5 wt% of different clays and 10 wt% of the same PP-g-MA (AC 950)

CHARACTERIZATION OF COMPATIBILIZER EFFECTIVENESS ON RHEOLOGY AND STRUCTURE

CHAPTER 4

4.1 INTRODUCTION

4.1.1 Objective

The object of this chapter is to investigate the importance of maleic anhydride distribution in maleated polypropylene (PP) compatibilizers for dispersion of nanolayers in PP melts. Selected grades of compatibilizers with a total maleic anhydride content of more than 1 wt% and different bound maleic anhydride contents were used for this study. 10 wt% of each of these compatibilizers were melt blended with 5 wt% nanoclay with the rest being bulk polypropylene. The structure of the resulting nanocomposites was investigated with XRD, TEM, controlled strain and controlled stress rheometry.

The main questions addressed in this chapter are as follows:

- For a fixed compatibilizer loading of 10wt% and 5wt% organo-clay and the rest being bulk polypropylene, how is the clay exfoliation levels affected by the maleic anhydride distribution: free, oligomeric and bound in four different PP-g-MA compatibilizers having total maleic anhydride contents varying from 1.2-4 wt%?
- To investigate the rheological response of composites with different levels of clay exfoliation using dynamic oscillatory shear as well as creep compliance measurements?

4.1.2 Background

The dispersion of layered silicates in polymeric matrices is of great interest in the polymer industry after the pioneering work done by researchers at Toyota for nylon-6 based materials [1-5]. Once the layered clay has been delaminated by different processing techniques, the polymer-clay hybrids exhibit unparalleled mechanical, thermal and gas barrier properties as compared to the base polymer matrices [7, 9-11, 13]. The nanoscopic fillers score over the conventional reinforcements in their ability to provide greater improvements in properties with a much reduced filler loading. These attributes of nanocomposites have made them suitable for applications ranging from automotive to food packaging to flame retardant materials.

Functionalized polyolefin oligomers (compatibilizers) are used in aiding clay dispersion for non-polar polymers like polypropylene and polyethylene[54-57], where the polar functionality (usually maleic anhydride) wets the clay surface and the oligomers are soluble in the bulk matrix. Using this approach, Okada and co-workers [53] synthesized the first PP-clay hybrids using maleic anhydride functionalized PP oligomers. The need to have a significant level of polar functionality has since been established by Hasegawa et al.[54-56], Gopakumar et al. [58] for polyethylene and by Ishida et al.[59] for a wide range of polymers. Theoretical studies done by Balazs et al. [27, 38-40] and molecular simulation studies by Minisini and Tsohnang [60] have also established that adding functionalized polymers leads to improved clay exfoliation levels. Strong interactions between the maleic anhydride moieties and the organoclay increase the system enthalpy, which compensates for the reduction in entropy due to the polymer chain intercalating in

the 1 nm gap between the clay platelets and leads to greater separation of the clay nanolayers.

The loading of the maleic anhydride functionalized polyolefins (PP-g-MA), the molecular weight of the PP-g-MA[64, 107] and the molar ratio of the maleic anhydride functionality [61] are the important variables, which dictate the choice of a compatibilizer. It is well established that functionalization with maleic anhydride leads to chain scission of the polypropylene [62] and therefore large amounts of low or modest molecular weight PP-g-MA will lead to unacceptable low mechanical properties. Marchant and Jayaraman[61] have investigated the polypropylene nanocomposite structure with varying amounts of different maleated polypropylenes and concluded that an optimum concentration of a compatibilizer with higher molar ratios of maleic anhydride moieties led to the most exfoliated structure. They also established a low shear relative viscosity calculated from a ratio of the plateau values of the composites and the silicate free melts as an index for clay exfoliation. Wang et al. [63, 64] investigated the effects of different molecular weight compatibilizers, maleic anhydride contents and the compatibilizer loadings on the clay exfoliation in polypropylene nanocomposites. Their results showed that the compatibilizer with lower molecular weight and higher MA content could lead to efficient clay dispersion in PP/clay composites.

The nature of the maleic anhydride functionality itself and its influence on the compatibilizer effectiveness to exfoliate the clay in polyolefin nanocomposites is one of the main objectives of this work. The maleic anhydride moieties in these materials may exist in three distinct forms. First as an unreacted small molecule, second as a maleic anhydride oligomer and third as maleic anhydride bound to a polymer chain [65, 66]. The

“bound” maleic anhydride moieties are grafted at the end of the polymer chains using a free radical reaction between polypropylene, maleic anhydride and an organic peroxide initiator[125]. The most probable structure from this reaction is an end group consisting of either a single maleic anhydride (succinic graft) or a multifunctional graft (poly maleic anhydride graft) as a result of the macro radical attacking another maleic anhydride molecule. De Roover and coworkers [125] have used titration and FTIR to identify these structures in 4 different modified polypropylenes. The percentage of bound maleic anhydride in the PP-g-MA turns out to be a critical variable and as is shown in the present work that a compatibilizer with a higher bound MA content results in higher levels of exfoliation in melt mixed polypropylene nanocomposites.

A detailed study of the low frequency viscoelastic response of nanocomposites with varying levels of clay exfoliation is the other important objective of this paper. Solomon and co-workers[97] have evaluated the melt phase properties of PP/clay hybrids and found that above a loading of 2wt% silicate, the nanocomposites exhibited a low frequency plateau in the storage modulus curve, which is indicative of a yield stress. The presence of an apparent yield stress for a polypropylene clay hybrid has also been observed by Galgali et al.[103], who attributed it to frictional interactions between the anisotropic clay platelets. In the present paper, when maleated polypropylenes with higher bound maleic anhydride are used, the nanocomposites showed a similar plateau for the storage modulus in the low frequency regime. The plot of the phase angle (δ) versus the complex shear modulus (G^*) is used to detect the subtle micro-structural differences in polypropylene nanocomposites with different levels of clay exfoliation. This plot often called the van-Gurp-Palmen (vGP) plot has been previously used for

verification of the time temperature superposition principle[119] and to elucidate the effects of polydispersity and long chain branching[120, 121]. The creep compliance measurements were also obtained in the linear viscoelastic range at a stress of 10Pa in order to get detailed information about the solid like response of these materials.

4.2 EXPERIMENTAL

4.2.1 Materials

This study uses organically modified montmorillonite clay, Nanocor I.30P, polypropylene homopolymer-Basell 6323 (MFR=12) and various grades of maleated polypropylenes. The original montmorillonite clay is sodium montmorillonite with a cation exchange capacity of over 120 meq/100 grams. The modified clay has 95-98% of the sodium ions exchanged with octadecyl ammonium ions and a specific gravity of 1.9. The modified clay has a basal spacing of 2.3 nm before compounding. This value was confirmed with X-ray diffraction patterns. The selected maleic anhydride modified polypropylenes had over 1wt% total maleic anhydride as confirmed by the suppliers. Two grades of maleic anhydride modified polypropylene (PP-g-MA) compatibilizers with acid numbers of 10 and 7 have been chosen from a set of *Eastman Epolenes*, as well as two grades from *Honeywell A-C waxes* with acid numbers of 9 and 23. The molecular weights, polydispersity and the acid number for all maleated polypropylenes are presented in Table 4.1. The chosen compatibilizers provide us a wide range of molecular weights and varying levels of maleic anhydride grafting. The results for the maleic anhydride distribution for the four PP-g-MA compatibilizers as obtained by using

titration were obtained from the previous work of Marchant[126] and have been included in Table 4.3.

4.2.2 *Melt Mixing*

The bulk PP, PP-g-MA's and clay were mixed in a lab scale Banbury mixer and compression molded following the mixing protocol as discussed in Chapter 2 (section 2.1). The compatibilizer and the organoclay loadings were kept fixed at 10wt% and 5wt% respectively. The compatibilizer grade and sample identification for each composite is given in Table 4.2.

4.2.3 *Structural Characterization:*

All nanocomposites were analyzed using TEM and XRD. The characterization of the structure by XRD was performed on the compression-molded disks with a Rigaku Rotaflex Ru-200BH X-ray diffractometer, which was equipped with a Ni-filtered Cu K α radiation source and operated at 45 kV and 100 mA. The sample was scanned over a 2θ range of 0.5° to 10° at a rate of $0.5^\circ/\text{min}$ and measurements were recorded at equal increments of 0.01° .

The TEM used in this study was a JEOL 100 CX with a 120 KeV electron accelerator. 90 nm thin sections were prepared from a disk formed for the rheological characterization. The sections were cryomicrotomed at a temperature of -120°C in order to create the required rigidity to produce the uniform thin sections required to obtain clear reproducible images. Several of these micrographs were analyzed using commercial image analysis software (Sigma Scan Pro 5.0, SPSS Inc.) to get a length distribution for

the clay platelets. The boundary of the single clay platelets in the micrograph was manually outlined by using the software, which then returned its major length. Particles were catalogued in several images for each composite so that a total of close to 100 single particles were analyzed for each composite. About four images were required for the composite NC14 and three images for the rest.

4.2.4 Rheological Characterization

Oscillatory shear measurements were performed with a Rheometrics RMS 800; the compression-molded disk was held between two parallel plates (50 mm) at 180°C and subjected to oscillatory shear over a frequency range of 0.05-100 rad/s at strain amplitude of 2%. The data were recorded only when the torque amplitude is above the recommended threshold of 2 g-cm. The chosen strain amplitude was confirmed to be within the linear viscoelastic regime by performing a strain sweep at a fixed frequency of 1 rad/sec at 180°C over a range of 0.5-30%. The samples were melted for 10 minutes before starting the test for homogenization.

The creep measurements were obtained at a stress of 10 Pa with an AR 2000 rheometer from TA Instruments. The chosen stress value of 10 Pa was confirmed to be in the linear viscoelastic regime, since similar compliance values were obtained at a higher stress of 15 Pa. The tests were performed at a temperature of 180°C and the samples were melted for 10 minutes before starting the test. A time sweep was performed at the test temperature to verify the absence of any micro-structural changes occurring in the experimental time frame during the annealing process as has been observed by Reichert et al. [84] and Solomon et al.[97].

4.3 RESULTS AND DISCUSSION

A primary focus for this study is the fraction of bound maleic anhydride and how it dictates the compatibilizer effectiveness in exfoliating the organoclay. The titration results summarized in Table 4.3 (modified from Reference [126]) indicate that different compatibilizers have different amounts of all three chemical forms of maleic anhydride. The compatibilizer PP-g-MA2 has a greater amount of total maleic anhydride than PP-g-MA3, but PP-g-MA3 has a larger amount of bound maleic anhydride. This turns out to be important for exfoliation. The compatibilizers PP-g-MA3 and PP-g-MA4 contain higher percentages of bound maleic anhydride with the latter containing the highest percentage of bound (2.6%) as well as total amount of maleic anhydride (4%)

The XRD patterns for the four composites along with the organoclay have been shown in Figure 4.1. The organoclay I.30P (curve A) shows a peak at 2θ values of 2.8 corresponding to a basal spacing of 2.3 nm. Based on the degree of dispersion, this peak can either shift to lower 2θ values for an intercalated composite or might yield a featureless curve indicative of the absence of any ordered platelet structures in an exfoliated nanocomposite. There is a small intercalation peak for the nanocomposite (NC11) with the lowest bound MA content as compared to the other three nanocomposites. This would indicate that the degree of exfoliation is the least for NC11. Further evaluation of the composite structure is possible by considering “shoulders” in the diffraction pattern. The length of this shoulder will indicate the population of intercalated as opposed to exfoliated species. The NC11 composite (Curve B) exhibits the longest shoulder of all the composites. The curves C and D for NC12 and NC13 respectively are very similar and no differences between the two can be readily discerned

from their XRD patterns. The composite NC14 has the most featureless XRD pattern implying the absence of ordered platelet structures.

Subtle differences in the structure of the four nanocomposites can be obtained from analysis of the transmission electron micrographs. The micrographs were obtained for composites NC12, NC13 and NC14, which appear from the XRD results to be significantly exfoliated. The representative micrographs are shown in Figures 4.2-4.4. The micrograph for the composite NC12 in figure 4.2 shows the presence of some intercalated clay tactoids in the composite. The composite micrographs for NC13 and NC14 have much fewer intercalated clay structures and have a large concentration of *single* clay platelets, implying that the nanolayers have been significantly separated in these two composites. Here a single platelet here is one, where no visible gaps can be located and it is at least half a particle length away from a neighboring particle.

The clay exfoliation levels can be compared quantitatively from an analysis of the fraction of single particles and the corresponding length distribution for such particles. Several transmission electron micrographs were used for this purpose. The results of this analysis are presented in Figure 4.5. The composites NC12 and NC13 have a uni-modal distribution with most probable length of 100 nm and 150 nm respectively. The composite NC14 has a bi-modal distribution with almost equal contributions from two most probable lengths of 125 nm and 210 nm, which identifies NC14 prepared with the PP-g-MA having the greatest bound MA fraction clearly as the most exfoliated sample with the highest average platelet length.

Small amplitude oscillatory shear rheology can yield useful information about the nanocomposite microstructure, since both storage modulus and the loss modulus of the

nanocomposite melts increase with the clay loadings [100]. For fixed silicate loadings and for nanocomposites with an intercalated morphology, the increase in dynamic storage modulus is highly sensitive to the intercalation levels and the flow induced alignment of the clay nanolayers [100, 127]. However for exfoliated nanocomposites for a fixed silicate loading, the relative viscosity of the composite provides a good index for the extent of clay delamination [61], since the relative viscosity is highly sensitive to the filler aspect ratio as has been well established for dilute suspensions [115] as well as for filled polymer melts [116]. The relative viscosity can be calculated by the ratio of the dynamic viscosity of the composite to the corresponding silicate free mixture at a fixed stress.

The dynamic viscosity for the composites and the corresponding silicate free melts containing both PP and PP-g-MA in the same proportion as the composites are plotted in figures 4.6-4.9. An analysis reveals two distinct types of viscosity curves. Figures 4.6 and 4.7 for the composites NC11 and NC12 fall into the first category, where the composite viscosity reaches a plateau value at low stresses. The other type of viscosity curve is observed for the composites NC13 and NC14, as shown in Figures 4.8 and 4.9. At low frequencies (or equivalently low stresses), the viscosity shows an abrupt increase with decreasing stresses, thereby indicating the presence of a yield stress for these systems.

The relative viscosity is plotted in Figure 4.10 over a wide G^* range. The composites NC14 and NC13 with higher contents of bound MA have higher relative viscosities as compared to the composites NC12 and NC11, thereby indicating that the levels of clay delamination are more pronounced in the former two cases. The composite NC11 with the compatibilizer PP-g-MA1 shows the least relative viscosity amongst the

four composite formulations. The rheology results are in agreement with the earlier reported XRD and TEM observations, with the exception of NC13. The relative viscosity difference between NC13 and NC14 is hardly discernible and doesn't clearly illustrate the different levels of clay exfoliation.

The dynamic storage modulus (G') curves have been plotted in Figure 4.11. The composites NC13 and NC14 have higher storage modulus values as compared to the composites NC12 and NC11 over most of the frequency range. A low frequency plateau in the G' plot is observed for the composites NC13 and NC14, which provides further evidence for the presence of a yield stress. Such viscoelastic behavior (liquid at shorter time scales and solid like at larger time scales) has been previously observed for other polymer-clay nanocomposite systems and has been attributed to the formation of a percolated network structure of the anisotropic clay platelets [102]. In a recent study with melt mixed polypropylene nanocomposites involving Cloisite-20A clay, PP-g-MA with 1 wt% maleic anhydride and MFI=6 PP, Lertwimolnum and Vergnes[118] have fitted a Carreau-Yasuda model to the complex viscosity curves to estimate the yield stress for these systems. They obtained excellent fits between the predicted and the experimental data, and found that the yield stress values reached a maximum of 800 Pa at a compatibilizer loading of 25wt% beyond which the value was almost constant.

A better understanding of the yield stress and its connection with the microstructure can be obtained by plotting the phase angle (δ) versus the complex shear modulus (G^*). The plots for the four nanocomposites are shown in Figure 4.12. Lowering in phase angle for most of the G^* range was the lowest for the highly exfoliated composites NC13 and NC14, which use the compatibilizer with the greatest amount of

bound maleic anhydride, thereby indicating the highly elastic nature for these composites. The lowering in the phase angle was the least for the intercalated composite NC11. There is a hint of the presence of a secondary minimum for the phase angle for the composites NC13 and NC14, however due to limited data in the lower G^* it cannot be conclusively established. Matsumoto et al.[117] have analyzed the long time viscoelastic response of polystyrene suspensions with spherical particles. The secondary minima in the low frequency regime was closely related to the yield stress, since both having similar relaxation mechanisms. The G^* value at the secondary minima can be interpreted as the yield stress for the system. The values are of the order of 960 Pa for the composites NC13 and NC14, with the former having slightly greater values. The van-Gurp-Palmen plots for all composites merge at large G^* values (of the order of 10^5 Pa), which is indicative of the plateau modulus for the polymer (G_n^0). Since all composites converge at the same point, it appears that the plateau modulus is unaffected by clay incorporation. However, it cannot be conclusively established in absence of data at higher G^* values. The corresponding plots for the silicate free matrices are shown in Figure 4.13. All the plots are essentially similar in nature and illustrate the effects of incorporation of low molecular weight maleated polypropylenes in the composite matrices. Trinkle and Friedrich[120] have also observed similar plots for three different molecular weights polystyrenes. It should be pointed here that the dynamic rheology studies with the nanocomposite formulations at 180°C yield an incomplete picture of the yield stress for the nanocomposite formulations. A better representative idea of the composite yield behavior can be obtained by conducting the tests at higher temperatures, which will yield the viscoelastic response of the material in the lower G^* regime.

Controlled stress rheometry is ideally suited to monitor the low frequency response of viscoelastic materials. Galgali et al.[103] used creep compliance measurements to monitor the hybrid formation kinetics for PP/clay hybrids upon addition of compatibilizer and also to elucidate the effects of annealing on the microstructure. They observed that the creep compliance for a compatibilized hybrid was progressively higher than the un-compatibilized hybrid for a 6wt% silicate loading. The creep compliance for the four composite formulations is plotted in Figure 4.14. The composite NC13 and NC14 have low compliance values as compared to the composites NC11 and NC12, which is a typical characteristic of a solid like response. The creep response at higher times also demonstrates the subtle structural differences between the composites NC13 and NC14, where in the creep compliance is progressively lower for the composite NC14 as compared to the composite NC13.

An average single platelet length was calculated from the earlier reported TEM analysis and is reported in Table 4.3. The greatest length (142 nm) is obtained for the composite NC14, which utilizes the compatibilizer with the highest amounts of both total as well as bound maleic anhydride. A greater average length is obtained for the composite NC13 (129), as compared to the composite NC12 (92nm). The nature of maleic anhydride grafting plays a crucial role here, since the total amount of maleic anhydride graft is higher for the compatibilizer PP-g-MA2 (1.8% versus 1.59%), but the bound maleic anhydride content is smaller than the compatibilizer PP-g-MA3 compatibilizer (0.94% versus 1.3%).

Overall the clay exfoliation levels scale as NC14>NC13>NC12>NC11 and are progressively higher, when compatibilizers containing higher grafting percentage of

bound maleic anhydride are used for nanocomposite preparation. This can be explained by considering the strength of the bond between the clay and the compatibilizer chains. When more than one maleic anhydride group is attached to a chain end, the potential for multiple interactions with the clay surface will enhance the ability of the compatibilizer to enter the clay gallery and also create a stronger bond between the clay and the compatibilizer. This will allow effective stress transfer from the polymer to the clay in the high shear melt mixing process and result in enhanced clay platelet separation. This is analogous to the polyamide work [52], where higher nanolayer exfoliation levels were achieved with higher molecular weight matrices.

4.4 CONCLUSION

This study reveals that the distribution of maleic anhydride in maleated PP-compatibilizers plays an important role in the process of clay delamination in a melt processed polypropylene nanocomposite system. The clay exfoliation levels were quantified with rheological analysis coupled with detailed image analysis of the composite micrographs. The three forms of maleic anhydride: bound, oligomeric and free were calculated by titration for four different compatibilizers and a higher fraction of bound maleic anhydride in the compatibilizer results in higher clay exfoliation for a fixed 10 wt% loading of the compatibilizer. This was explained by the formation of a stronger bond between the clay and the compatibilizer, which should facilitate transfer of stresses from the PP matrix chains to slide the clay nanolayers during melt blending.

The dynamic storage modulus curves approached a steady plateau at low frequencies indicating the presence of a yield stress. The relative viscosity for the

composites was calculated from the dynamic viscosities for the composites and the corresponding silicate free melts in order to quantify clay delamination levels, and it indicated a progressive increase with incorporation of compatibilizers with higher bound maleic anhydride grafting. The average length for the single clay platelet was obtained by analysis of several TEM images for each specimen and it also followed the same trend.

Table 4.1: Molecular information on compatibilizers

	M _w	M _n	Polydispersity	Acid Number
PP-g-MA1 ^a	52,000	27,400	1.9	7
PP-g-MA2 ^a	47,000	24,800	1.9	10
PP-g-MA3 ^b	28,250	7,700	3.7	9
PP-g-MA4 ^b	22,000	3,700	5.9	23

a) Molecular weight values obtained from Eastman Chemicals

b) Molecular weight and MAH functionality obtained from Honeywell International, Inc.

Table 4.2: Composite identification and compatibilizer grade in each composite

Composite ID	PP-g-MA grade
NC11	PP-g-MA1
NC12	PP-g-MA2
NC13	PP-g-MA3
NC14	PP-g-MA4

Table 4.3: Nature and concentration of maleic anhydride in maleated polypropylenes obtained by titration and average length of clay platelet

	Wt % maleic anhydride in PP-g-MA ^(a)				Platelet length (nm)
	Small Molecule	Oligomeric	Bound	Total	
PP-g-MA1	0.69	0.14	0.37	1.20	—
PP-g-MA2	0.65	0.21	0.94	1.80	92
PP-g-MA3	0.00	0.29	1.30	1.59	129
PP-g-MA4	0.83	0.56	2.61	4.00	142

a) Titration results obtained from Marchant [126]

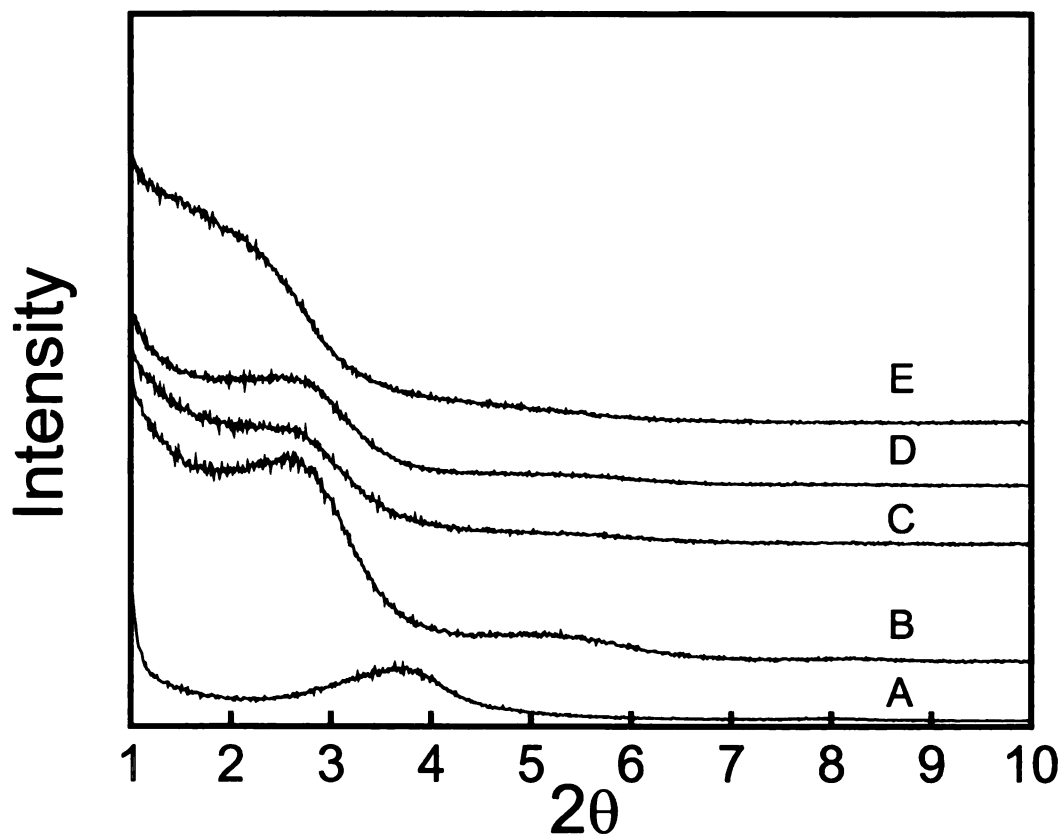


Figure 4.1: XRD patterns for polypropylene/clay nanocomposites: Curve A: I.30P organoclay, curve B: NC11, curve C: NC12, curve D: NC13, curve E: NC14. All composites have a fix loading of 85wt% PP6323, 10 wt% PP-g-MA and 5wt% I.30P Clay. The composite NC11 is based on PP-g-MA1 (Acid Number =7), the composite NC12 is based on PP-g-MA2 (Acid Number=10), the composite NC13 is based on PP-g-MA3 (Acid Number=9) and the composite NC14 is based on PP-g-MA4 (Acid Number =23)



Figure 4.2: Transmission Electron Micrograph for the composite NC12. The composite NC12 consists of 85wt% PP6323, 10wt% PP-g-MA2 (Acid Number =10) and 5wt% I.30P clay. The scale bar in the picture is 200 nm

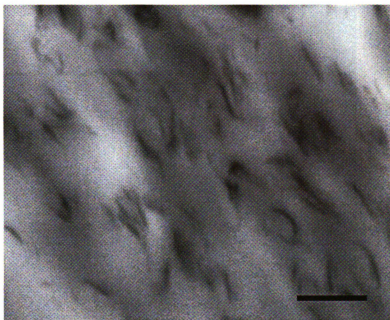


Figure 4.3: Transmission Electron Micrograph for the composite NC13. The composite NC13 consists of 85wt% PP6323, 10wt% PP-g-MA3 (Acid Number =9) and 5wt% I.30P clay. The scale bar in the picture is 200 nm

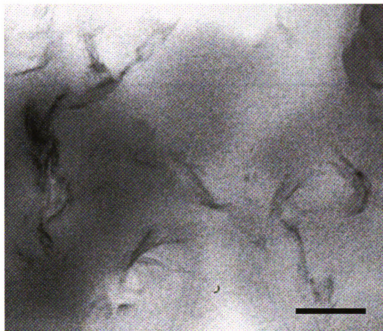


Figure 4.4: Transmission Electron Micrograph for the composite NC14. The composite NC14 consists of 85wt% PP6323, 10wt% PP-g-MA4 (Acid Number =23) and 5wt% I.30P clay. The scale bar in the picture is 200 nm

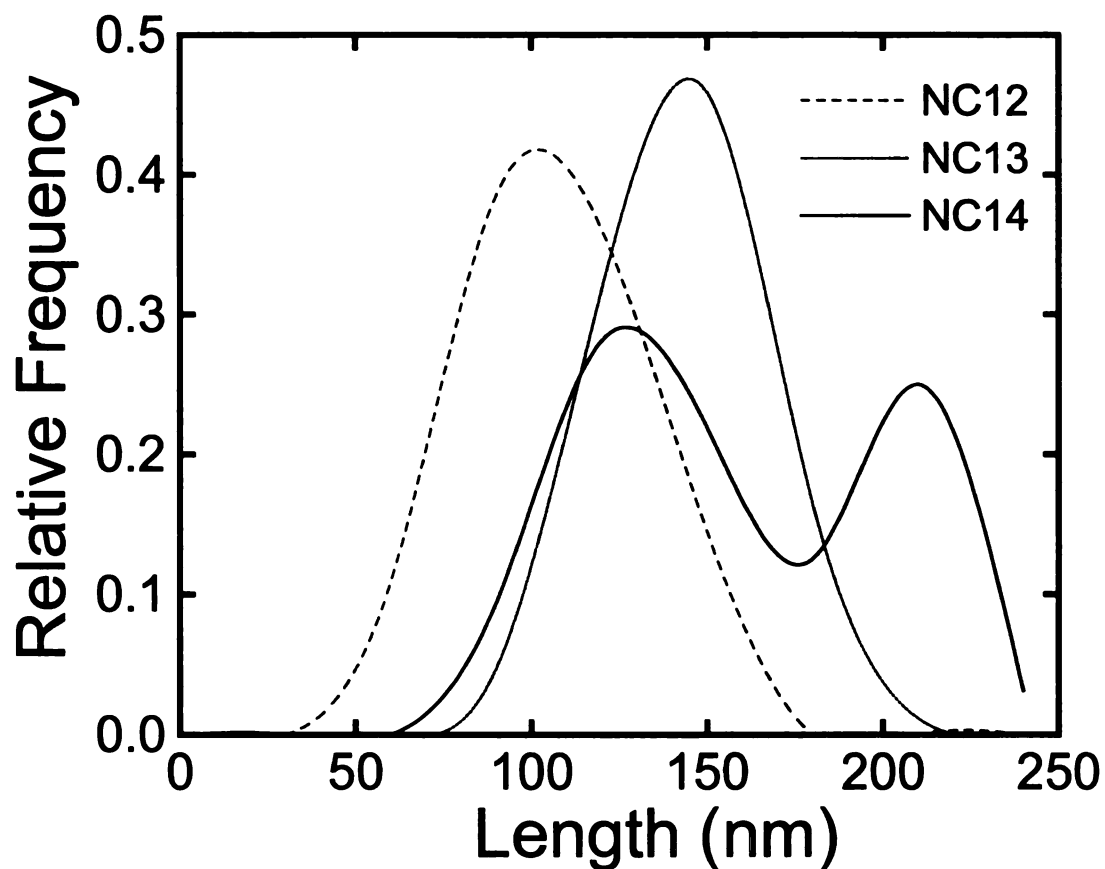


Figure 4.5: Length distributions of single particles for composites: (---) NC12, (....) NC13 and (—) NC14. All composites have a fix loading of 85wt% PP6323, 10 wt% PP-g-MA and 5wt% I.30P Clay. The composite NC12 is based on PP-g-MA2 (Acid Number=10), the composite NC13 is based on PP-g-MA3 (Acid Number=9) and the composite NC14 is based on PP-g-MA4 (Acid Number =23)

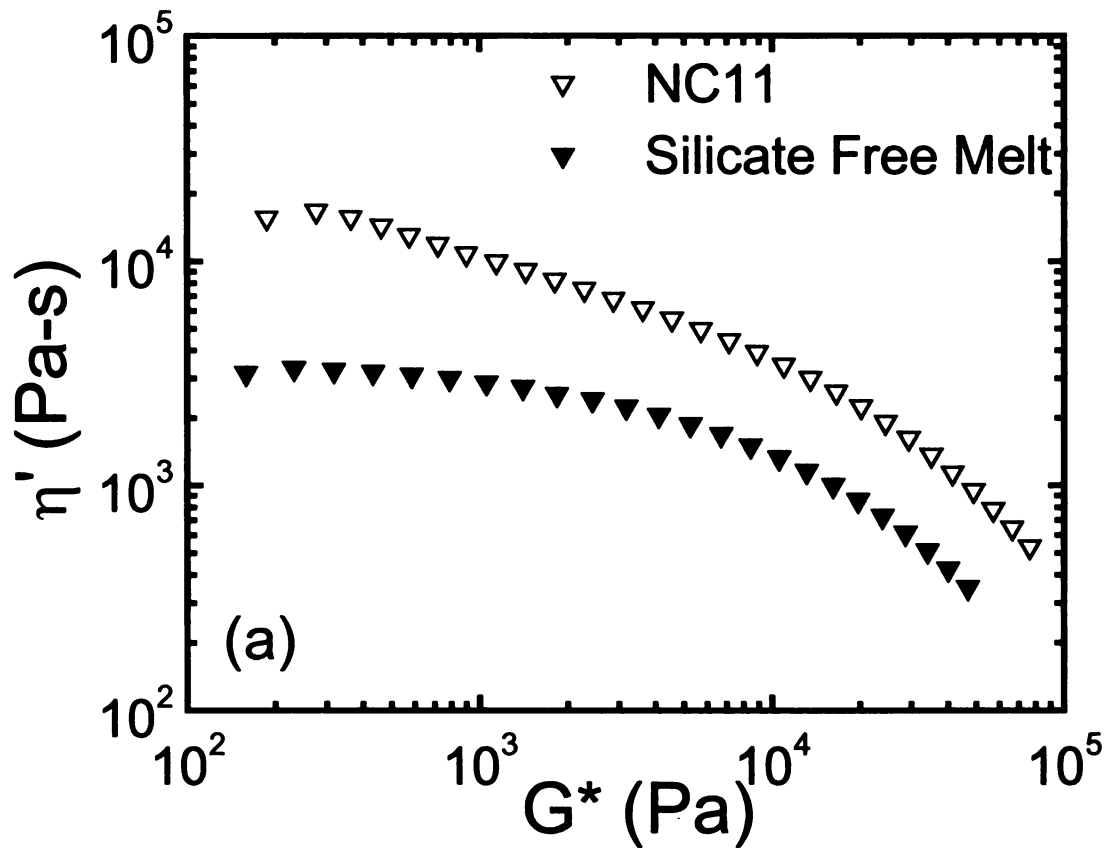


Figure 4.6: Dynamic viscosity curves for composite NC11 (∇) and the silicate free melt of PP6323 and PP-g-MA1 (\blacktriangledown) at 180°C. The composite NC11 consists of 85wt% PP6323, 10wt% PP-g-MA1 (Acid Number =7) and 5wt% I.30P clay

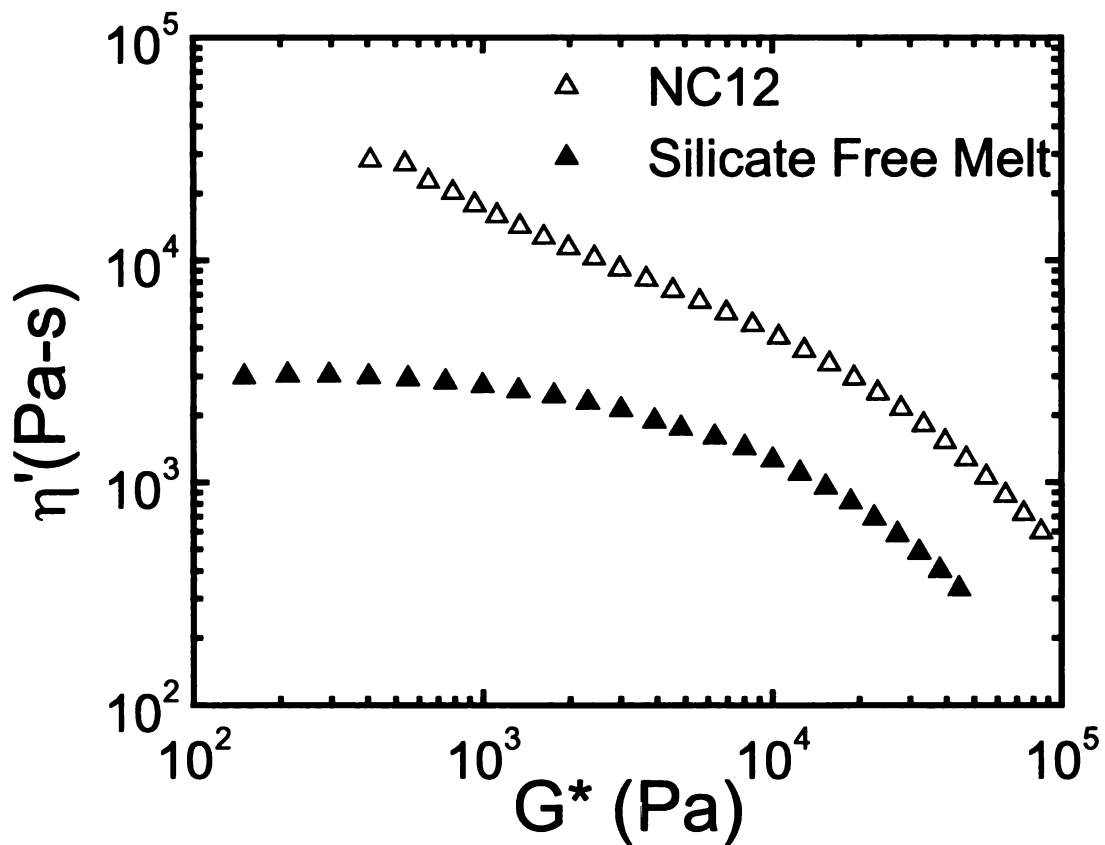


Figure 4.7: Dynamic viscosity curves for composite NC12 (Δ) and the silicate free melt of PP6323 and PP-g-MA2 (\blacktriangle) at 180°C. The composite NC12 consists of 85wt% PP6323, 10wt% PP-g-MA2 (Acid Number =10) and 5wt% I.30P clay

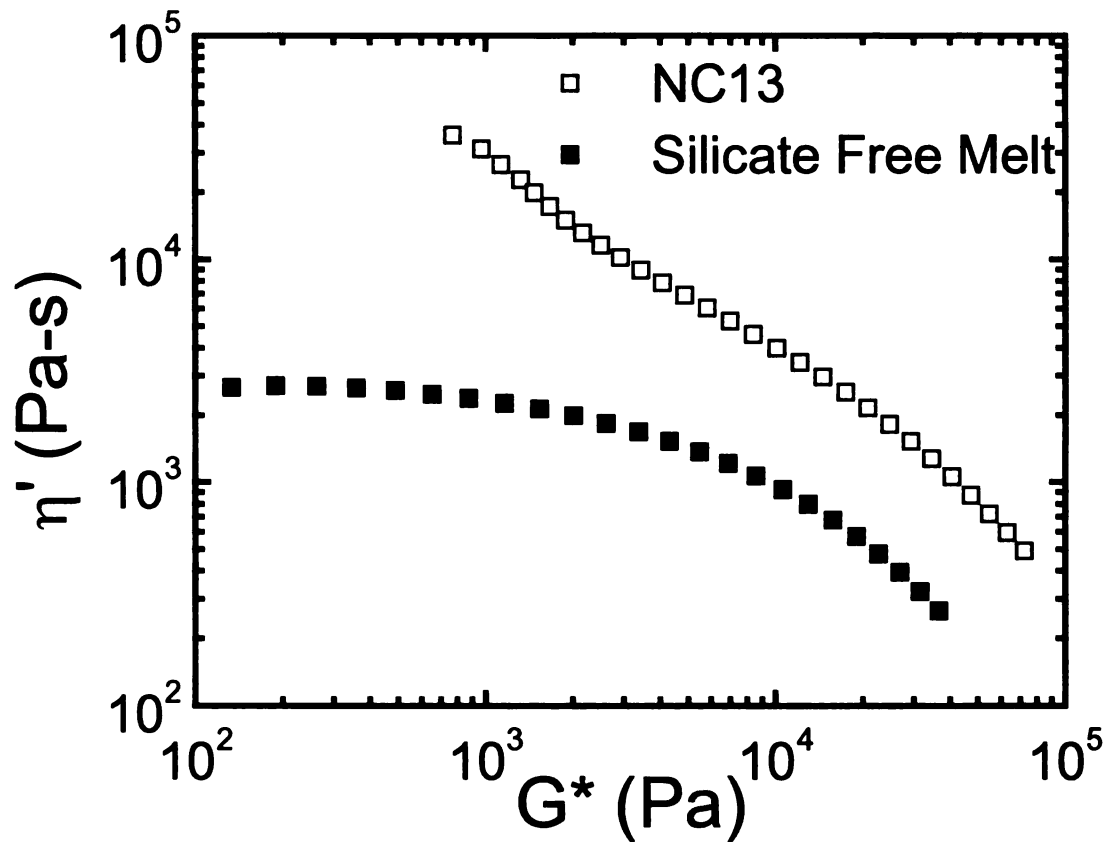


Figure 4.8: Dynamic viscosity curves for composite NC13 (\square) and the silicate free melt of PP6323 and PP-g-MA3 (\blacksquare) at 180°C. The composite NC13 consists of 85wt% PP6323, 10wt% PP-g-MA3 (Acid Number =9) and 5wt% I.30P clay

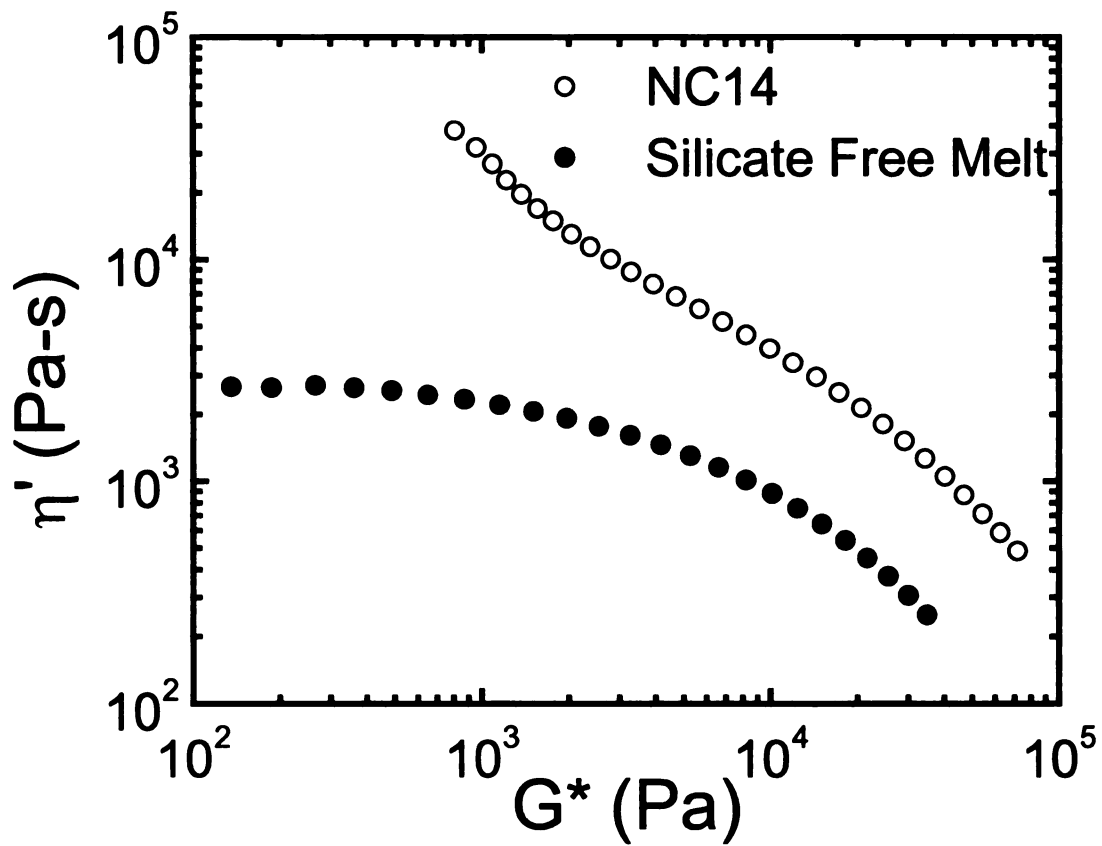


Figure 4.9: Dynamic viscosity curves for composite NC14 (○) and the silicate free melt of PP6323 and PP-g-MA4 (●) at 180°C. The composite NC14 consists of 85wt% PP6323, 10wt% PP-g-MA4 (Acid Number =23) and 5wt% I.30P clay

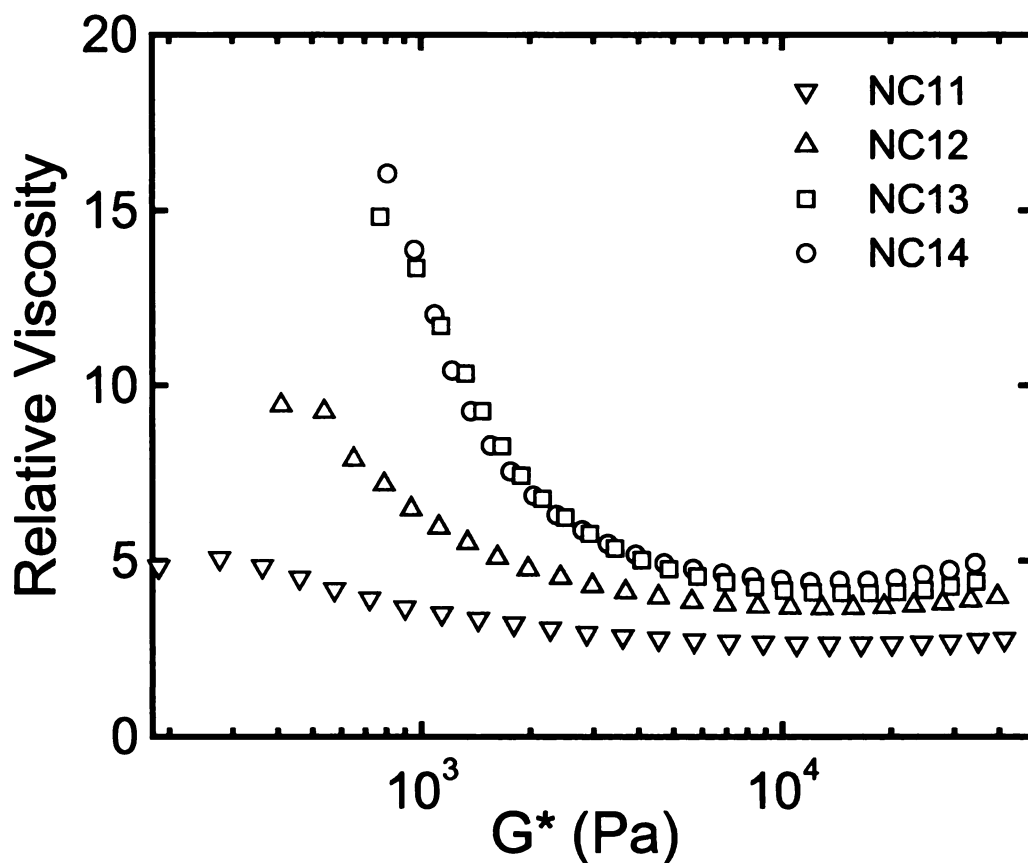


Figure 4.10: Relative viscosity curves obtained at similar G^* for the composites with different compatibilizers at 180°C: (▽) NC11, (△) NC12, (□) NC13, (○) NC14. All composites have a fix loading of 85wt% PP6323, 10 wt% PP-g-MA and 5wt% I.30P Clay. The composite NC11 is based on PP-g-MA1 (Acid Number =7), the composite NC12 is based on PP-g-MA2 (Acid Number=10), the composite NC13 is based on PP-g-MA3 (Acid Number=9) and the composite NC14 is based on PP-g-MA4 (Acid Number =23)

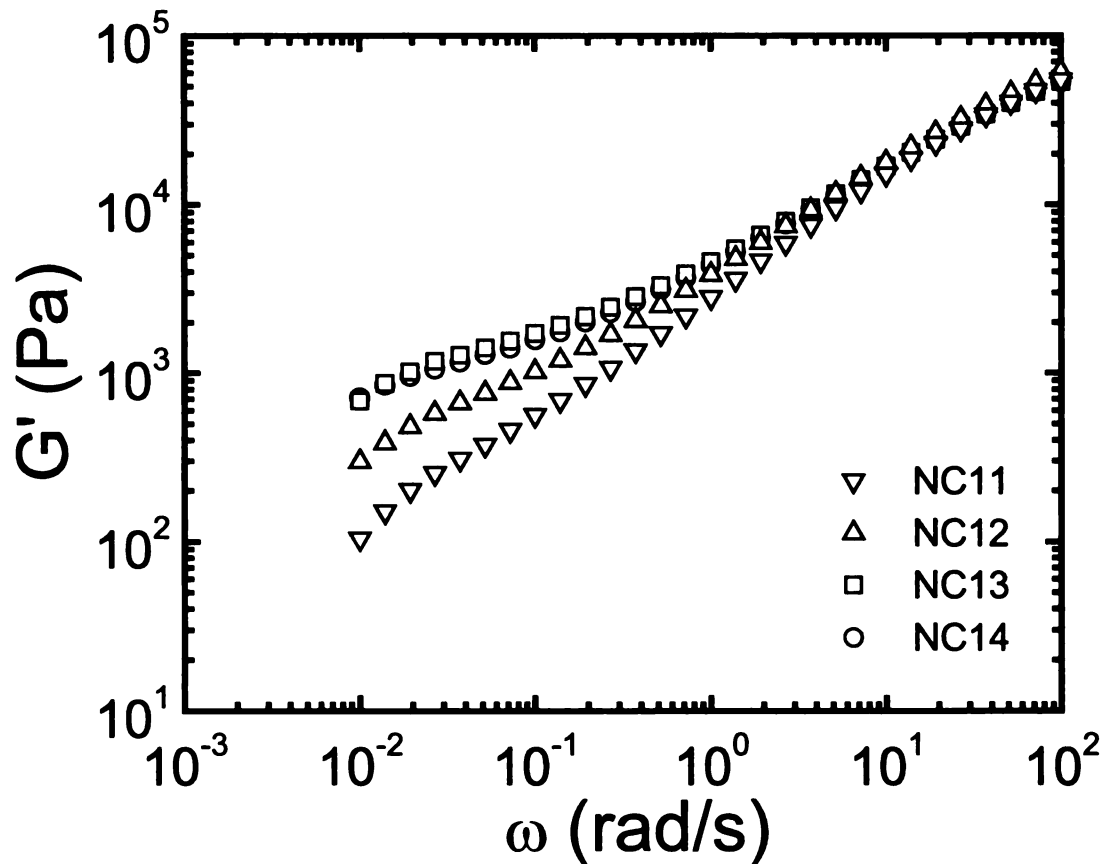


Figure 4.11: Storage Modulus (G') curves versus frequency (ω) for the composites with different compatibilizers at 180°C: (∇) NC11, (Δ) NC12, (\square) NC13, (\circ) NC14. All composites have a fix loading of 85wt% PP6323, 10 wt% PP-g-MA and 5wt% I.30P Clay. The composite NC11 is based on PP-g-MA1 (Acid Number =7), the composite NC12 is based on PP-g-MA2 (Acid Number=10), the composite NC13 is based on PP-g-MA3 (Acid Number=9) and the composite NC14 is based on PP-g-MA4 (Acid Number =23)

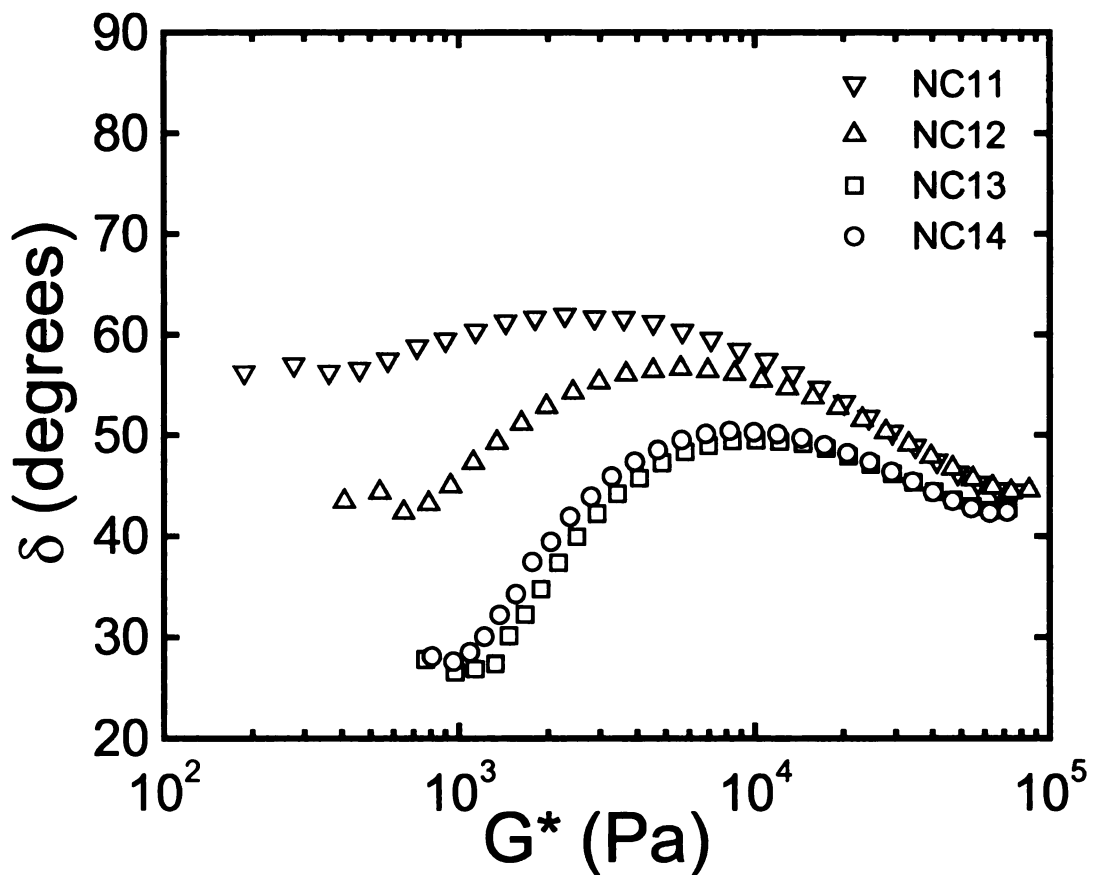


Figure 4.12: Phase Angle (δ) versus Complex Shear Modulus (G^*) for the composites with different compatibilizers at 180°C: (∇) NC11, (Δ) NC12, (\square) NC13, (\circ) NC14. All composites have a fix loading of 85wt% PP6323, 10 wt% PP-g-MA and 5wt% I.30P Clay. The composite NC11 is based on PP-g-MA1 (Acid Number =7), the composite NC12 is based on PP-g-MA2 (Acid Number=10), the composite NC13 is based on PP-g-MA3 (Acid Number=9) and the composite NC14 is based on PP-g-MA4 (Acid Number =23)

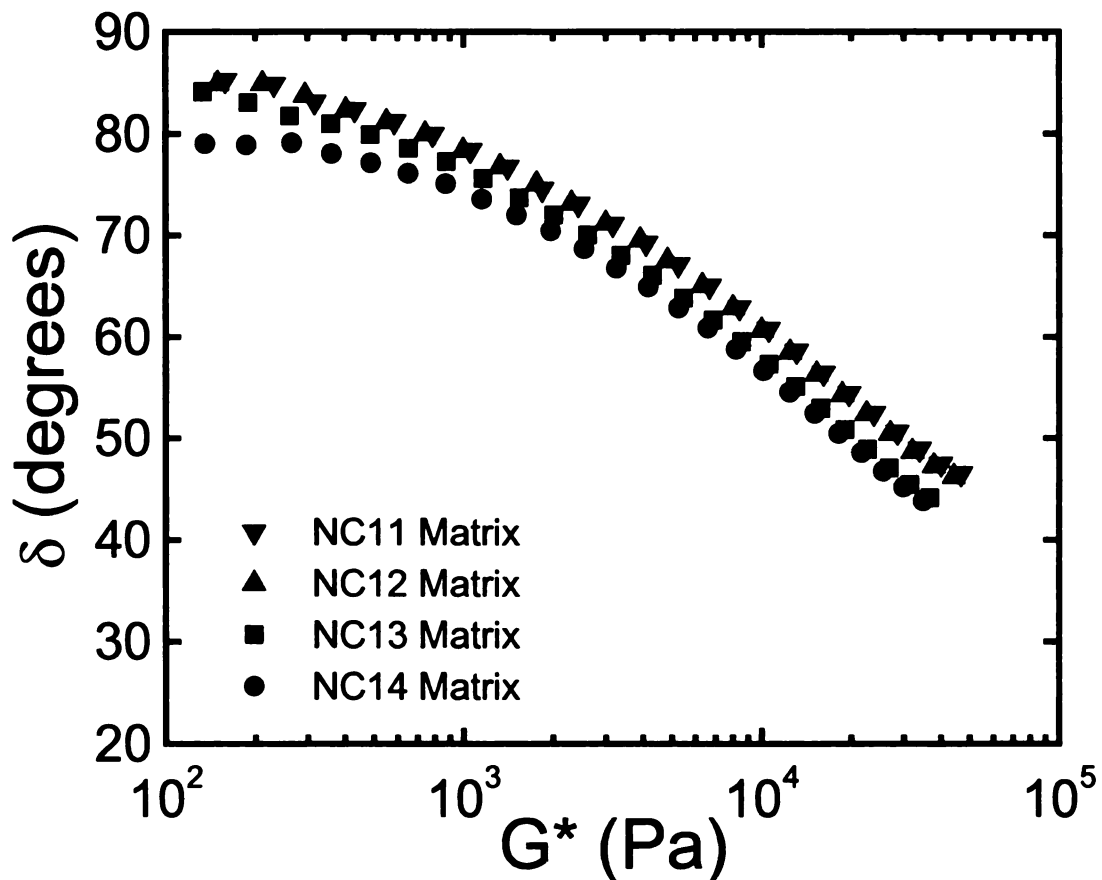


Figure 4.13: Phase Angle (δ) versus Complex Shear Modulus (G^*) for the silicate free composite matrices at 180°C: (\blacktriangledown) NC11, (\blacktriangle) NC12, (\blacksquare) NC13, (\bullet) NC14. All composites have a fix loading of 85wt% PP6323, 10 wt% PP-g-MA and 5wt% I.30P Clay. The composite NC11 is based on PP-g-MA1 (Acid Number =7), the composite NC12 is based on PP-g-MA2 (Acid Number=10), the composite NC13 is based on PP-g-MA3 (Acid Number=9) and the composite NC14 is based on PP-g-MA4 (Acid Number =23)

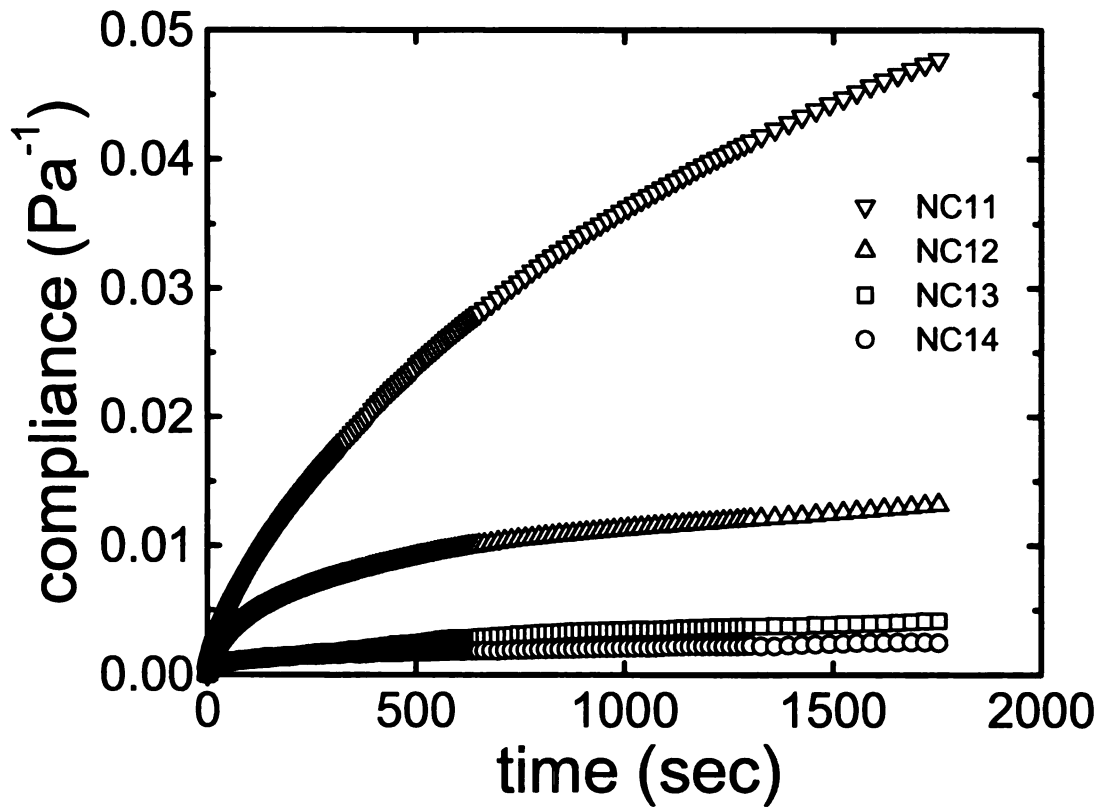


Figure 4.14: Creep Compliance $J(t)$ as a function of time at a stress of 10 Pa at 180°C: (∇) NC11, (Δ) NC12, (\square) NC13, (\circ) NC14. All composites have a fix loading of 85wt% PP6323, 10 wt% PP-g-MA and 5wt% I.30P Clay. The composite NC11 is based on PP-g-MA1 (Acid Number =7), the composite NC12 is based on PP-g-MA2 (Acid Number=10), the composite NC13 is based on PP-g-MA3 (Acid Number=9) and the composite NC14 is based on PP-g-MA4 (Acid Number =23)

CONCLUSIONS AND RECOMMENDATIONS

CHAPTER-5

5.1 CONCLUSIONS

This study was focused towards improving the interactions between the different components of a polypropylene nanocomposite system — bulk polypropylene, maleated polypropylene and the nanoclay intercalated with long chain alkyl ammonium surfactants, in order to boost the clay exfoliation levels. There were two primary issues addressed in this work.

- How can the interactions between the organoclay and the bulk polypropylene be improved to facilitate effective clay dispersion?
- How is the nanolayer morphology affected by additional processing and does a careful control of the interactions between the different system components provide additional stability to the nanocomposite structure?

The silicate fillers offer two interaction sites: the negatively charged clay faces, which have long chain alkyl ammonium surfactants tethered to them and the hydroxylated clay edges. The early research attempts were targeted towards improving the extent of coupling by adding maleated polypropylenes (compatibilizer), where the maleic anhydride moiety has favorable interactions with the clay and facilitates the polymer intercalation in the clay galleries. Previous authors[6] have attributed it to the

strong hydrogen bonding interactions of the maleic anhydride with the polar clay surfaces, which provides the required coupling between the clay and the bulk polymer. The strength of the hydrogen bond is an order of magnitude higher than the attractive Van-der-Waals forces and therefore dominates over the attractive forces between the clay platelets. This also explains why the distribution of maleic anhydride in maleated polypropylene plays an important role in the process of clay delamination (as discussed in Chapter 4) and the clay exfoliation levels were higher when compatibilizers with more bound maleic anhydride were used. Recent studies by Eastwood et al.[128] indicate that the clay exfoliation levels are higher in the presence of optimum amounts of intermolecular hydrogen bonding and these interactions provide a driving force for the polymer to exfoliate the layered silicate. The clay edges also have a few hydroxyl groups on the edges, which can serve as anchoring points for the maleic anhydride moiety.

Another way to increase the interactions between polymer and the filler is to use silane coupling agents to provide the necessary interfacial coupling during the process of melt compounding. The choice of the silane coupling agent is important and a solubility parameter match between the bulk polymer and the non-hydrolyzable group of the silane can be used for silane selection. Our results show that nanocomposites with the most exfoliated structure are obtained, when the chosen silane is located at the edges of the organoclay and doesn't intercalate the clay galleries. A schematic of the interactions between the different components after the silane treatment has been discussed in Figure 5.1. It lays down the interactions, when organoclay is modified with phenyltrimethoxy silane and subsequently the silane treated organoclay is melt blended with PP-g-MA and bulk polypropylene. We have previously established that the phenyltrimethoxy silane

functionalizes the edge hydroxyls and doesn't intercalate the clay galleries (Chapter 3). Treatment of the organoclay with phenyltrimethoxy silane results in the formation of a strong covalent bond between the clay and the silicon atom of the silane coupling agent and the phenyl functionality improves the interactions with the bulk polypropylene. Previous studies with silane coupling agents have attributed this improved interfacial coupling to the formation of an interpenetrating network (IPN). The phenyltrimethoxy silane treatment also results in the creation of two additional hydroxyl functionalities per coupling edge site, which offer additional anchoring points for hydrogen bonding with the maleic anhydride. This should further facilitate the sliding of the clay nanolayers during melt blending.

The other object of this study was to investigate the clay nanolayer morphology in shear and extensional flows. The idea was to investigate if improved interfacial coupling limits the extent of restacking/re-aggregation. Strong intermolecular interactions will limit the polymer chain mobility and provide stable structures. A high level of nanolayer re-stacking was observed in extrusion studies (Chapter 3) particularly at higher residence times in shear flows. However the levels of re-aggregation and restacking were reduced for the nanocomposites reinforced with phenyltrimethoxy silane functionalized clay particularly at higher residence times in shear flows. This could be attributed to two factors: the first owing to better interfacial interactions between the phenyl group and the bulk polypropylene. The second factor might be improved hydrogen bonding interactions between the PP-g-MA and the clay edge hydroxyls when the phenyltrimethoxy silane treated organoclay is used for melt blending, which provide additional morphological stability to the clay structure. On the other hand, the presence of a large amount of

hydrogen bonding interactions between the PP-g-MA and the clay faces seems to result in more clay restacking and aggregation. The other factor, which needs to be carefully investigated in this regard is the effect of temperature on hydrogen bonding interactions between the filler and the compatibilizer. The reduced restacking levels obtained in this study with the appropriate silane treatment provides evidence of better interfacial contacts between the clay and PP and can serve as a useful tool to render morphological stability to the clay nanolayers.

5.2 RECOMMENDATIONS

Based on the results of this investigation, the following recommendations can be made for future research efforts:

1. The overall goal of this study was to systematically evaluate the interactions between the multi-component polypropylene/PP-g-MA/organoclay systems and optimize it to boost the clay exfoliation levels. Two additional recommendations can be made in this field. The use of longer alkyl chain silane coupling agents needs to be evaluated in order to study the effects of chain length on the coupling between the clay and the bulk polypropylene. The second recommendation can be made with regard to the surfactant treatment of the clay. Recent studies evaluate the positive effects of using polymerically modified surfactants to facilitate clay exfoliation in melt mixed systems. Wilkie and coworkers[129, 130] have prepared two new organically modified clays that contain an oligomeric styrene or methacrylate, which were melt-blended with different nanocomposite systems. In the case of polypropylene[130], they obtained good levels of

clay exfoliation without using any maleated PP. Similar studies were carried out successfully by Kurian et al.[131], where polystyrene (PS)/clay composites by using a PS surfactant modified clay.

2. In this study, the surfactant treatment for the organoclay involved a single long alkyl tail. A recent study with polyethylene/clay hybrids suggests that the presence of two alkyl tails gives better exfoliation, owing to the preferential affinity of the non-polar polyolefin with the alkyl tails and not with the clay faces. This needs to be evaluated for the polypropylene system and should lead to the most optimum structure.
3. This study was based on a batch mixing technique, where all ingredients were mixed together and melt blended. Owing to the positive effects of masterbatching, a comparative study needs to be undertaken to contrast the effects of masterbatching to batch compounding.
4. The sequence of feeding the system components (clay, polypropylene and PP-g-MA) also needs careful consideration. Effects of adding clay in a secondary step after the PP and PP-g-MA have been mixed in the first step needs to be evaluated, because recent studies point out towards this protocol as being beneficial for effective clay dispersion.
5. In the nanoclay morphological stability studies, the core of the extruded strand was analyzed for effects of extensional flow on nanostructure. To complete eliminate wall shear contamination; a core-skin flow has to be used. Here the skin can layer can be comprised of a linear low-density

polyethylene (LLDPE), which will offer the desired lubrication to the composite during extrusion through the semi-hyperboloidal dies.

6. The van-Gurp-Palmen plot as used in this research work can be used to characterize the yield behavior of the nanocomposite materials. In order to further establish it, the data should be supplemented with yield stress measurements obtained from alternate techniques. The yield stress measurements can be obtained by monitoring the creep response[103] to progressive increase in stress. The stress at which the zero shear viscosity drops by a magnitude can be identified as the yield stress of the material. For some of the nanocomposite materials, the rheology data in the low G^* regime could not be obtained and therefore the yield stress information obtained by the van-Gurp-Palmen plots was insufficient. For those cases, the rheology experiments should be performed at slightly higher temperatures (200°C is recommended).

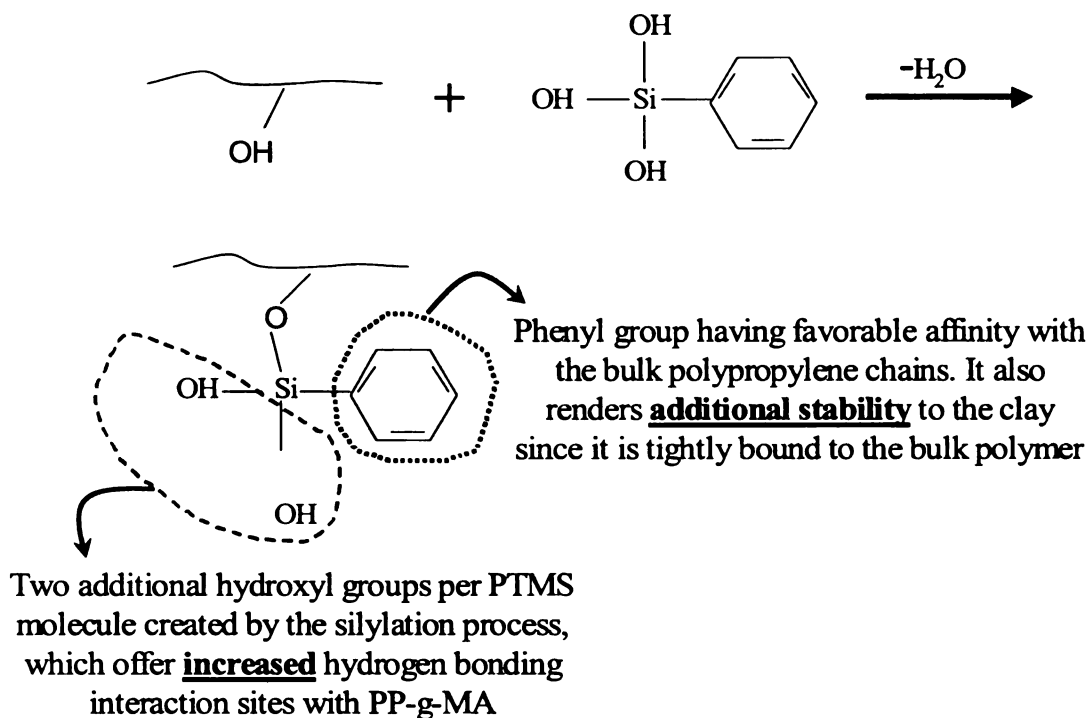


Figure 5.1: Proposed mechanism for the enhancement in the stability of nanolayers by careful control of the interactions between the different system components. This is achieved by favorable interactions of the phenyl end-capped silane with the bulk polypropylene and also increased hydrogen bonding interactions between the PP-g-MA and the hydroxyl groups.

BIBLIOGRAPHY

1. Usuki, A., Kawasumi, M., Kojima, Y., Okada, A., Kurauchi, T., and Kamigaito, O., "Swelling Behavior of Montmorillonite Cation Exchanged for Omega-Amino Acids by Epsilon-Caprolactam." *J. Mater. Res.*, **8**, (5), 1174-1178 (1993)
2. Usuki, A., Kojima, Y., Kawasumi, M., Okada, A., Fukushima, Y., Kurauchi, T., and Kamigaito, O., "Synthesis of Nylon 6-Clay Hybrid." *J. Mater. Res.*, **8**, (5), 1179-1184 (1993)
3. Kojima, Y., Usuki, A., Kawasumi, M., Okada, A., Fukushima, Y., Kurauchi, T., and Kamigaito, O., "Mechanical-Properties of Nylon 6-Clay Hybrid." *J. Mater. Res.*, **8**, (5), 1185-1189 (1993)
4. Kojima, Y., Usuki, A., Kawasumi, M., Okada, A., Kurauchi, T., and Kamigaito, O., "Synthesis of Nylon-6-Clay Hybrid by Montmorillonite intercalated with epsilon-caprolactam." *J. Polym. Sci. Pol. Chem.*, **31**, (4), 983-986 (1993)
5. Kojima, Y., Usuki, A., Kawasumi, M., Okada, A., Kurauchi, T., Kamigaito, O., and Kaji, K., "Fine-Structure of Nylon-6-Clay Hybrid." *J. Polym. Sci. Pol. Phys.*, **32**, (4), 625-630 (1994)
6. Giannelis, E., Krishnamoorti, R., and Manias, E., "Polymer-silicate nanocomposites: Model systems for confined polymers and polymer brushes." *Adv. Polym. Sci.*, **138**, 107-147 (1999)
7. Giannelis, E.P., "Polymer layered silicate nanocomposites." *Adv. Mater.*, **8**, (1), 29-35 (1996)
8. Giannelis, E.P., "Polymer-layered silicate nanocomposites: Synthesis, properties and applications." *Appl. Organomet. Chem.*, **12**, (10-11), 675-680 (1998)
9. Kato, M., Usuki, A., and Okada, A., "Synthesis of polypropylene oligomer-clay intercalation compounds." *J. Appl. Polym. Sci.*, **66**, (9), 1781-1785 (1997)
10. Kawasumi, M., Hasegawa, N., Kato, M., Usuki, A., and Okada, A., "Preparation and mechanical properties of polypropylene-clay hybrids." *Macromolecules*, **30**, (20), 6333-6338 (1997)
11. Yasue, K., Kathira, S., Yoshikawa, M., and Fujimoto, K., "In Situ Polymerization Route to Nylon 6-Clay Nanocomposites." Polymer Clay Nanocomposites, T.J. Pinnavaia and G.W. Beall, Editors. (2000)

12. Alexandre, M. and Dubois, P., "Polymer-layered silicate nanocomposites: preparation, properties and uses of a new class of materials." *Mat. Sci. Eng.*, **28**, (1-2), 1-63 (2000)
13. Ray, S. and Okamoto, M., "Polymer/layered silicate nanocomposites: a review from preparation to processing." *Prog. Polym. Sci.*, **28**, (11), 1539-1641 (2003)
14. Messersmith, P.B. and Giannelis, E.P., " Synthesis and Barrier Properties of Poly(Epsilon-Caprolactone)-Layered Silicate Nanocomposites." *J. Polym. Sci. Pol. Chem.*, **33**, (7), 1047-1057 (1995)
15. Qian, G., Cho, J.W. and Lan, T., "Preparation and Properties of Polyolefin Nanocomposites." Polyolefins 2001, Houston, TX (2001)
16. Bartholmai, M. and Scharrel, B., "Layered silicate polymer nanocomposites: new approach or illusion for fire retardancy? Investigations of the potentials and the tasks using a model system." *Polym. Advan Technol.*, **15**, (7), 355-364 (2004)
17. Gilman, J., Jackson, C., Morgan, A., Harris, R., Manias, E., Giannelis, E., Wuthenow, M., Hilton, D., and Phillips, S., "Flammability properties of polymer - Layered-silicate nanocomposites. Polypropylene and polystyrene nanocomposites." *Chem. Mater.*, **12**, (7), 1866-1873 (2000)
18. Manias, E., Touny, A., Wu, L., Strawhecker, K., Lu, B., and Chung, T., "Polypropylene/Montmorillonite nanocomposites. Review of the synthetic routes and materials properties." *Chem. Mater.*, **13**, (10), 3516-3523 (2001)
19. Tang, Y., Hu, Y., Li, B., Liu, L., Wang, Z., Chen, Z., and Fan, W., "Polypropylene/montmorillonite nanocomposites and intumescent, flame-retardant montmorillonite synergism in polypropylene nanocomposites." *J. Poly. Sci. Poly. Chem.*, **42** (23), 6163-6173 (2004)
20. Tang, Y., Hu, Y., Wang, S., Gui, Z., Chen, Z., and Fan, W., "Intumescent flame retardant-montmorillonite synergism in polypropylene-layered silicate nanocomposites." *Poly. Int.*, **52** (8), 1396-1400 (2003)
21. Pinnavaia, T.J., Lan, T., Kaviratna, P.D., Wang, Z. and Shi, H.H., "Clay-Reinforced Epoxy Nanocomposites- Synthesis, Properties and Mechanism of Formation." *Abstr. Pap. Am. Chem. S.*, **210**, 61 (1995)
22. Van Olphen, H., An Introduction to Clay Colloid Chemistry; Interscience Publishers: New York, 1962
23. Theng, B.K.G., Soils with Variable Charge., New Zealand: Offset Publications (1980)

24. Delozier, D.M., Orwoll, R.A., Cahoon, J.F., Ladislaw, J.S., Smith, J.G., and Connell, J.W., "Polyimide nanocomposites prepared with a novel aromatic surfactant." *High. Perform. Polym.*, **15**, (3), 329-346 (2003)
25. Vaia, R. and Giannelis, E., "Lattice model of polymer melt intercalation in organically-modified layered silicates." *Macromolecules*, **30**, (25), 7990-7999 (1997)
26. Vaia, R. and Giannelis, E., "Polymer melt intercalation in organically-modified layered silicates: Model predictions and experiment." *Macromolecules*, **30**, (25), 8000-8009 (1997)
27. Balazs, A., Singh, C., and Zhulina, E., "Modeling the interactions between polymers and clay surfaces through self-consistent field theory." *Macromolecules*, **31**, (23), 8370-8381 (1998)
28. Kuznetsov, D. and Balazs, A., "Phase behavior of end-functionalized polymers confined between two surfaces." *J. Chem. Phys.*, **113**, (6), 2479-2483 (2000)
29. Huh, J., Ginzburg, V., and Balazs, A., "Thermodynamic behavior of particle/diblock copolymer mixtures: Simulation and theory." *Macromolecules*, **33**, (21), 8085-8096 (2000)
30. Gee, R., Maxwell, R., and Balazs, B., "Molecular dynamics studies on the effects of water speciation on interfacial structure and dynamics in silica-filled PDMS composites." *Polymer*, **45**, (11), 3885-3891 (2004)
31. Lee, J., Shou, Z., and Balazs, A., "Predicting the morphologies of confined copolymer/nanoparticle mixtures." *Macromolecules*, **36**, (20), 7730-7739 (2003)
32. Buxton, G., Lee, J., and Balazs, A., "Computer simulation of morphologies and optical properties of filled diblock copolymers." *Macromolecules*, **36**, (25), 9631-9637 (2003)
33. Lee, J., Thompson, R., Jasnow, D., and Balazs, A., "Entropically driven formation of hierarchically ordered nanocomposites." *Phys. Rev. Lett.*, **89**, (15), (2002)
34. Buxton, G. and Balazs, A., "Lattice spring model of filled polymers and nanocomposites." *J. Chem. Phys.*, **117**, (16), 7649-7658 (2002)
35. Thompson, R., Ginzburg, V., Matsen, M., and Balazs, A., "Predicting the mesophases of copolymer-nanoparticle composites." *Science*, **292**, (5526), 2469-2472 (2001)

36. Kuznetsov, D. and Balazs, A., "Scaling theory for end-functionalized polymers confined between two surfaces: Predictions for fabricating polymer/clay nanocomposites." *J. Chem. Phys.*, **112**, (9), 4365-4375 (2000)
37. Ginzburg, V., Singh, C., and Balazs, A., "Theoretical phase diagrams of polymer/clay composites: The role of grafted organic modifiers." *Macromolecules*, **33**, (3), 1089-1099 (2000)
38. Ginzburg, V. and Balazs, A., "Calculating phase diagrams for nanocomposites: The effect of adding end-functionalized chains to polymer/clay mixtures." *Adv. Mater.*, **12**, (23), 1805-1809 (2000)
39. Zhulina, E., Singh, C., and Balazs, A., "Attraction between surfaces in a polymer melt containing telechelic chains: Guidelines for controlling the surface separation in intercalated polymer-clay composites." *Langmuir*, **15**, (11), 3935-3943 (1999)
40. Ginzburg, V. and Balazs, A., "Calculating phase diagrams of polymer-platelet mixtures using density functional theory: Implications for polymer/clay composites." *Macromolecules*, **32**, (17), 5681-5688 (1999)
41. Lyatskaya, Y. and Balazs, A., "Modeling the phase behavior of polymer-clay composites." *Macromolecules*, **31**, (19), 6676-6680 (1998)
42. Singh, C., Pickett, G., Zhulina, E., and Balazs, A., "Modeling the interactions between polymer-coated surfaces." *J. Phys. Chem. B*, **101**, (50), 10614-10624 (1997)
43. Reichert, P., Nitz, H., Klinke, S., Brandsch, R., Thomann, R., and Mulhaupt, R., "Poly(propylene)/organoclay nanocomposite formation: Influence of compatibilizer functionality and organoclay modification." *Macromol. Mater. Eng.*, **275**, (2), 8-17 (2000)
44. Ton-That, M., Perrin-Sarazin, F., Cole, K., Bureau, M., and Denault, J., "Polyolefin nanocomposites: Formulation and development." *Polym. Eng. Sci.*, **44**, (7), 1212-1219 (2004)
45. Hotta, S. and Paul, D., "Nanocomposites formed from linear low density polyethylene and organoclays." *Polymer*, **45**, (22), 7639-7654 (2004)
46. Fornes, T., Hunter, D., and Paul, D., "Nylon-6 nanocomposites from alkylammonium-modified clay: The role of alkyl tails on exfoliation." *Macromolecules*, **37**, (5), 1793-1798 (2004)

47. Lee, J., Lim, Y., and Park, O., "Thermal characteristics of organoclay and their effects upon the formation of polypropylene/organoclay nanocomposites." *Polym. Bull.*, **45**, (2), 191-198 (2000)
48. Kim, K., Utracki, L.A., and Kamal, M.R., "Numerical simulation of polymer nanocomposites using self-consistent mean-field model." *J. Chem. Phys.*, **121**, (21), 10766-10777 (2004)
49. Lan, T., Kaviratna, P.D., and Pinnavaia, T.J., "Mechanism of Clay Tactoid Exfoliation in Epoxy-Clay Nanocomposites." *Chem. Mater.*, **7**, (11), 2144-2150 (1995)
50. Lan, T. and Pinnavaia, T., "Clay-Reinforced Epoxy Nanocomposites." *Chem. Mater.*, **6**, (12), 2216-2219 (1994)
51. Sun, T. and Garces, J., "High-performance polypropylene-clay nanocomposites by in-situ polymerization with metallocene/clay catalysts." *Adv. Mater.*, **14**, (2), 128-130 (2002)
52. Fomes, T.D., Yoon, P.J., Keskkula, H., and Paul, D.R., "Nylon 6 nanocomposites: the effect of matrix molecular weight." *Polymer*, **42**, (25), 9929-9940 (2001)
53. Usuki, A., Kato, M., Okada, A., and Kurauchi, T., "Synthesis of polypropylene-clay hybrid." *J. Appl. Polym. Sci.*, **63**, (1), 137-139 (1997)
54. Hasegawa, N., Kawasumi, M., Kato, M., Usuki, A., and Okada, A., "Preparation and mechanical properties of polypropylene-clay hybrids using a maleic anhydride-modified polypropylene oligomer." *J. Appl. Polym. Sci.*, **67**, (1), 87-92 (1998)
55. Hasegawa, N., Okamoto, H., Kato, M., and Usuki, A., "Preparation and mechanical properties of polypropylene-clay hybrids based on modified polypropylene and organophilic clay." *J. Appl. Polym. Sci.*, **78**, (11), 1918-1922 (2000)
56. Hasegawa, N., Okamoto, H., Kawasumi, M., Kato, M., Tsukigase, A., and Usuki, A., "Polyolefin-clay hybrids based on modified polyolefins and organophilic clay." *Macromol. Mater. Eng.*, **280**, (7-8), 76-79 (2000)
57. Hasegawa, N. and Usuki, A., "Silicate layer exfoliation in polyolefin/clay nanocomposites based on maleic anhydride modified polyolefins and organophilic clay." *J. Appl. Polym. Sci.*, **93**, (1), 464-470 (2004)
58. Gopakumar, T., Lee, J., Kontopoulou, M., and Parent, J., "Influence of clay exfoliation on the physical properties of montmorillonite/polyethylene composites." *Polymer*, **43**, (20), 5483-5491 (2002)

59. Ishida, H., Campbell, S., and Blackwell, J., "General approach to nanocomposite preparation." *Chem. Mater.*, **12**, (5), 1260-1267 (2000)
60. Minisini, B. and Tsobnang, F., "Molecular mechanics studies of specific interactions in organomodified clay nanocomposite." *Compos. Part A-Appl. S.*, **36**, (4), 531-537 (2005)
61. Marchant, D. and Jayaraman, K., "Strategies for optimizing polypropylene-clay nanocomposite structure." *Ind. Eng. Chem. Res.*, **41**, (25), 6402-6408 (2002)
62. Minoura, Y., Ueda, M., Mizunuma, S., and Oba, M., "The Reaction of Polypropylene with Maleic Anhydride." *J. Appl. Polym. Sci.*, **13**, 1625 (1969)
63. Wang, Y., Chen, F., Li, Y., and Wu, K., "Melt processing of polypropylene/clay nanocomposites modified with maleated polypropylene compatibilizers." *Compos. Part B-Eng.*, **35**, (2), 111-124 (2004)
64. Wang, Y., Chen, F., and Wu, K., "Twin-screw extrusion compounding of polypropylene/organoclay nanocomposites modified by maleated polypropylenes." *J. Appl. Polym. Sci.*, **93**, (1), 100-112 (2004)
65. Sclavons, M., Carlier, V., DeRoover, B., Franquinet, P., Devaux, J., and Legras, R., "The anhydride content of some commercial PP-g-MA: FTIR and titration." *J. Appl. Polym. Sci.*, **62**, (8), 1205-1210 (1996)
66. Sclavons, M., Franquinet, P., Carlier, V., Verfaillie, G., Fallais, I., Legras, R., Laurent, M., and Thyron, F., "Quantification of the maleic anhydride grafted onto polypropylene by chemical and viscosimetric titrations, and FTIR spectroscopy." *Polymer*, **41**, (6), 1989-1999 (2000)
67. Sun, T. and Garces, J., "High-performance polypropylene-clay nanocomposites by in-situ polymerization with metallocene/clay catalysts." *Adv. Mater.*, **14**, (2), 128-130 (2002)
68. Lee, E., Mielewski, D., and Baird, R., "Exfoliation and dispersion enhancement in polypropylene nanocomposites by in-situ melt phase ultrasonication." *Polym. Eng. Sci.*, **44**, (9), 1773-1782 (2004)
69. Wang, Z.M., Nakajima, H., Manias, E., and Chung, T.C., "Exfoliated PP/clay nanocomposites using ammonium-terminated PP as the organic modification for montmorillonite." *Macromolecules*, **36**, (24), 8919-8922 (2003)
70. Liu, X. and Wu, Q., "PP/clay nanocomposites prepared by grafting-melt intercalation." *Polymer*, **42**, (25), 10013-10019 (2001)

71. Kato, M., Matsushita, M., and Fukumori, K., "Development of a new production method for a polypropylene-clay nanocomposite." *Polym. Eng. Sci.*, **44**, (7), 1205-1211 (2004)
72. Shi, H.Z., Lan, T., and Pinnavaia, T.J., "Interfacial effects on the reinforcement properties of polymer-organoclay nanocomposites." *Chem. Mater.*, **8**, (8), 1584-1587 (1996)
73. Lan, T. and Qian, G., "Preparation of high performance polypropylene nanocomposites." *Additives 2000*. Clearwater Beach, FL (2000)
74. Song, K. and Sandi, G., "Characterization of montmorillonite surfaces after modification by Organosilane." *Clay Clay Miner.*, **49**, (2), 119-125 (2001)
75. Le Pluart, L., Duchet, J., Sautereau, H., and Gerard, J.F., "Surface modifications of montmorillonite for tailored interfaces in nanocomposites." *J. Adhesion*, **78**, (7), 645-662 (2002)
76. Le Pluart, L., Duchet, J., Sautereau, H., and Gerard, J.F., "Tailored interfaces in nanocomposites." *Macromol. Symp.*, **194**, 155-160 (2003)
77. Zhao, C., Feng, M., Gong, F., Qin, H., and Yang, M., "Preparation and characterization of polyethylene-clay nanocomposites by using chlorosilane-modified clay." *J. Appl. Polym. Sci.*, **93**, (2), 676-680 (2004)
78. Miller, A. and Berg, J., "The prediction of adhesion between polymer matrices and silane-treated glass surfaces in filled composites." *J. Adhes. Sci. Technol.*, **16**, (5), 495-507 (2002)
79. Miller, A. and Berg, J., "Predicting adhesion between a crystalline polymer and silane-treated glass surfaces in filled composites." *J. Adhes. Sci. Technol.*, **16**, (14), 1949-1956 (2002)
80. Miller, A., Knowlton, M., and Berg, J., "The use of UNIFAC for the estimation of adhesion enhancement between polymers and mineral surfaces treated with silane coupling agents." *J. Adhes. Sci. Technol.*, **14**, (12), 1471-1484 (2000)
81. Garces, J.M., Moll, D.J., Bicerano, J., Fibiger, R., and McLeod, D.G., "Polymeric nanocomposites for automotive applications." *Adv. Mater.*, **12**, (23), 1835-1839 (2000)
82. Hong, C., Lee, Y., Bae, J., Jho, J., Nam, B., and Hwang, T., "Performance of polypropylene/clay nanocomposites for automotive parts applications." *J. Ind. Eng. Chem.*, **11**, (1), 76-82 (2005)

83. Gilman, J., "Flammability and thermal stability studies of polymer layered-silicate (clay) nanocomposites." *Appl. Clay Sci.*, **15**, (1-2), 31-49 (1999)
84. Reichert, P., Hoffmann, B., Bock, T., Thomann, R., Mulhaupt, R., and Friedrich, C., "Morphological stability of poly(propylene) nanocomposites." *Macromol. Rapid Comm.*, **22**, (7), 519-523 (2001)
85. Okamoto, M., Sato, H., Taguchi, H., and Kotaka, T., "Shear-induced aggregation behavior in lipophilized smectite clay/styrene suspension." *Nihon Reoroji. Gakk.*, **28**, (4), 199-200 (2000)
86. Kumar, S. and Jayaraman, K., "Process Induced Orientation of nanolayers in Polyolefin Nanocomposites." *Society of Plastics Engrs. Annual Tech. Conf.*, **62**, 1498-1502. Chicago, IL (2004)
87. Zhang, Q., Wang, Y., and Fu, Q., "Shear-induced change of exfoliation and orientation in polypropylene/montmorillonite nanocomposites." *J. Polym. Sci. Pol. Phys.*, **41**, (1), 1-10 (2003)
88. Sekelik, D., Stepanov, E., Nazarenko, S., Schiraldi, D., Hiltner, A., and Baer, E., "Oxygen barrier properties of crystallized and talc-filled poly(ethylene terephthalate)." *J. Polym. Sci. Pol. Phys.*, **37**, (8), 847-857 (1999)
89. Bafna, A., Beaucage, G., Mirabella, F., and Mehta, S., "3D Hierarchical orientation in polymer-clay nanocomposite films." *Polymer*, **44**, (4), 1103-1115 (2003)
90. Kojima, Y., Usuki, A., Kawasumi, M., Okada, A., Kurauchi, T., Kamigaito, O., and Kaji, K., "Novel Preferred Orientation in Injection-Molded Nylon 6-Clay Hybrid." *J. Polym. Sci. Pol. Phys.*, **33**, (7), 1039-1045 (1995)
91. Schmidt, G., Nakatani, A.I., Butler, P.D., Karim, A., and Han, C.C., "Shear orientation of viscoelastic polymer-clay solutions probed by flow birefringence and SANS." *Macromolecules*, **33**, (20), 7219-7222 (2000)
92. Varlot, K., Reynaud, E., Kloppfer, M.H., Vigier, G., and Varlet, J., "Clay-reinforced polyamide: Preferential orientation of the montmorillonite sheets and the polyamide crystalline lamellae." *J. Polym. Sci. Pol. Phys.*, **39**, (12), 1360-1370 (2001)
93. Okamoto, M., Nam, P.H., Maiti, P., Kotaka, T., Hasegawa, N., and Usuki, A., "A house of cards structure in polypropylene/clay nanocomposites under elongational flow." *Nano Lett.*, **1**, (6), 295-298 (2001)
94. Fasulo, P.D., Rodgers, W.R., and Ottaviani, R.A., "Extrusion Processing of TPO Nanocomposites." *Polym. Eng. Sci.*, **44**, (6), 1036-1045 (2004)

95. Dolgovskij, M.K., Fasulo, P.D., Lortie, F., Macosko, C.W., Ottaviani, R.A., and Rodgers, W.R., "Effect of Mixer type on exfoliation of Polypropylene Nanocomposites." Society of Plastics Engrs. Annual Tech. Conf., 2255-2259. 2003. Nashville, TN
96. Gopakumar, T. and Page, D., "Compounding of nanocomposites by thermokinetic mixing." *J. Appl. Polym. Sci.*, **96**, (5), 1557-1563 (2005)
97. Solomon, M., Almusallam, A., Seefeldt, K., Somwangthanaroj, A., and Varadan, P., "Rheology of polypropylene/clay hybrid materials." *Macromolecules*, **34**, (6), 1864-1872 (2001)
98. Cullity, B.D., "Elements of X-ray Diffraction. 2nd ed., Massachusetts: Addison-Wesley (1978)
99. Krishnamoorti, R., "Rheology and structure of polymer layered-silicate nanocomposites." *Abstr. Pap. Am. Chem. S.*, **218**, U558-U558 (1999)
100. Krishnamoorti, R. and Giannelis, E., "Rheology of end-tethered polymer layered silicate nanocomposites." *Macromolecules*, **30**, (14), 4097-4102 (1997)
101. Krishnamoorti, R. and Giannelis, E., "Strain hardening in model polymer brushes under shear." *Langmuir*, **17**, (5), 1448-1452 (2001)
102. Aubry, T., Razafinimaro, T., and Mederic, P., "Rheological investigation of the melt state elastic and yield properties of a polyamide-12 layered silicate nanocomposite." *J. Rheol.*, **49**, (2), 425-440 (2005)
103. Galgali, G., Ramesh, C., and Lele, A., "A rheological study on the kinetics of hybrid formation in polypropylene nanocomposites." *Macromolecules*, **34**, (4), 852-858 (2001)
104. Auhl, D., Stange, J., Munstedt, H., Krause, B., Voigt, D., Lederer, A., Lappan, U., and Lunkwitz, K., "Long-chain branched polypropylenes by electron beam irradiation and their rheological properties." *Macromolecules*, **37**, (25), 9465-9472 (2004)
105. Ellis, T.S. and D'Angelo, J.S., "Thermal and mechanical properties of a polypropylene nanocomposite." *J. Appl. Polym. Sci.*, **90**, (6), 1639-1647 (2003)
106. Oya, T., Polypropylene-Clay Nanocomposites, in *Polymer Clay Nanocomposites*, T.J. Pinnavaia and G.W. Beall, Editors. (2000)

107. Svoboda, P., Zeng, C., Wang, H., Lee, L., and Tomasko, D., "Morphology and mechanical properties of polypropylene/organoclay nanocomposites." *J. Appl. Polym. Sci.*, **85**, (7), 1562-1570 (2002)
108. Cho, Y.G. and Kamal, M.R., "Estimation of stress for separation of two platelets." *Polym. Eng. Sci.*, **44**, (6), 1187-1195 (2004)
109. Milczewska, K., Voelkel, A. and Jeczalik, J. "The use of Flory-Huggins parameters to characterization of polymer/filler interactions." *Macromol. Symp.*, **194**, 305-311 (2003)
110. Voelkel, A., Milczewska, K. and Jeczalik, J. "Characterization of the interactions in polymer/silica systems by inverse gas chromatography." *Macromol. Symp.*, **169**, 45-55 (2001)
111. Wang, K., Liang, S., Du, R.N., Zhang, Q. and Fu, Q. "The interplay of thermodynamics and shear on the dispersion of polymer nanocomposite." *Polymer*, **45**, (23), 7953-7960 (2004)
112. Marchant, D. and Jayaraman, K., "Effectiveness Of PPMA Compatibilizers For Nanolayer Dispersion In PP: Bound Vs Free Anhydride." Society of Plastics Engrs. Annual Tech. Conf., **61**, 2200-2204. Nashville, TN (2003)
113. Voeks, J.F., "Cohesive Energy Density and Internal Pressure of High Polymers." *J. Polym. Sci. Part A*, **2**, 5319-5325 (1964)
114. Xu, L., Reeder, S., Thopasridharan, M., Ren, J., Shipp, D.A. and Krishnamoorti, R. "Structure and melt rheology of polystyrene-based layered silicate nanocomposites." *Nanotechnology*, **16**, S514-S521 (2005)
115. Luciani, A., Leterrier, Y., and Manson, J., "Rheological behaviour of dilute suspensions of platelet particles." *Rheol. Acta*, **38**, (5), 437-442 (1999)
116. Utracki, L., Favis, B., and Fisa, B., "Dynamic and Steady-state flow of Polypropylene Systems." *Polym. Composite*, **5**, (4), 277-288 (1984)
117. Matsumoto, T., Hitomi, C., and Onogi, S., "Rheological Properties of Disperse Systems of Spherical-Particles in Polystyrene Solution at Long Time-Scales." *T. Soc. Rheol.*, **19**, (4), 541-555 (1975)
118. Lertwilmolnun, W. and Vergnes, B., "Influence of compatibilizer and processing conditions on the dispersion of nanoclay in a polypropylene matrix." *Polymer*, **46**, (10), 3462-3471 (2005)
119. Van Gorp, M. and Palmen, J., "Time temperature superposition for polymeric blends." *Rheology Bulletin*, **67**, 5-8 (1998)

120. Trinkle, S. and Friedrich, C., "Van Gurrp-Palmen-plot: a way to characterize polydispersity of linear polymers." *Rheol. Acta*, **40**, (4), 322-328 (2001)
121. Trinkle, S., Walter, P., and Friedrich, C., "Van Gurrp-Palmen Plot II - Classification of long chain branched polymers by their topology." *Rheol. Acta*, **41**, (1-2), 103-113 (2002)
122. Galgali, G., Agarwal, S., and Lele, A., "Effect of clay orientation on the tensile modulus of polypropylene-nanoclay composites." *Polymer*, **45**, (17), 6059-6069 (2004)
123. Miller, A. and Berg, J., "Effect of silane coupling agent adsorbate structure on adhesion performance with a polymeric matrix." *Compos. Part A-Appl. S.*, **34**, (4), 327-332 (2003)
124. Nygard, P., Grundke, K., Mader, E., and Bellmann, C., "Wetting kinetics and adhesion strength between polypropylene melt and glass fibre: influence of chemical reactivity and fibre roughness." *J. Adhes. Sci. Technol.*, **16**, (13), 1781-1808 (2002)
125. Deroover, B., Sclavons, M., Carlier, V., Devaux, J., Legras, R., and Momtaz, A., "Molecular Characterization of Maleic Anhydride-Functionalized Polypropylene." *J. Polym. Sci. Pol. Chem.*, **33**, (5), 829-842 (1995)
126. Marchant, D. "PhD Dissertation" Michigan State University, (2003)
127. Krishnamoorti, R., Ren, J., and Silva, A., "Shear response of layered silicate nanocomposites." *J. Chem. Phys.*, **114**, (11), 4968-4973 (2001)
128. Eastwood, E., Viswanathan, S., O'Brien, C.P., Kumar, D., and Dadmun, M.D., "Methods to improve the properties of polymer mixtures: optimizing intermolecular interactions and compatibilization." *Polymer*, **46**, 3957-3970 (2005)
129. Su, S., Jiang, D., and Wilkie, C., "Novel polymerically-modified clays permit the preparation of intercalated and exfoliated nanocomposites of styrene and its copolymers by melt blending." *Polym. Degrad. Stabil.*, **83**, (2), 333-346 (2004)
130. Su, S., Jiang, D., and Wilkie, C., "Poly(methyl methacrylate), polypropylene and polyethylene nanocomposite formation by melt blending using novel polymerically-modified clays." *Polym. Degrad. Stabil.*, **83**, (2), 321-331 (2004)
131. Kurian, M., Dasgupta, A., Beyer, F.L., and Galvin, M.E., "Investigation of the effects of silicate modification on polymer-layered silicate nanocomposite morphology." *J. Polym. Sci. Pol. Phys.*, **42**, (22), 4075-4083 (2004)

MICHIGAN STATE UNIVERSITY LIBRARIES



3 1293 02736 8756